

**MEGAKARYOCYTE-MEMBRANE WRAPPED NANOPARTICLES FOR  
TARGETED DELIVERY TO HEMATOPOIETIC STEM CELLS**

by

Erica Winter

A thesis submitted to the Faculty of the University of Delaware in partial fulfillment of the requirements for the degree of Master of Science in Biological Sciences

Fall 2018

© 2018 Erica Winter  
All Rights Reserved

**MEGAKARYOCYTE-MEMBRANE WRAPPED NANOPARTICLES FOR  
TARGETED DELIVERY TO HEMATOPOIETIC STEM CELLS**

by

Erica Winter

Approved: \_\_\_\_\_  
Eleftherios T. Papoutsakis, Ph.D.  
Professor in charge of thesis on behalf of the Advisory Committee

Approved: \_\_\_\_\_  
E. Fidelma Boyd, Ph.D.  
Chair of the Department of Biological Sciences

Approved: \_\_\_\_\_  
John Pelesko, Ph.D.  
Interim Dean of the College of Arts and Sciences

Approved: \_\_\_\_\_  
Douglas J. Doren, Ph.D.  
Interim Vice Provost for the Office of Graduate and Professional  
Education

## ACKNOWLEDGMENTS

I would like to thank the University of Delaware and the Department of Biological Sciences for providing me with opportunities to learn and perform research. Through the Graduate program I was able to make new friends and interact with caring professors all while learning and improving skills that will stay with me during my scientific career.

I would like to thank my advisor, Dr. Terry Papoutsakis, who accepted me into his lab and provided me with the opportunity to study stem cells, something I was always interested in. He provided me with support and guidance whenever necessary throughout this project and I know that his support will continue in the coming years post-graduation. I would also like to thank my committee members, Dr. Donna Woulfe and Dr. Jessica Tanis, who were very caring and provided critical feedback necessary to complete this project. Dr. Emily Day and Jenna Harris for providing the nanoparticles as well as critical feedback. Dr. Matt Hudson and Eric Munoz for use of their time and equipment.

I would like to thank all the Papoutsakis lab members who helped improve my critical thinking and experimental design skills. Chen-Yuan Kao was a wonderful mentor and friend to me and without his help during the first year I would have been lost in the lab. When joining the lab, I met Christian Escobar and Hannah Streett who provided great support and friendship throughout my time in the Papoutsakis lab.

Finally, I would like to thank my friends and family for understanding the devotion and time it takes to perform graduate research. With their support and

encouragement, I was able to push myself to go back to school and complete the biology graduate program!

## TABLE OF CONTENTS

LIST OF TABLES .....	vii
LIST OF FIGURES .....	viii
ABSTRACT .....	xvi

### Chapter

1	INTRODUCTION .....	1
1.1	Hematopoietic Stem Cells .....	1
1.2	Challenges Associated with Therapeutic Gene Delivery to HSPCs .....	2
1.3	Megakaryocyte-derived Microparticles (MkMPs) Target and Interact with HSPCs .....	5
1.4	PLGA NPs are Capable of Encapsulating Genetic Cargo .....	10
1.5	PLGA NPs can be Decorated with Cell Membrane for Targeted Delivery .....	13
1.6	NPs can Escape Endosomes .....	14
1.7	Mk-membrane Wrapped NPs (MkNPs) would Target and Interact with HSPCs .....	17
2	MEMBRANE COLLECTION, NANOPARTICLE WRAPPING, AND CHARACTERIZATION .....	20
2.1	Background.....	20
2.2	Materials and Methods .....	20
2.2.1	Culture of CHRF-288-11 Cell Line.....	20
2.2.2	Culture of Human Hematopoietic Stem Cells to Mature Megakaryocytes.....	21
2.2.3	Preparation of PMA-CHRF or Mk Membranes .....	23
2.2.4	PLGA NP Preparation .....	24
2.2.5	PMA-CHRF and Mk-membrane Wrapped NP Synthesis .....	24
2.2.6	Transmission Electron Microscopy (TEM).....	24
2.2.7	Nanoparticle Tracking Analysis (NTA) .....	25
2.2.8	Wrapping Using NTA .....	25
2.2.9	Streptavidin Bead Assay.....	26
2.3	Results .....	26

2.3.1	Confirmation of Membrane-wrapped NPs as Visualized Under TEM.....	26
2.3.2	Confirming Wrapping by NTA .....	33
2.3.3	Assessing the Membrane Protein Content of Wrapped NPs Using a Magnetic Bead Assay.....	49
2.4	Discussion.....	55
3	<b>MK-WRAPPED NANOPARTICLES INTERACT WITH HEMATOPOIETIC STEM CELLS .....</b>	<b>59</b>
3.1	Background.....	59
3.2	Materials and Methods .....	60
3.2.1	Co-Culture with HSPCs and Mk-wrapped NPs .....	60
3.2.2	Confocal and Super Resolution Microscopy .....	60
3.2.3	Endocytosis of Bare PLGA NPs and Mk-wrapped NPs .....	61
3.3	Results .....	61
3.3.1	Mk-wrapped NPs Interact with HSPCs after 24hrs.....	61
3.3.2	Uptake of Mk-wrapped NPs is Dynamin-Dependent.....	74
3.4	Discussion.....	80
4	<b>FUTURE DIRECTIONS.....</b>	<b>82</b>
	<b>REFERENCES .....</b>	<b>86</b>
 Appendix		
A	MEMBRANE-COLLECTION AND NP WRAPPING.....	90
B	FURTHER CHARACTERIZATION OF MK-WRAPPED NPs.....	94
C	MK-WRAPPED NPS INTERACTING WITH HSPCs .....	96
D	HUMAN CONSENT FORM .....	103
E	INSTITUTIONAL ANIMAL CARE AND USE COMMITTEE FORM AUP# 1326-2017-0 .....	105
F	INSTITUTIONAL ANIMAL CARE AND USE COMMITTEE FORM AUP# 1290-2016-0 .....	109

## LIST OF TABLES

Table 1.	Calculating wrapping ratio based on concentration .....	38
Table 2.	Sample calculation of wrapped and bare NPs to add to HSPCs .....	47
Table 3.	Calculating the wrapping ratio based on Surface Area .....	48
Table 4.	Brief description of major endocytic pathways (Verma and Stellacci 2010, Mulcahy 2014). .....	74

## LIST OF FIGURES

- Figure 1. Scheme of Mk-wrapped PLGA NPs targeting HSPCs *in vitro*. Mk-membrane vesicles (MkMVs) will be derived from Megakaryocytes (Mks). The MkMVs will wrap around PLGA NPs to create Mk-membrane wrapped NPs (MkNPs), which target HSPCs. .... 18
- Figure 2. Morphology of PMA-CHRF-membrane-coated PLGA nanoparticles. (A) Day 3 extracted PMA-CHRF membranes. (B) Bare NPs. (C) PMA-CHRF wrapped NPs display the clear polymeric core surrounded by a “halo” or secondary layer suggesting membrane wrapping. Green arrow points to the membrane layer. All samples were placed on a 400nm Carbon coated grid and negatively stained with 1% Phosphotungstate (PTA) (sodium) (pH 7.2) and visualized with TEM. .... 30
- Figure 3. Mk membranes form vesicles post extrusion. Day 12 Mk cells ( $2.0 \times 10^7$  cells) were subjected to membrane extraction process and then extruded through 400nm pore membrane 11 times. Sample was placed on a 400nm Carbon coated grid and negatively stained with 1% Phosphotungstate (PTA) (sodium) (pH 7.2) and visualized with TEM.. 31
- Figure 4. Morphology of Mk-membrane-coated PLGA nanoparticles. (A) Membranes generated from Day12 Mk cells from differentiated CD34<sup>+</sup> HSPCs. (B) Bare, DiD-loaded NPs were sonicated with Mk membrane vesicles resulting in (C) wrapped NPs. Wrapped NPs display the clear polymeric core surrounded by a “halo” or secondary layer suggesting membrane wrapping. A green arrow points to the membrane layer. All samples were placed on a 400nm Carbon coated grid and negatively stained with 1% PTA (sodium) (pH 7.2) and visualized with TEM. .... 32
- Figure 5. Mk membranes are 7-10nm thick. Mk membranes were extracted and wrapped around NPs. All samples were placed on a 400nm Carbon coated grid and negatively stained with 1% PTA (sodium) (pH 7.2) and visualized with TEM. Membrane thickness was determined by tools used on Libra 120 software. .... 34

Figure 6.	Mk-membrane wrapping increases the size of NPs. Top structure is a bare NP and bottom structure is a Mk-wrapped NP. Vesicles were isolated from $4.4 \times 10^6$ Day 12 Mk cells and used to wrap NPs ranging in size of 50-75nm on 1/10/2018. Yellow arrow points to the Mk membrane wrapped around the NP. ....	35
Figure 7.	Mean diameter size of MkMVs. Day 12 MkMVs were extruded through 400nm membrane pore filter 11 times. NTA (NS300) was performed on extruded vesicles with three replicates per individual membrane extraction. Error bars represent standard deviation (n=11). ..	37
Figure 8.	Size distribution of bare NPs, MkMVs, and MkNPs as determined by NTA. Wrapping was performed using the 400nm-pore membrane. The size of bare NPs and extruded MkMVs were determined using NS300 (Malvern). Ratios of NP to MkMVs were calculated (number of NPs: number of MkMVs, wrapped samples were generated and measured for mean size. NTA was performed on each sample with three technical replicates each. Error bars represent standard deviation (n=4). ....	39
Figure 9.	Excess MkMVs and debris are present after wrapping. (A). Bare NPs were wrapped with MkMVs at a 1:60 NP to MkMV ratio (1 NP for 60 MkMVs). Blue arrows point to excess MkMVs or debris. (B). Wrapped NPs in A above were magnified to show wrapping. Green arrows point to wrapped NPs. Samples were placed on 400nm Carbon Cu grids and negatively stained with 2% uranyl acetate and examined under TEM. Scale bars represent 100 $\mu$ m. ....	40
Figure 10.	Excess MkMVs are removed after additional ultracentrifugation step. (A) NPs wrapped by MkMVs in a 1:60 NP: MkMV were ultracentrifuged at 17,000rpm for 30mins and then resuspended in water. (B) The samples in A were magnified to show wrapping. Green arrow points to wrapping. Samples were placed on 400nm Carbon Cu grids and negatively stained with 2% uranyl acetate and examined under TEM. Scale bars represent 100 $\mu$ m. ....	41
Figure 11.	Particle size distribution of bare and wrapped NPs determined by NTA. Bare NPs were wrapped with MkMVs, and synthesized MkNPs were subjected to ultracentrifugation to remove excess MkMVs and generate Purified MkNPs. NTA determined size distribution with three technical replicates. ....	43

Figure 12.	Mean Diameter of Purified MkNPs. Bare DiD-loaded NPs were wrapped with Day 12 MkMVs via extrusion in a 1 to 60 ratio (NP: MkMV) and analyzed on NanoSight300 (Malvern). Synthesized MkMVs were ultracentrifuged to remove excess MkMVs. Once “cleaned” the wrapped NP is referred to as Purified MkNPs. NTA was performed on each sample with three technical replicates each. Error bars represent standard deviation. ....	44
Figure 13.	Mean Diameters of Synthesized MkNPs and Purified MkNPs. Bare DiD-loaded NPs were wrapped with Day 12 MkMVs via extrusion and analyzed on NanoSight300 (Malvern). Synthesized MkMVs were ultracentrifuged to remove excess MkMVs. Once “cleaned” wrapped NPs were called Purified MkNPs. NTA was performed on each sample with three technical replicates. Error bars represent standard deviation. (n=3) .....	45
Figure 14.	Size distribution curves of Bare NPs, Synthesized MkNPs, and Purified MkNPs. Bare NPs were wrapped with MkMVs via 400nm membrane pore. Synthesized MkNPs were placed in PBS overnight to induce swelling of Bare NPs. The Bare NPs were filtered and excess MkMVs were removed by ultracentrifugation to produce Purified MkNPs. NTA determined size distribution with three technical replicates.....	46
Figure 15.	Scheme of Magnetic Bead-antibody assay. The streptavidin-coated magnetic beads will be attracted to biotin-conjugated anti CD41 antibodies. Any material that is CD41 <sup>+</sup> (MkMVs and MkNPs) will be attracted to the antibody bound to the magnetic beads. The bare DiD NPs will remain unbound and wash away.....	51
Figure 16.	Streptavidin-coated Magnetic beads and biotin-conjugated anti-CD41 antibodies capture MkMVs and MkNPs. Magnetic beads (grey) were mixed with biotin-conjugated anti-CD41 antibodies. MkMVs (red), bare NPs (green), and MkNPs (yellow) were each mixed separately with the magnetic beads and antibodies. Samples were placed on a magnetic stand and washed three times, ensuring only captured material remained. Washed magnetic beads were analyzed via flow cytometry. Goat anti-mouse antibody (blue) was used as a proof-of-principle.....	53

- Figure 17. Colocalization of signals suggests NPs are wrapped and targeting HSPCs. NPs (green) were wrapped with PKH-26 dyed Mk membranes (red) and exposed to Day 3 HSPCs in a co-culture system. Yellow signal suggests colocalization. Live cells were washed with PBS and visualized under Confocal (LMS880) under 40x oil. Arrows point to examples of MkNPs. Scale bar represents 10 $\mu$ m. .... 63
- Figure 18. HSPCs uptake Mk-wrapped NPs after 24hrs. (A) Static image of HSPC with taken in MkNPs indicated by the yellow colocalization of signals. (B) Static images taken from Z-stacks in sequence. Z-stacks and image taken on Confocal LMS880. Red arrow points to uropod region of HSPC. White arrow points to the MkNPs in cytoplasm. Nuclei stained with DAPI. Scale bar represents 10 $\mu$ m. .... 64
- Figure 19. Super Resolution Microscopy further confirms MkNPs are inside HSPCs. Mk membranes were stained with PKH26 (red). NPs were loaded with DiD (light blue). HSPCs' membranes were stained with phalloidin (green) and nuclei were stained with DAPI. Z-stack recorded on SuperRes Zeiss Elyra PS 1 under 63x oil and static images taken from Z-stack video in sequence are presented. Yellow arrows point to colocalization in static images. .... 66
- Figure 20. MkNPs interact with HSPCs at 24hrs, as detected by flow cytometry. Mk membranes stained with PKH26 (red) and NPs loaded with DiD (green) were extruded to form MkNPs (yellow). Particles were co-cultured with Day 3 HSPCs for 24 hours and then measured using flow cytometry (FACS Aria). Gate in upper right corner represents wrapped NPs. Blue color shows live cells positive for interaction. .... 67
- Figure 21. Transwell membrane and additional centrifugation step allow for increase uptake of MkNPs by HSPCs. HSPCs were co-cultured with 44,000 MkNPs/cell for 24hrs. (A) Static image of HSPC with MkNPs taken in (B) Split screen of static image displaying different channels. Mk membranes stained with PKH26 membrane dye (red), NPs loaded with DiD dye (green), nuclei stained with DAPI (blue). Arrows point to uptake when nuclei are in focus. Yellow signals suggest colocalization. Visualized with Confocal LMS880 under 40x oil. Scale bar is 5 $\mu$ m. .... 69

- Figure 22. HSPCs take up MkNPs after 24 hrs. Day 3 HPSCs were seeded with 10,000 MkNPs/cell. Mk membranes stained with PKH26 membrane dye (red), NPs loaded with DiD dye (green), nuclei stained with DAPI (blue). Arrows point to uptake when nuclei are in focus. Yellow signals suggest colocalization. Visualized with Confocal LMS880 under 40x oil. Images are static images taken from Z-stacks in sequence Scale bar is 5 $\mu$ m..... 70
- Figure 23. MkNPs are in cell cytoplasm of HSPCs. Day 3 HSPCs were co-cultured with 77,000 MkNPs for 24hrs. Mk membranes were dyed with PKH26 (red), NPs were loaded with DiD (green), nuclei were stained with DAPI (blue), and HSPCs' membranes stained with phalloidin (white). Samples were fixed to slides and visualized on Confocal LMS880 under 63x oil. Scale bars are 5 $\mu$ m. Arrows point to uptake of wrapped NPs..... 71
- Figure 24. Static images taken from Z-stack in sequence display internalization of MkNPs in cell cytoplasm. Day 3 HSPCs were co-cultured with 77,000 MkNPs for 24hrs. Mk membranes were dyed with PKH26 (red), NPs were loaded with DiD (green), nuclei were stained with DAPI (blue), and HSPCs' membranes stained with phalloidin (white). Samples were fixed to slides and visualized on Confocal LMS880 under 63x oil. Scale bars are 5 $\mu$ m. Arrows point to uptake of wrapped NPs. .... 72
- Figure 25. Comparison of HSPCs exposed to 10,000 particles/cell for 24hrs. Day 3 HSPCs were co-cultured with either 10,000 MkNPs (left panels) or 10,000 bare NPs (right panels) for 24hrs, as determined NTA. Mk membranes are dyed with PKH26(red), NPs are dyed with DiD (green), nuclei are stained with DAPI (blue). The yellow signals suggest colocalization. Visualized using Confocal LMS880. Scale bars are 5 $\mu$ m. .... 73

- Figure 26. Lipid rafts and Dynamin are involved in the uptake bare PLGA NPs by HSPCs. Day 3 HSPCs were pre-incubated with specific inhibitors of endocytic pathways. Inhibitors used were Dimethylamiloride (DMA), Methyl- $\beta$ -cyclodextrin (M $\beta$ CD), Dynasore, and LY29400, which target macropinocytosis, lipid raft, dynamin-dependent endocytosis, and macropinocytosis through PI3K, respectively. 5mM M $\beta$ CD, 10 $\mu$ M DMA, 80 $\mu$ M Dynasore, and 50 $\mu$ M LY29400 for 45mins at 37°C, before co-culture with bare NPs for 30mins. Uptake of Bare NPs were analyzed by flow cytometry. Data represent the average of 6 biological replicates  $\pm$  standard error of the mean. \*, p<0.05; \*\*, p<0.01 ..... 78
- Figure 27. Dynamin-dependent endocytosis is involved in uptake of MkNPs by HSPCs. Day 3 HSPCs were pre-incubated with specific inhibitors against endocytic pathways. Inhibitors used were Dimethylamiloride (DMA), Methyl- $\beta$ -cyclodextrin (M $\beta$ CD), Dynasore, and LY29400, which target macropinocytosis, lipid raft, dynamin-dependent endocytosis, and macropinocytosis through PI3K, respectively. 10 $\mu$ M DMA, 5mM M $\beta$ CD, 80 $\mu$ M Dynasore, and 50 $\mu$ M LY29400 for 45mins at 37°C, before co-culture with Mk-wrapped NPs for 30mins. Uptake of MkNPs were analyzed by flow cytometry. Data represent the average of 6 biological replicates  $\pm$  standard error of the mean. \*, p<0.05; \*\*, p<0.01 ..... 79
- Figure A1. PMA-CHRF membrane vesicles visualized on TEM. PMA-CHRF vesicles were generated by membrane extraction process and extruded through 400nm membrane pore. All samples were placed on a 400nm Carbon coated grid and negatively stained with 1% PTA (sodium) (pH 7.2) and visualized with TEM. .... 90
- Figure A2. PMA-CHRF wrapped NPs visualized on TEM. (A) PMA-CHRF wrapped 5.2mg/mL NPs generated on 9/26/17 (B) PMA-CHRF wrapped 4.83 mg/mL NPs generated on 10/03/17. All samples were placed on a 400nm Carbon coated grid and negatively stained with 1% PTA (sodium) (pH 7.2) and visualized with TEM. .... 91
- Figure A3. MkMVs. Top row: MkMVs isolated from 2.0x10<sup>7</sup> Day 12 Mk cells on 5/28/2018. Middle row: Mk membrane vesicles isolated from 1.1x10<sup>7</sup> Day 12 Mk cells on 6/19/2018. Bottom row: Mk membrane vesicles isolated from 6.0x10<sup>6</sup> D12 Mk cells on 7/10/2018. All membrane vesicles were extruded through 400nm membrane pore 11 times. All samples were placed on a 400nm Carbon coated grid and negatively stained with 2% uranyl acetate and visualized with TEM. .... 92

Figure A4.	MkNPs visualized on TEM. Day 12 Mk membranes wrapped 0.25 mg/mL NPs through extrusion of 400nm pore on 2/02/2018. All samples were placed on a 400nm Carbon coated grid and negatively stained with 1% PTA (sodium) (pH 7.2) and visualized with TEM. ....	93
Figure B1.	Secondary layer surrounding the NP indicates wrapping and increases size of NPs. Top structure is a bare NP and bottom structure is a Mk-wrapped NP. Vesicles were isolated from $4.4 \times 10^6$ Day 12 Mk cells and use to wrap NPs ranging in size of 50-75nm on 1/10/2018. Particles labeled using a tool on Libra 120 Software to show size increase. ....	94
Figure B2.	MkNPs are FITC-CD41 <sup>+</sup> . Bare NPs (A) loaded with DiD (red) were wrapped with un-dyed Mk membranes. Wrapped NPs (B) were exposed to FITC-CD41 (green) and visualized under 40X oil on Confocal 880. The scale bare is 20 $\mu$ m. Any yellow suggests colocalization of both signals. ....	95
Figure C1.	MkNPs appear to aggregate at HSPCs' membrane surface at 12hrs. MkNPs show colocalization of signals but no uptake when exposed to Day 3 HSPCs for 12hrs. Images taken on Confocal LMS880. Nuclei stained with DAPI. Scale bar represents 10 $\mu$ m. ....	96
Figure C2.	HSPCs take in MkMVs and Bare NPs at 12hrs. (A) Static images of HSPCs with MkMVs stained with PKH26 (red) and Bare NPs (green) (B) Static images taken taken from Z-stacks in sequence. Z-stacks and images taken on Confocal LMS880. Arrows point to uptake of either MkMVs or Bare NPs. Nuclei stained with DAPI. Scale bar represents 10 $\mu$ m. ....	97
Figure C3.	HSPCs take in MkMVs and Bare NPs at 24hrs. (A) Static images of HSPCs with MkMVs stained with PKH26 (red) and Bare NPs (green). (B) Static images taken from Z-stacks in sequence. Z-stacks and images taken on Confocal LMS880. Arrows point to uptake of either MkMVs or Bare NPs. Nuclei stained with DAPI. Scale bar represents 10 $\mu$ m. ....	98
Figure C4.	MkNPs detected on flow cytometry interacting with HSPCs at 12hrs. Mk membranes stained with PKH26 (red) and NPs loaded with DiD (green) were extruded to form MkNPs (yellow). Particles were co-cultured with Day 3 HSPCs for 12 hours and then measured using flow cytometry (FACS Aria). Gate represents wrapped NPs. Blue color shows live cells positive for interaction. ....	99

- Figure C5. Uptake of MkMVs by HSPCs after 24hrs. Day 3 HSPCs were co-cultured with 175,000 MkMVs per cell for 24hrs. Mk membranes were dyed with PKH26 (red). Nuclei stained with DAPI (blue). Arrow points to uptake as nucleus comes into focus. Static images taken from Z-stack in sequence. Visualized on Confocal LMS880 under 40x oil. Scale bar is 5 $\mu$ m. .... 99
- Figure C6. Uptake of bare NPs by HSPCs after 24hrs. Day 3 HSPCs were co-cultured with 43,900 bare NPs per cell for 24hrs. Bare NPs were dyed with DiD. Nuclei stained with DAPI. Arrow points to uptake as nucleus comes into focus. Static images taken from Z-stack in sequence. Visualized on Confocal LMS880 under 40x oil. Scale bar is 5 $\mu$ m..... 100
- Figure C7. HSPCs uptake Mk-wrapped NPs after 24 hrs. Day 3 HPSCs were seeded with 77,000 MkNPs/cell. Mk membranes stained with PKH26 membrane dye (red), NPs loaded with DiD dye (green), Nuclei stained with DAPI (blue). Arrows point to uptake when nuclei are in focus. Yellow signals suggest colocalization. Visualized on Confocal LMS880 under 40x oil. Static images are taken from Z-stacks in sequence. Scale bar is 5 $\mu$ m..... 100
- Figure C8. Comparison of HSPCs exposed to 43,000 particles/cell for 24hrs. Day 3 HSPCs were co-cultured with 43,000 MkNPs (left panels) or bare NPs (right panels) for 24hrs. Mk membranes are dyed with PKH26(red), NPs are dyed with DiD (green), Nuclei are stained with DAPI (blue). The yellow signals indicate colocalization. Visualized under Confocal LMS880. Scale bars are 5 $\mu$ m..... 101
- Figure C9. Split screens showing different channels. HSPCs were co-cultured with 77,000 MkNPs per cell for 24hrs. Mk-membranes were dyed with PKH26 (red), NPs were loaded with DiD dye (green), and nuclei were stained (blue), HSPCS were stained with phalloidin (white). Slides were fixed in 4% formaldehyde and visualized using Confocal LMS880 under 63X oil. Scale bar is 5 $\mu$ m. .... 102

## ABSTRACT

Hematopoietic Stem and Progenitor Cells (HSPCs) are promising targets for gene therapy as they are self-renewing and differentiate into many blood-related cells. However, they are considered very difficult to transfect. Current delivery methods, such as viral vectors (i.e. lentiviruses), produce poor gene delivery as well as cytotoxicity. However, synthetic PLGA Nanoparticles (NPs) produce low toxicity and can encapsulate genetic cargo. To improve targeted delivery to HSCs *in vivo*, PLGA NPs can be decorated with the cell membrane removed from Megakaryocytes (Mks) or Mk-derived Microparticles (MkMPs), which we have previously shown to interact with HSCs *in vitro* and *in vivo* (Escobar 2017, Jiang 2017). A NP disguised with a Mk membrane will be able to avoid innate immune responses and specifically target HSPCs *in vivo* where it will deliver its genetic cargo once taken in by the HSPC.

Here, we demonstrate that the protocol for extracting the membranes from Mks to generate Mk-membrane vesicles (MkMVs) has been optimized, that PLGA NPs are successfully wrapped to produce Mk-membrane wrapped NPs (MkNPs), and we explore the mechanism by which MkNPs enter the cell. Wrapping is characterized by Transmission Electron Microscope and internalization of MkNPs in the cytoplasm of HSPCs is seen after 24hrs of introduction *in vitro*.

In this study, novel methods such as Nanoparticle Tracking Analysis (NTA) and flow cytometry have been used to further characterized MkNPs; these methods have not been utilized by other published literature. Size and concentration of the

MkNPs was determined by NTA. As wrapped NPs are too small for detection on flow cytometry, magnetic beads capturing MkNPs were used to confirm wrapping.

The methods developed and optimized in this study will be used in the future to generate Mk-wrapped cargo-loaded NPs for targeted delivery to HSPCs.

## Chapter 1

### INTRODUCTION

#### 1.1 Hematopoietic Stem Cells

The hematopoietic system consists of many cell types with different, specialized functions all deriving from a specific cell type: Hematopoietic Stem Cells (HSCs) (Domen 2006). HSCs are self-renewing and possess the ability to differentiate into multiple hematopoietic lineages (Ogawa 1993). HSCs differentiate into either myeloid blood cells (erythrocytes, megakaryocytes, eosinophils, basophils, neutrophils, and monocytes) and lymphoid blood cells (B cells, T cells, and natural killer cells)(Cabrita, Ferreira et al. 2003). These differentiated cells make up about 0.01-0.05% of the cells found in the bone marrow (Cabrita, Ferreira et al. 2003), and many of these types of blood cells are short lived and need to be replenished continuously(Domen 2006) The average human requires approximately one hundred billion new hematopoietic-lineage cells each day which requires the presences of HSCs, the only source of these cells (Domen 2006). Differentiating into the different cell types is triggered by the release of cytokines, which are secreted glycoproteins that trigger the stem cells to differentiate along a certain lineage (Cabrita, Ferreira et al. 2003). HSCs can be collected from murine and human systems, identified by specific selectable markers (CD34<sup>+</sup>), and cultured in an *ex vivo* environment. The ability to grow HSCs *ex vivo* has greatly helped to understand the different differentiation mechanisms and to learn how to deliver therapeutic materials to HSCs.

## 1.2 Challenges Associated with Therapeutic Gene Delivery to HSPCs

Due to their ability to self-renew and multipotency, HSPCs (Hematopoietic Stem and Progenitor Cells) offer great therapeutic potentials for corrective gene delivery. Gene therapy is described as the direct transfer of genetic material to cells or tissues for the treatment of inherited disorders and acquired diseases (Dizaj, Jafari et al. 2014). This therapeutic method aims to introduce a gene encoding a functional protein altering the expression of an endogenous gene or possessing the capacity to cure or prevent the progression of a disease (Dizaj, Jafari et al. 2014). It has been proposed that a small number of genetically modified HSPCs could accomplish lifelong, corrective reconstitution of the entire hematopoietic system in patients with various hematologic disorders (Yu, Natanson et al. 2016). Such disorders include but are not limited to HIV, sickle cell anemia, X-linked severe combined immunodeficiency (SCID-X1), adenosine deaminase deficiency (ADA), and Wiskott-Aldrich syndrome (WAS) (Yu, Natanson et al. 2016).

The current and most efficient gene therapies in place is to deliver transgenes of interest via integrating and non-integrating viral vectors (Yu, Natanson et al. 2016). A patient's HSPCs are harvested from the bone marrow, peripheral blood, or umbilical cord blood. The HSPCs are cultured *ex vivo* and then exposed to gene-editing tools such as a viral vector designed to modify the cell's genome. However, modification may not occur in every cell when HSPCs are directly modified (Goodman and Malik 2016). The HSPCs are transplanted back into the patient where the modified cells proliferate and repopulate, a process known as engraftment. Highly efficient gene transfer must occur to modify enough cells able to achieve long-term engraftment (Goodman and Malik 2016).

Traditional gene therapy was developed using gamma-retroviruses. However, gamma-retrovirus-based HSPC gene therapy led to limited capacity to insert transgenes into long term repopulating HSPCs and substantial associated risk of insertional mutagenesis due to activation of adjacent proto-oncogenes (Yu, Natanson et al. 2016). Instead, lentiviruses offer more advantages compared to gammaretroviral vectors; they possess the ability to infect quiescent cells, the ability to package large cassettes, and reduced genotoxicity due to the viral enhancers being removed (Goodman and Malik 2016, Yu, Natanson et al. 2016). Lentiviruses were previously used to deliver sgRNA and Cas9 to murine HSPCs generating loss-of-function mutations in associated with human acute myeloid leukemia (Yu, Natanson et al. 2016). However, in an experiment performed by Yu et al., a lentiviral vector delivering large genetic editing components (sgRNA and Cas9) to human HSPCs resulted in significant cytotoxicity (Yu, Natanson et al. 2016). The cytotoxicity could be caused by dysregulated transgene expression or residual genotoxicity (Yu, Natanson et al. 2016). Integrating viral vectors also result in permanent expression in HSPCs and their progeny, which would not be acceptable for clinical settings (Yu, Natanson et al. 2016). Non-integrating viral vectors like adeno-associated viral vectors (rAAVs) have been used to transport nucleases or gene correction cassettes, but they have low levels of integration, cytotoxic, or have small packaging limitations (Yu, Natanson et al. 2016). Although viral vectors make up 70% of gene therapy in clinical trials and they have a high transfection efficiency, they often lead to carcinogenesis, immunogenicity, and broad tropism, and in addition, they have limited DNA packaging capacity, on top of difficulties in vector production (Yin 2014). These disadvantages hinder clinical applications.

Due to the limitations observed with viral vectors, research has moved towards the use of non-viral vectors for nucleic-acid delivery. Non-viral vectors either consist of natural vectors (plasmid DNA or small nucleic acids, antisense oligonucleotides, small interfering RNAs (siRNA), microRNA (miRNA)) or synthetic vectors composed of lipid complexes, and polymers (Dizaj, Jafari et al. 2014). Synthetic vectors are usually easier to synthesize than viral vectors, tend to have lower immunogenicity than viral vectors, and have the potential to deliver larger genetic payloads than viral vectors (Yin 2014).

Delivery of naked natural vectors often results in lower transformation efficiency due to the negative charge nucleic acids and negative cell membrane charges (Dizaj, Jafari et al. 2014). Physical (electroporation) and chemical (liposomes) transfection agents have been utilized to enhance transformation efficiency *in vitro* (Dizaj, Jafari et al. 2014). However, these methods cannot be utilized when trying to deliver therapeutic cargo in a clinical *in vivo* setting.

*In vivo* delivery of natural therapeutic cargo needs to overcome several barriers before it can elicit a response. Naked genetic cargo risks potential degradation by endonucleases in physiological fluids and extracellular spaces. It has been shown that the half-life of plasmid DNA is 10 mins following intravenous injection into mice (Dizaj, Jafari et al. 2014). Therefore, for successful delivery of the therapeutic gene to target cells *in vivo*, the genetic material must be protected or entrapped in a synthetic carrier. First, the cargo loaded synthetic carrier will enter the bloodstream and it must protect the genetic cargo from degradation by endonuclease and evade immune detection and avoid renal clearance (Yin 2014). Second, the synthetic carrier must be able to exit the bloodstream, identify and reach its target cell (Yin 2014). This step is

crucial for delivery. Finally, the synthetic carrier must be able to enter the target cells through endocytosis and escape from the endosome to deliver its cargo to the cytoplasm or nucleus of the target cell (Yin 2014). Synthetic carriers that are easy to generate, provide safety, are compact enough to enter target cells, and can induce a controlled release of their cargo, are viable options for clinical use.

To target HSPCs, we must develop or utilize a delivery system that both targets HSPCs *in vivo* and enables HSPCs to take up the cargo thus leading to a strong phenotype. One way of targeting HSPCs *in vivo* is by using key components of “systems” (cells or cell parts or vesicles) that we already know interact with HSPCs.

### **1.3 Megakaryocyte-derived Microparticles (MkMPs) Target and Interact with HSPCs**

HSCs can differentiate into any blood lineage cells. Megakaryocytes (Mks) are HSC-derived, polyploid myeloid cells that upon fragmentation give rise to circulating platelets, which are responsible for vascular repair and hemostasis, stopping of blood flow at a site of injury by inducing blood coagulation. Mks are the largest (50-100 $\mu$ m) and rarest cells residing in the bone marrow; accounting for 0.01% of nucleated bone marrow cells (Machlus and Italiano 2013). During their maturation, under the influence of thrombopoietin (TPO), an HSC will undergo megakaryopoiesis to differentiate into an Mk. TPO will bind to the Mk specific receptor c-Mpl allowing the Mk to undergo endomitosis that allows Mks to become polyploid through cycles of DNA replication without cell division (Patel 2005, Machlus and Italiano 2013). Through endomitosis, Mks accumulate DNA content of 4N, 8N, 32N, 64N, and 128N in a single polylobulated nucleus (Machlus and Italiano 2013). During this time, the Mks increase in size, become full of platelet-specific granules, and develop an

invaginated membrane system (Machlus and Italiano 2013). Mature Mks migrate to the endothelial lining of blood-marrow sinusoids where they extend long branches called proplatelets through gaps of the endothelium into circulating blood (Machlus and Italiano 2013, Jiang, Woulfe et al. 2014). As the proplatelets extend into circulation, shear forces and fission cause the proplatelet to separate from Mks, and the proplatelet fragments will then mature into platelets in circulation (Machlus and Italiano 2013, Jiang, Woulfe et al. 2014).

In addition to producing platelets, Mks also shed small vesicles called microparticles (MPs). MPs are submicron vesicles (0.1 to 1 $\mu$ m in diameter) budding off the plasma membrane of mammalian cells (Jiang 2017). They possess distinct biological properties and participate in intercellular communication in various physiological processes such as coagulation, inflammation, tumorigenesis, and differentiation (Jiang 2017). MPs derived from platelets were previously thought to be the most abundant type of MPs circulating blood (Flaumenhaft, Dilks et al. 2009). At the time, it was found that 70 to 90% of circulating MPs in the bloodstream expressed cluster of differentiation (CD) marker CD41. Mature Mks express CD41 and since platelets are derived from Mks they also express CD41. Platelets also express platelet activation markers CD62P and LAMP1<sup>-</sup> (Flaumenhaft, Dilks et al. 2009). When MPs were isolated from mouse and human circulating blood plasma it was found that the majority of the MPs were CD41<sup>+</sup> and CD62P<sup>-</sup> (Flaumenhaft, Dilks et al. 2009). This finding suggested that these MPs did not express platelet activation markers and therefore, were not derived from platelets but were actually derived from Mks (Flaumenhaft, Dilks et al. 2009). Similarly, Jiang et al found that Mks differentiated *in*

*vitro*, produced MPs that were CD41<sup>+</sup> and CD62P<sup>-</sup> (Flaumenhaft, Dilks et al. 2009), confirming that most of the MPs are derived from Mks not platelets.

Mks produce MPs through continuous blebbing off the Mk plasma membrane, whereby MkMPs form “as beads along the length of slender, unbranched micropodia” (Flaumenhaft, Dilks et al. 2009). When Mks were exposed to increased shear forces *in vitro*, MkMP production increased by 30-to 40- fold (Jiang, Woulfe et al. 2014), suggesting that, *in vivo*, when Mks enter the bone marrow sinusoids and are exposed to shear forces, numerous MkMPs are likely generated (Jiang, Woulfe et al. 2014). To determine a potential physiological function, MkMPs were co-cultured with HSPCs and it was found that MkMPs promoted survival and Mk differentiation of HSPCs in the absence of TPO (Jiang, Woulfe et al. 2014). MPs naturally carry membrane and cytosolic proteins, mRNA, and miRNAs and upon interacting with their target hosts they can deliver these endogenous cargo to the target cell (Dragovic, Gardiner et al. 2011, Jiang 2017). Interaction with the target cell is initiated and mediated by ligand receptor binding, leading to uptake of the MPs through endocytosis or membrane fusion (Jiang 2017). Upon intake, the MP will deliver its cargo to HSPCs thus altering the fate of the target cell. As previously shown, MkMPs target HSPCs and enhance Mk differentiation as demonstrated by increased Mk polyploidization (2N, 4N, 8N, etc.) (Jiang, Woulfe et al. 2014, Jiang 2017). To test their specificity, MkMPs were also co-cultured with mesenchymal stem cells (MSCs), human umbilical vein endothelial cells (HUVECs) and granulocytes (myeloid white cells), which are ontologically and physiologically related to HSPCs and, *in vivo*, are in contact with HSPCs (Jiang 2017). MkMPs could not transdifferentiate these cells possibly because these cells were not capable of taking up MkMPs or because they lacked the specific

signaling molecules to transdifferentiate (Jiang 2017). These findings suggest that MkMPs specifically target and deliver cargo to HSPCs that promotes their differentiation towards Mks in the absence of TPO. Uptake of MkMPs by HSPCs occurred after 3-5hrs (Jiang 2017). Scanning and Transmission Electron microscopy images revealed that the MkMPs were fusing with the membrane of the HSPCs, while blocking uptake through endocytic inhibitors revealed that, in addition to membrane fusion, MkMPs may be taken up by HSPCs through endocytic processes involving macropinocytosis and lipid rafts (Jiang 2017). Furthermore, it was shown that the MkMPs interact at the uropod region of the HSPCs and blocking of surface proteins CD54, CD11b and CD18 reduced uptake of MkMPs, thus suggesting that CD54 and CD11b/CD18 (Mac-1) pair MkMPs with HSPCs (Jiang 2017).

MPs deliver proteins, mRNA, microRNAs, or phospholipids (endogenous cargo) to target cells (Jiang 2017). To better understand the endogenous cargo MkMPs are delivering, MkMPs were treated with RNases to reduce their RNA content. When RNase-treated MkMPs were delivered to the HSPCs *in vitro*, the ploidy, or chromosome number, of Mks decreased by 50% compared to control, suggesting that MkMPs are delivering RNA to HSPCs, and that uptake of MkMPs by the HSPCs is necessary to transfer the RNA (Jiang 2017).

As it was demonstrated that MkMPs target HSPCs *in vitro*, the next question to address and test was if MkMPs target HSCs *ex vivo*. Murine HSCs were extracted from murine bone marrow and were co-cultured with human MkMPs and the human MkMPs interacted with the murine HSCs inducing megakaryocytic differentiation (Escobar 2017). *Ex vivo* interaction of murine HSCs and human MkMPs led us to examine if human MkMPs can be a delivery method/treatment for *in vivo* platelet

biogenesis in mice (Escobar 2017). Human MkMPs were intravenously injected into wild-type mice, and it was shown that murine platelet production increased significantly compared to mice who received an injection of saline (Escobar 2017). Next, mice were treated with anti-CD41 antibody to induce thrombocytopenia, i.e. to decrease their platelet levels. Upon injection of human MkMPs, platelet levels in thrombocytopenic mice increased compared to thrombocytopenic mice who did not receive human MkMPs (Escobar 2017). Furthermore, the fraction of reticulated (newly synthesized) murine platelets increased upon injection of human MkMPs, thus suggesting that the MkMPs are targeting the HSCs naturally found in the bone marrow or in circulation, thus inducing them to differentiate into Mks, which produce platelets (Escobar 2017). Human platelet transfusions are costly and the amount of platelets needed to be effective is high (one effective transfusion has  $\sim 1-5 \times 10^{11}$  platelets) and platelets have such a short lifespan ( $\sim 10^{11}$  platelets are made in the body every day and only last for 7-10 days) that transfusions are needed often (Machlus and Italiano 2013). Therefore, if enough MkMPs are derived from human HSPCs *in vitro*, direct injection of MkMPs into the bloodstream may be a substitute treatment for patients suffering from low platelet count due to pregnancy, chemotherapy, or genetic disorders.

A study to test the biodistribution of MkMPs into the murine system is currently underway. From this study, we expect to learn if the MkMPs are targeting the bone marrow, by injecting the mice with fluorescently labeled MkMPs and collecting their organs (heart, brain, liver, kidney, spleen, blood, and bone marrow) and analyzing them for fluorescence intensity. As MkMPs target HSCs we expect to see a high fluorescence intensity in the bone marrow suggesting that the injected

MkMPs cleared the innate immune system and entered the bone marrow to interact with HSCs.

To sum, these data demonstrated that MkMPs target and interact with HSPCs both *in vitro* and *in vivo*. The MkMPs' ability to interact with HSCs can be utilized for cargo delivery for gene therapy or engineering them to carry exogeneous molecules for delivery to HSPCs (Jiang 2017). Transfer of genetic cargo through MPs is now under investigation in the Papoutsakis lab. At the moment, loading of MPs or exosomes with exogenous cargo seems to be difficult. Further experiments and optimization are under way to determine the optimal voltage for loading the exogenous cargo via electroporation. In addition, both MPs and exosomes themselves carry largely unknown mixture of endogenous proteins and nucleic acids that is transferred together with the desired cargo (Diener, Bosio et al. 2016). Their ability to be loaded, deliver cargo, and their impact on target cells still needs to be understood. Meanwhile, nanoparticles may provide a synthetic tool to utilize in the protection and delivery of exogenous cargo.

#### **1.4 PLGA NPs are Capable of Encapsulating Genetic Cargo**

Nanoparticles (NPs) are small, spherical structures around 100 nm in size (Danhier, Ansorena et al. 2012). They can be made of synthetic or natural polymers. The versatility of NPs is attractive because they can be engineered to be at a desirable size, have prolonged circulation time, have hydrophobic/hydrophilic properties, increased drug encapsulation, and controlled drug release (Luk and Zhang 2015). NPs can also be made using biocompatible and biodegradable materials. Poly-lactic-co-glycolic acid (PLGA) NPs are widely used since the breakdown of the polymer leads to lactic- and glycolic-acid formation, which are recognized by the body and are easily

metabolized by the Krebs Cycle (Danhier, Ansorena et al. 2012). The minimal toxicity associated with PLGA has led the FDA to approve PLGA for drug delivery applications in humans (Danhier, Ansorena et al. 2012). These carriers are composed of natural biomaterials and are small enough to be internalized by cells and enter the nucleus passing through the cytoplasm and escaping the endosome/lysosome process following endocytosis (Dizaj, Jafari et al. 2014).

In addition to drug delivery, PLGA NPs are also being explored as gene vectors due PLGA's ability to encapsulate DNA/RNA (Chen, Guo et al. 2016). PLGA protects nucleic acids from endonuclease degradation *in vivo*, thus increasing the NP's circulation time and avoiding clearance by the innate immune system (Yin 2014). The promising features of NPs as genetic carriers have led several researchers to test the NP's ability to deliver genetic cargo to HSPCs.

Many studies have relied on delivering oligonucleotides to human HSPCs through electroporation, nucleofection, or microinjection, but these methods can be toxic to the cells and cannot be used *in vivo* (McNeer, Chin et al. 2011). Researchers are now using PLGA NPs to encapsulate nucleic acids. McNeer and colleagues used biodegradable PLGA NPs to encapsulate triplex-forming peptide nucleic acids (PNA) and DNA and delivered these NPs to CD34<sup>+</sup> HSPCs (McNeer, Chin et al. 2011). The goal of the study was to see if delivery via NPs (a safe, biodegradable system) performed as well as delivery of the PNA/DNA through nucleofection (a system that often produces cytotoxicity). When exposed to the PNA/DNA loaded NPs, cell viability and CD34<sup>+</sup> expression in the NP-treated HSPCs was "nearly identical" to untreated cells (McNeer, Chin et al. 2011). Cell survival was substantially lower and CD34<sup>+</sup> expression decreased in HSPCs treated through the nucleofection process

(McNeer, Chin et al. 2011). NP treatment led to much higher rates of recombination (0.2% modification frequencies) compared to nucleofection (0.05% modification frequencies) (Yin 2014). Although successful, the gene modification frequencies observed by McNeer is low compared to the suggested frequency of 10-15% required in HSPCs for treatment of clinical hemoglobinopathies (McNeer, Schleifman et al. 2011).

In a study similar to McNeer's, Diener and colleagues explored delivery methods to HSPCs by delivering siRNA via chemical transfection, electroporation, and PLGA NPs (Diener 2015). CD45, a blood cell marker expressed on all hematopoietic cells (including HSPCs) except for mature erythrocytes, was chosen as the target protein and CD45-siRNA was encapsulated in PLGA NPs through double emulsion (Diener 2015). In a proof-of-principle study, Diener showed that the CD45-siRNA NPs cultured with monocytes decreased CD45 expression, showing that the NPs encapsulated the siRNA and released the siCD45, knocking down expression. However, when the siCD45 NPs were delivered to HSPCs, CD45 expression levels were not affected (Diener 2015). Diener concluded that although the HSPCs internalized the siRNA-NPs, the uptake was not efficient enough to induce CD45 knockdown (Diener 2015). Although both groups had low delivery yields, these two reports demonstrated that genetic cargo can be encapsulated by PLGA NPs and delivered to HSPCs.

*Ex vivo* therapies on HSPCs provide immediate clinical applications, but *in vivo* genome editing eliminates the need to extract and manipulate HSPCs *ex vivo* (McNeer, Schleifman et al. 2011). Multiple treatments with PLGA NPs could be used to increase gene modification frequencies *in vivo* while eliminating any *ex vivo*

handling of HSPCs (McNeer, Schleifman et al. 2011). However, for successful delivery of genetic materials, the NPs need to have effective cellular internalization (Chen 2016). The challenge now becomes about increasing target specificity so that NPs can directly interact with HSPCs *in vivo* at a higher efficiency thus increasing internalization and their rate of delivery. The delivery of genetic cargo via NPs *in vivo* has been hampered by the lack of targeting ability of the NPs and the inability of the genetic cargo to escape from the endosome (Chen 2016). Fortunately, the surface of PLGA can be easily modified to enhance specific targeting.

### **1.5 PLGA NPs can be Decorated with Cell Membrane for Targeted Delivery**

The challenges of selective accumulation at the target cell of interest, cellular internalization and endosomal escape can be addressed by “decorating” the NP carrier (Yin 2014). The surface of NPs can be decorated with targeting ligands, peptides, antigens, antibodies, and lipids, thus allowing for more specific targeting (Luk and Zhang 2015). New engineering strategies have emerged that combine synthetic NPs with natural biomaterials to create a nature-inspired biomimetic delivery system (Luk and Zhang 2015). Cell membranes are composed of phospholipids and embedded with functional surface proteins that are crucial for their bio-functions (Zhai, Su et al. 2017). When the properties of a naturally occurring cell membrane are preserved and are coated onto a synthetic NP surface, a bio-hybrid system is created (Luk and Zhang 2015). The membrane-wrapped NPs possess the “tunable physiochemical properties” of synthetic NPs as well as the “complex functions” of the host cell membrane (Luk and Zhang 2015).

The first evidence of a cell-membrane coated NP was created by the Zhang group using membranes derived from red blood cells (RBCs) by a hypotonic treatment

and coating the membranes onto negatively charged PLGA NPs by extrusion (Hu, Zhang et al. 2011, Kroll, Fang et al. 2017). Cell membranes from RBCs are easily derived, while membranes from nucleated cells require more physical force (Zhai, Su et al. 2017). Membranes from nucleated cells are physically disrupted and collected by separating the plasma membrane from the nuclear and mitochondrial components through sucrose gradient or differential centrifugation (Kroll, Fang et al. 2017). The NPs are coated with membranes by either extrusion (physically forcing the membrane to interact with the NPs through tiny pores) or through sonication. The coating results from the asymmetric charge of the cell membrane causing them to coat the NP cores to minimize charge repulsion (Luk, Hu et al. 2014, Kroll, Fang et al. 2017). Both methods of wrapping were found to fully coat the NPs and retain cell surface proteins in a right-side-out-manner (Luk, Hu et al. 2014, Kroll, Fang et al. 2017). The translocation of many membrane proteins, glycans, and lipids to the surface of the nanoparticles makes them excellent vehicles for drug delivery, detoxification, and gene therapies (Kroll, Fang et al. 2017). When RBC membrane-wrapped NPs were delivered *in vivo* they have remained stable under shear-stress conditions, had long circulation times, interacted with target cells through specialized markers, or recognized and penetrated tumors (Kroll, Fang et al. 2017). It was also found that, compared to bare NPs, platelet-wrapped NPs showed a reduction in macrophage consumption suggesting that the membrane cloak disguises the NP from the innate immune system (Hu, Zhang et al. 2011).

## **1.6 NPs can Escape Endosomes**

Once the NPs are constructed and characterized, they are brought in contact with their presumed target cells. NPs acquire different physiochemical properties in

biological fluids (Verma and Stellacci 2010, Behzadi 2017). Once bare NPs enter a biological fluid such as cell culture media or blood, it begins to absorb any biomolecules within the fluid and its surface is altered (Behzadi 2017). The cells now “see” this surface-covered NP and recognize that layer of coverage as the biological identity of the NPs (Behzadi 2017) and not the pure bare NP. The biological identity of the NP is affected by its size, shape, surface charge, the biological fluids present, and experimental factors like temperature, and osmolarity (Behzadi 2017). The microenvironment surrounding the target cell (extracellular matrix, pH, among others) also affects how well the NP will interact with the target cell (Behzadi 2017). Therefore, when designing the NPs and coating the NPs all these factors must be taken into consideration for ideal targeting and delivery.

Once the NPs reach the exterior membrane of the target cell they can interact with the membrane-receptors, extracellular matrix, and enter the cell through endocytosis (Chou 2011, Behzadi 2017). Again, the physical properties of the NPs (size, shape, surface charge and coating) and cell type and cellular environment influence how the NP will be taken into the cell and the down-stream response of the cell (Kuhn, Vanhecke et al. 2014). There are 5 different endocytic pathways that will be discussed in this study. Phagocytosis involves the engulfment of large particles, such as microorganisms and cell debris (Kuhn, Vanhecke et al. 2014). Pinocytosis involves the fluid uptake of particles and is composed of macropinocytosis, clathrin-mediated endocytosis, caveolae-mediated endocytosis, and clathrin- and caveolin-independent endocytosis (Kuhn, Vanhecke et al. 2014). Macropinocytosis acts by using actin to make the outer membrane of the cell “ruffle” or form protrusions and capture particles floating nearby (Verma and Stellacci 2010, Kuhn, Vanhecke et al.

2014). Clathrin-mediated endocytosis is a form of receptor-mediated endocytosis that utilizes the protein clathrin that collects at the site of internalization and clathrin-coated pits are formed as the membrane invaginates (Behzadi 2017). Caveolin-mediated endocytosis involves the protein caveolin that form flask-shaped membrane invaginations (Kuhn, Vanhecke et al. 2014, Behzadi 2017). Clathrin- and caveolae-independent endocytosis take place in areas on the membrane with higher lipid content without clathrin or caveolae (Behzadi 2017).

Surface charges of NPs also determine how the NP will interact with the cell and effect their uptake. Positively charged NPs seem to experience a higher extent of internalization due to interacting with negatively charged cell membranes (Danhier, Ansorena et al. 2012). There has been evidence of internalization of negatively charged NPs despite the NPs interacting with a mostly negatively charged cell membrane (Verma and Stellacci 2010). It is believed that the negatively charged NPs cluster at cationic sites on the plasma membrane and then endocytosed (Verma and Stellacci 2010).

The pathway through which NPs enter the cell also dictates how the NP and its cargo will escape the vesicle once internalized. PLGA NPs are internalized through fluid pinocytosis and clathrin-mediated endocytosis (Danhier, Ansorena et al. 2012). Once internalized, PLGA NPs rapidly escape the endo-lysosome and enter the cytoplasm within 10mins of incubation (Danhier, Ansorena et al. 2012). To escape the endo-lysosome, the PLGA NPs interact with the endo-lysosome due to selective reversal of the surface charge of the PLGA (from anionic to cationic) under acidic conditions (Paulo, Pires das Neves et al. 2011).

Therefore, the size, charge, and surface coverings of the NPs and interaction with its target cell is crucial for delivery. To overcome the barriers preventing NPs from associated with and internalized by their target cells, a natural cell membrane should be utilized. The cell membrane will cloak the NPs, concealing them from the target cells. This will allow for easier recognition by the target cell and enhance uptake. However, it is not clear yet how the cellular membrane dissociates from the NP once inside the endosome to deliver its cargo. It would be interesting to compare the endocytic pathways between the membrane wrapped NPs and bare NPs.

### **1.7 Mk-membrane Wrapped NPs (MkNPs) would Target and Interact with HSPCs**

As we have previously shown that MkMPs interact with HSPCs *in vitro*, *ex vivo*, and *in vivo*, we believed the next step is to use membranes isolated from MkMPs or Mks to wrap genetic cargo loaded-PLGA NPs. We hypothesized that wrapping the NPs with membranes from MkMPs would enhance targeting towards HSPCs *in vivo*, allowing the HSPCs to uptake the wrapped NPs and deliver genetic cargo. Our proposed plan was to isolate Day 12 (D12) MkMPs differentiated from human CD34<sup>+</sup> primary HSPCs. The MkMPs would be washed and MkMP-membrane vesicles would be generated by physical disruption of the cells and differential centrifugation. The membrane vesicles would fuse to cargo loaded PLGA NPs through extrusion or sonication. Membrane-wrapped cargo loaded NPs would be delivered HSPCs both *in vitro* and *in vivo*.

Our first aim was to synthesize BioNPs comprised of MkMP and/or Mk membranes surrounding spherical PLGA NP cores. MP production from Mks has a low MP productivity, and the MPs are very small (0.1 to 1 $\mu$ m in diameter), producing

only small amounts of membranes from MkMPs. The amount of membrane required to coat the NPs would not be enough. Therefore, we used membranes from Mks as they are larger and more abundant (Figure 1). Since MkMPs have all the same attributes (cellular components and markers) as their parent cell, Mk, the membrane derived from an Mk should suffice as a substitute.

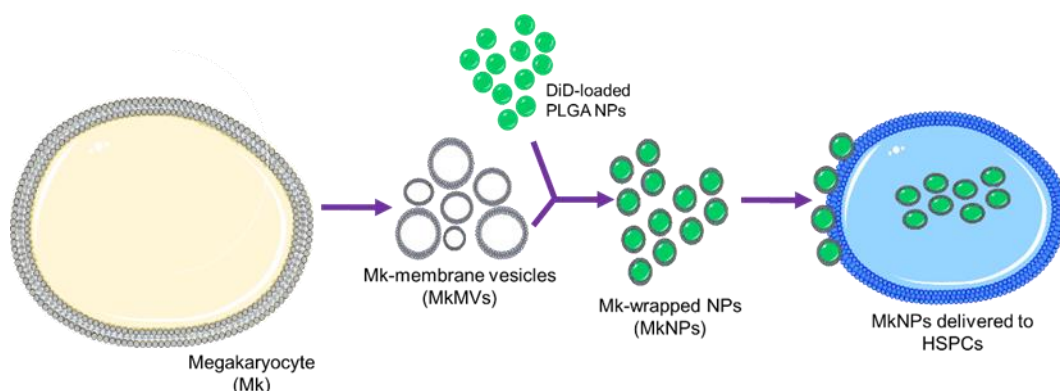


Figure 1. Scheme of Mk-wrapped PLGA NPs targeting HSPCs *in vitro*. Mk-membrane vesicles (MkMVs) will be derived from Megakaryocytes (Mks). The MkMVs will wrap around PLGA NPs to create Mk-membrane wrapped NPs (MkNPs), which target HSPCs.

Once we synthesized our coated MkNPs, we characterized them using Dynamic Light Scattering (DLS), Transmission Light Microscopy (TEM), flow cytometry, and Nanoparticle Tracking Analysis (NTA) and confirmed wrapping so that we could better understand their targeting mechanism.

Our second aim was to examine the mechanism by which our Mk-wrapped NPs interacted with and entered HSPCs *in vitro*. This aim involved using confocal and super-resolution microscopy to visualize interaction and uptake, as well as using

endocytic inhibitors to better understand the mechanism by which MKNPs interact and enter HSPCs.

## Chapter 2

### MEMBRANE COLLECTION, NANOPARTICLE WRAPPING, AND CHARACTERIZATION

#### 2.1 Background

As previously shown, MkMPs target and induce Mk differentiation in CD34<sup>+</sup> HSPCs (Jiang, Woulfe et al. 2014, Jiang 2017). MkMPs target CD34<sup>+</sup> HSPCs through a receptor mediated process that allows the MPs to directly fuse with the target HSPCs' membranes resulting in uptake by HSPCs (Jiang 2017). Utilizing the natural ability of the MkMPs to specifically target HSPCs may be the key to delivering genetic cargo to HSPCs *in vitro* and *in vivo*. Cell membranes extracted from Mks or MkMPs can be used to decorate PLGA NPs loaded with genetic cargo. During the membrane extraction process the natural composition of the Mk/MkMP membrane is preserved so the membrane vesicles will still be able to offer their unique HSPC targeting specificity and provide innate immunity. Using the extracted membrane for target specificity and PLGA NPs ability to protect genetic cargo, the cargo will be delivered safely to HSPCs.

#### 2.2 Materials and Methods

##### 2.2.1 Culture of CHRF-288-11 Cell Line

CHRF cells (CHRF-288-11, provided by Dr. R. Smith of NIH, Bethesda, MD) (Fuhrken, Chen et al. 2007) treated with phorbol 13-myristate12-acetate (PMA, Sigma Aldrich) were maintained in Iscove's Modified Dulbecco's Medium (IMDM, Sigma

I7633) supplemented with 0.1% Fetal Bovine Serum (FBS, Sigma), Sodium Bicarbonate (Sigma S6014) and Antibiotic-Antimycotic (Anti-Anti, Thermo Fisher). Cells were incubated for 3 days in 5% CO<sub>2</sub>, 20% O<sub>2</sub>, 95% relative-humidity, and 37°C. On Day 3, adherent and non-adherent cells were collected, and membranes were isolated.

### **2.2.2 Culture of Human Hematopoietic Stem Cells to Mature Megakaryocytes**

Frozen human G-SCF-mobilized peripheral blood CD34<sup>+</sup> cells (purchased from Fred Hutchinson Cancer Research Center) were cultured as previously described (Panuganti, Schlinker et al. 2013). Cells were thawed and plated for five days in IMDM supplemented with 20% Bovine Serum Albumin, Insulin, and Transferrin (BIT) (StemCell Technologies, Canada 09500), and 1% Anti-Anti with 2.5ng/mL recombinant human interleukin (rhIL)-3 (Perprotech Inc. 200-03), 10 ng/mL of rhIL-6, rhIL-11 (Perprotech Inc. 200-06, 200-11), 100 ng/mL recombinant human Thrombopoietin (rhTPO) (Perprotech Inc. 300-18), 100ng/mL of recombinant human stem cell factor (rhSCF) (Perprotech Inc. 300-07) and 1µg/mL of low density lipoprotein from human plasma (hLDL) (Sigma-Aldrich L7914). Cells were incubated at 5% CO<sub>2</sub>, 5% O<sub>2</sub>, 95% relative humidity, 37°C. On Day 5, the cell-culture suspension was collected and centrifuged at 300x g for 10 mins to collect cells for re-suspension in new media. For Days 5-7, the culture media of the cells is comprised of IMDM, 20% BIT, 1% Anti-Anti, 100ng/mL rhTPO and rhSCF, 10ng/mL rhIL-3, rhIL-9, and rhIL-11, and 1µg/mL of hLDL. The culture was incubated in 5% CO<sub>2</sub>, 20% O<sub>2</sub>, 95% relative humidity, and 37°C.

On Day 7, dead cell removal and CD41<sup>+</sup> enrichment was performed. The cell culture was spun down at 300xg for 10mins. Supernatant was removed, and cells were

resuspended in Dead Cell Removal Beads (Miltenyi 130-090-101) to remove dead cells. For every  $10^7$  cells, 100 $\mu$ L of Dead Cell removal microbeads were added and the solution incubated at room temperature for 15mins. After 15mins, 500 $\mu$ L of 1x Binding Buffer (Miltenyi) was added to the solution and the solution was passed through an MS column (Miltenyi 130-042-201) setup utilizing the MACs system and the manufacturer's protocol. Dead cells were collected in the magnetic column and any live cells were collected in a 15mL conical tube. The column was washed three times with 500 $\mu$ L 1X Binding Buffer to elute out any remaining live cells. After collection, 7mL of PEB buffer (PBS+5% BSA + 2mM EDTA) was added to the live cells and the suspension was centrifuged at 300xg for 10mins. Supernatant was discarded, and cells were resuspended in PEB and CD61 microbeads (Miltenyi 130-051-101). For every  $10^7$  cells, 20 $\mu$ L of CD61 microbeads and 80 $\mu$ L of PEB were added. The suspension was incubated at 4°C for 15mins. After incubation, 10mL of PEB was added and the suspension was centrifuged at 300xg for 10mins. The cell suspension was resuspended in 500 $\mu$ L PEB and passed through an LD column (Miltenyi 130-042-901). CD61<sup>+</sup> cells were captured in the column and then released from the column by removing the column from the MACs setup and passing 3mL PEB through the column. Finally, 7mL of IMDM was added to the CD61<sup>+</sup> cells and the cells were centrifuged at 300xg for 10mins. After enrichment, CD41<sup>+</sup> cells were cultured in IMDM, 20% BIT, 1% Anti-Anti, 100ng/mL rhTPO and rhSCF, 6.25 mM nicotinamide, 1 $\mu$ g/mL LDL and incubated in 5% CO<sub>2</sub>, 20% O<sub>2</sub>, 95% relative-humidity, and 37°C. On Day 12, the cell suspension was collected, and membranes were isolated.

### **2.2.3 Preparation of PMA-CHRF or Mk Membranes**

To harvest membranes, PMA-CHRF cells were collected on Day 3 and detached from flask using Accutase (Thermo Fisher Scientific). Both adherent and non-adherent PMA-CHRF cells were collected and utilized in membrane extraction. Mature Mk cells were collected on Day 12.

Membrane collection from both cell types underwent the following membrane extraction procedure: Cells were collected and washed with 1X Phosphate buffered saline (PBS, Corning) by centrifuge at 400x *g* for 5mins. Whole cell membranes were dyed with PKH26 (PKH26 Red Fluorescent Cell Linker Kit for General Cell Membrane Labeling-Sigma). Briefly, 8 $\mu$ l of PKH26 is added 1mL of Dil C (PKH26 Red Fluorescent Cell Linker Kit for General Cell Membrane Labeling-Sigma) and the dye-mixture is added to the cells that have already been suspended in 1mL Dil C. Cells were suspended in the dye mixture for 5mins following the manufacturer's protocol. Dyeing is quenched by adding 4mL 1% BSA. Cells were centrifuged at 400x *g* for 10mins followed by washing twice with 1X PBS. After washing, cells were suspended in a hypotonic lysis buffer consisting of 20 mM Tris HCl, 10mM KCl, 2mM MgCl<sub>2</sub> and protease inhibitor (p8340, Sigma) per 5mL of solution, and disrupted using a Dounce homogenizer with a tight-fitting pestle (Kimble) (Fang, Hu et al. 2014). The entire solution was subjected to 20 passes before spinning down at 3,200x *g* for 5mins at 4°C (Fang, Hu et al. 2014). The supernatant was saved while the pellet was resuspended in hypotonic lysing buffer and subjected to another 20 passes and spun down again. The supernatants were collected and spun down at 18,000rpm (20,000x *g*) for 20mins at 4°C, after which the pellet was discarded, and supernatant was centrifuged at 40,000rpm (100,000x *g*) for 50mins at 4°C (Fang, Hu et al. 2014).

Supernatant was discarded, and pelleted cell membranes were resuspended in 100 $\mu$ L of Biology Grade Molecular Water (Corning).

#### **2.2.4 PLGA NP Preparation**

Nanoparticles were generated by Jenna Harris of Dr. Emily Day's lab and were provided to us for use by Erica Winter in this collaborative project. Briefly, poly (lactic-co-glycolic acid) (PLGA, B6013-2, Lactel) is dissolved in acetone, and mixed with DiD fluorescent dye (D7757, Fisher). The mixture is added dropwise to H<sub>2</sub>O and stirred for 2hrs to evaporate the acetone. After 2hrs., the mixture was centrifuged in 10kDa MWCO filters (Amicon, EMD Millipore™ UFC801096). at 4200rpm for 30mins. Filtered sample is resuspended in 2mL H<sub>2</sub>O and centrifuged at 4200rpm for 30mins. Collected NPs were analyzed by Dynamic Light Scattering (DLS) and found to be approximately 60nm-120nm in size.

#### **2.2.5 PMA-CHRF and Mk-membrane Wrapped NP Synthesis**

To prepare empty PMA-CHRF or MkMVs, membranes, derived as described above, were physically extruded through 400nm polycarbonate membrane for 11 passes (Avanti Mini Extruder) (Fang, Hu et al. 2014). The vesicles were then coated onto PLGA NPs by co-extruding vesicles and NPs through 400nm polycarbonate membrane for 7 passes.

#### **2.2.6 Transmission Electron Microscopy (TEM)**

Transmission electron microscopy (TEM) imaging was carried out by glow discharging carbon-coated 400 square mesh copper grids. 20 $\mu$ l of sample was placed in 72-well plate (Nunc) and the grids were dipped into the wells containing 20 $\mu$ l of sample and then dipped into 20 $\mu$ l H<sub>2</sub>O four times. Finally, the grids were negatively

stained with 1% Phosphotungstate (PTA) or 2% uranyl acetate, dried, and visualized using Carl Zeiss Libra 120.

### **2.2.7 Nanoparticle Tracking Analysis (NTA)**

To determine the size and concentration of our bare NPs, empty Mk membranes, and MkNPs, samples were analyzed using the Nano Sight NS300 instrument (Malvern). Each sample was diluted in 700 $\mu$ L Molecular Biology-grade Water to an optimal concentration of  $1 \times 10^8$  to  $1 \times 10^9$  particles per milliliter or 30-80 particles per frame. Samples were mixed before introduction into the sample chamber and a video recording, typically 1 minute, initiated (Dragovic, Gardiner et al. 2011). Three technical replicates for each sample were analyzed. NTA post-acquisition settings were optimized and kept constant between samples, and each video was then analyzed by the NTA software to give the mean, mode, and median particle size together with an estimate of the concentration (Dragovic, Gardiner et al. 2011). Eric Munoz of Dr. Matthew Hudson's lab analyzed all samples.

### **2.2.8 Wrapping Using NTA**

Once the size and the concentrations of the bare NPs and the membrane vesicles were determined via NTA, a wrapping ratio of NPs: membranes were chosen (See example in Table 1 in Sec. 2.3.2). Membranes were coated onto PLGA NPs by co-extruding MVs and NPs through the 400nm membrane pore for 7-11 passes.

After wrapping with extrusion, the sample was ultracentrifuged at 17,000rpm for 30mins at 4°C to pellet coated NPs and remove excess MVs (Fang, Hu et al. 2014). Pellet was resuspended in Molecular Biology Grade Water and a final NTA reading was taken to determine the size and concentration of the purified wrapped

sample. Swelling of bare NPs was induced by adding PBS to the sample and letting sit overnight. Swollen bare NPs were removed by filtering through at 0.22 $\mu$ m filter and sample was ultracentrifuged at 17,000rpm to remove excess MVs.

### **2.2.9 Streptavidin Bead Assay**

Approximately 1 $\mu$ L of Dynabeads MyOne Streptavidin T1 (Thermo Fisher) magnetic beads were washed and mixed with 2 $\mu$ L of biotin-conjugated CD41 antibodies (Thermo Fisher). MKNPs were gently rotated with the magnetic beads for a couple of hours at room temperature. Samples were washed four times using 0.1% BSA in PBS, following manufacturer's protocol and analyzed using flow cytometry (FACS Aria II, BD Biosciences). Beads 1 $\mu$ m in size were selected for and membrane dye, PKH26, was detected using the PE channel while NP dye, DiD, was detected using the APC channel. Gates displaying PKH26<sup>+</sup> were created to select for anything PKH26<sup>+</sup> and DiD<sup>+</sup>.

To determine the amount of CD41 present in the samples, 10 $\mu$ L FITC-conjugated CD41 antibodies (BD Biosciences) were added to the magnetic bead-Mk mem/bare NP/MkNP mixtures and rotated at room temperature for 2hrs. Fluorescence was detected using the FITC channel on flow cytometer. Paired student's t-test was used to determine statistical significance using Excel.

## **2.3 Results**

### **2.3.1 Confirmation of Membrane-wrapped NPs as Visualized Under TEM**

To create cell-membrane coated NPs, membranes from whole-intact cells must first be extracted. Cell membranes are bilayers composed of phospholipids and embedded with functional surface proteins, which are crucial for their bio-functions

(Zhai, Su et al. 2017). To preserve the functional contents of the membranes (i.e. membrane-functional proteins and membrane organization), the plasma membrane must be extracted as gently as possible (Zhai, Su et al. 2017). The extraction of plasma membrane was optimized by Hu et al in 2011 using membranes from red blood cells (RBCs)(Hu, Zhang et al. 2011). RBCs were isolated from whole blood and placed in a hypotonic treatment for hemolysis and placed in an ice bath for 20 mins (Hu, Zhang et al. 2011). The resulting RBC “ghosts” were sonicated for 5 mins and then extruded through a 400nm polycarbonate porous membrane using an Avanti mini extruder (Hu, Zhang et al. 2011). Initially, this process was used to extract membranes from the megakaryoblastic cell line CHRF-288-11. This cell line acts a strong model to study megakaryopoiesis, as it was shown that when treated with phorbol 13-myristate 12-acetate (PMA), the CHRF cells had a gene expression pattern similar to primary Mks and constitutively expressed Mk marker CD41 (Fuhrken, Chen et al. 2007). PMA-CHRFs become adherent to tissue-culture flask surface, have multilobate nuclei and extended proplatelet-like structures (Fuhrken, Chen et al. 2007). These PMA-treated cells also undergo endomitosis and show signs of polyploidization similar to primary Mks, further developing into mature Mks (Fuhrken, Chen et al. 2007). Since PMA-treated CHRF cells mimic Mk differentiation, they were used to optimize the cell membrane extraction process.

However, when the RBC membrane extraction process was used on PMA-CHRF cells, very few membranes were generated. Membranes from nucleus-free cells, such as RBCs, are easier to extract and require little to no mechanical force. As nucleated eukaryotic cells are biomechanically stronger, the extraction method is more complicated (Zhai, Su et al. 2017). A large quantity of nucleated eukaryotic cells

should be harvested from culture. Once harvested, the cells are lysed in hypotonic solution and disrupted through mechanical membrane destruction (i.e. Dounce homogenization). The disrupted cells are placed in a discontinuous sucrose gradient centrifugation or differential centrifugation to remove intracellular components. The plasma membrane is collected and further sonicated or extruded through porous polycarbonate membrane to create the nanosized membrane vesicles (Zhai, Su et al. 2017).

The megakaryoblastic cell line CHRF-288-11 was treated with PMA, and on Day 3 membranes were collected from  $2.3 \times 10^7$  cells and were subjected the extraction procedure. Briefly, PMA-CHRFs were placed in a hypotonic solution treatment and physically crushed through homogenization followed with the removal of intracellular components through differential centrifugation. Finally, PMA-CHRF membranes were extruded through 400nm polycarbonate pore to create membrane vesicles under 400nm in size (Supplementary Figure A1). The membrane vesicles were visualized using transmission electron microscopy (TEM) (Carl Zeiss Libra 120). TEM is considered one of the strongest tools to characterize wrapped NPs (Zhai, Su et al. 2017). Once wrapped, the cell membrane composed of lipids and proteins are usually of different electron density compared to the inner core of the NPs (Zhai, Su et al. 2017). Typical images of wrapped NPs show a white spherical core NP enveloped by light gray circles indicating that the core is covered by a cell membrane (Zhai, Su et al. 2017). Bare NPs show sharp contrasts against the background and empty MVs appear as hollowed out, collapsed shells (Zhai, Su et al. 2017).

PMA-CHRF MVs appeared shallow and collapsing with extracellular membrane components/debris sprinkled throughout the sample (Figure 2a).

Constructed empty 1mg/mL PLGA NPs (not loaded with dye or cargo) prepared from 5.2mg/ $\mu$ L PLGA were mixed with extruded PMA-CHRF MVs and sonicated for 2 mins (5 sec on/off) using a cup horn ultrasonic water bath (Qsonica) and visualized under TEM. The polymeric cores appear clear on TEM (Figure 2b) while the PMA-CHRF wrapped NPs have a “halo”, or a darker, secondary layer around the NP suggesting membrane wrapping (Figure 2c). The constructed bare NPs ranged between 50-90nm in size and the PMA-CHRF-wrapped NPs displayed a diameter of 90-120nm under TEM.

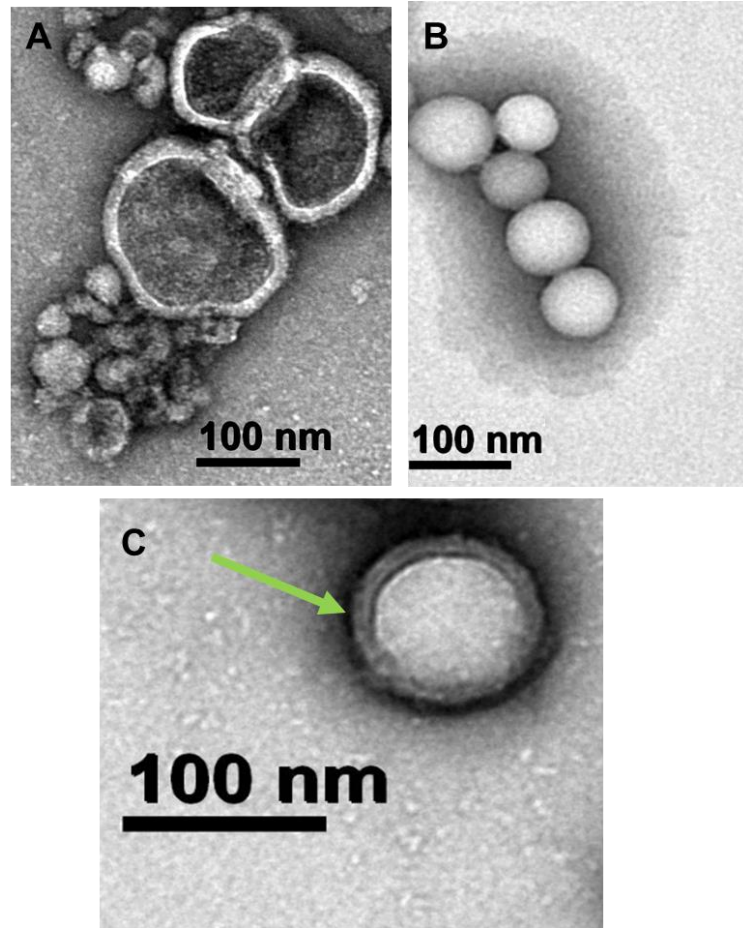


Figure 2. Morphology of PMA-CHRF-membrane-coated PLGA nanoparticles. (A) Day 3 extracted PMA-CHRF membranes. (B) Bare NPs. (C) PMA-CHRF wrapped NPs display the clear polymeric core surrounded by a “halo” or secondary layer suggesting membrane wrapping. Green arrow points to the membrane layer. All samples were placed on a 400nm Carbon coated grid and negatively stained with 1% Phosphotungstate (PTA) (sodium) (pH 7.2) and visualized with TEM.

As the membrane extraction protocol was optimized and wrapping was displayed, the focus of the study moved towards using MVs isolated from primary Mks. Human donor CD34<sup>+</sup> HSPCs were differentiated into Mks over the course of twelve days using interleukins (IL3, IL6, IL9, and IL11), Stem Cell Factor (SCF), and

thrombopoietin (TPO). Day 12 Mks were harvested and the membranes from  $3 \times 10^6$  cells were collected through the extraction process previously mentioned. A sample of MkMVs were visualized under TEM and empty shell-like structures, or vesicles, were displayed ranging in size from 25 to 300nm. (Figure 3).

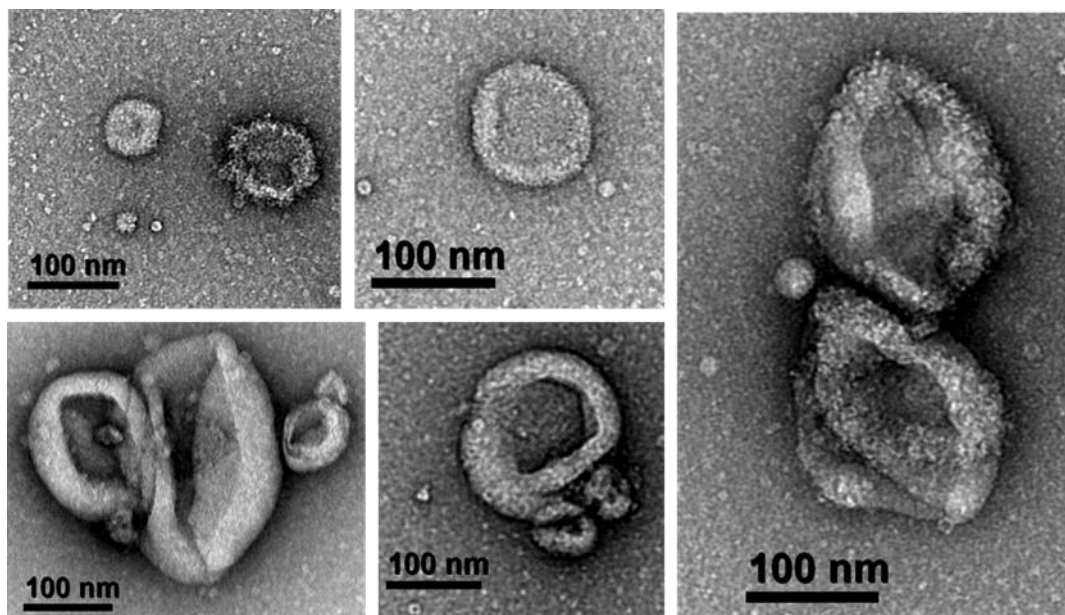


Figure 3. Mk membranes form vesicles post extrusion. Day 12 Mk cells ( $2.0 \times 10^7$  cells) were subjected to membrane extraction process and then extruded through 400nm pore membrane 11 times. Sample was placed on a 400nm Carbon coated grid and negatively stained with 1% Phosphotungstate (PTA) (sodium) (pH 7.2) and visualized with TEM

The extruded Mk vesicles were fused to 0.25mg/mL DiD-loaded PLGA NPs, roughly 112nm in size, through 400nm-pore membranes four times using the Avanti Mini Extruder. Again, the MkMVs appear shallow and collapsed (Figure 4a). The MkNPs display the “halo”, darker secondary layer suggesting the membrane has

wrapped the NP (Figure 4c). The size of the bare DiD-loaded NPs was 60-75 nm, while the Mk-membrane wrapped DiD-loaded NPs pictured are around 80nm and 100nm in diameter.

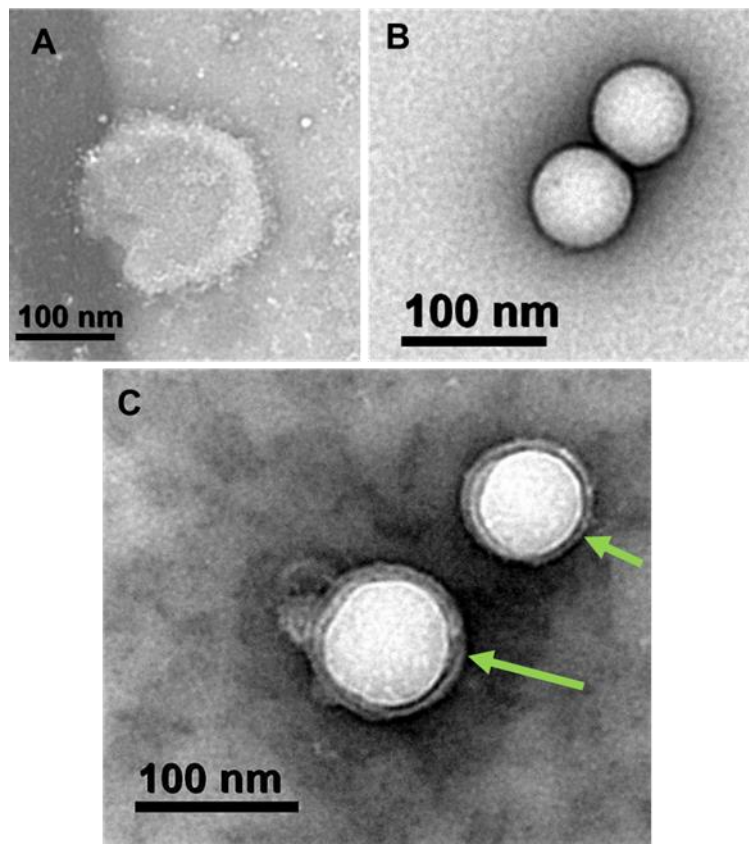


Figure 4. Morphology of Mk-membrane-coated PLGA nanoparticles. (A) Membranes generated from Day12 Mk cells from differentiated CD34<sup>+</sup> HSPCs. (B) Bare, DiD-loaded NPs were sonicated with Mk membrane vesicles resulting in (C) wrapped NPs. Wrapped NPs display the clear polymeric core surrounded by a “halo” or secondary layer suggesting membrane wrapping. A green arrow points to the membrane layer. All samples were placed on a 400nm Carbon coated grid and negatively stained with 1% PTA (sodium) (pH 7.2) and visualized with TEM.

Our bare and wrapped NP TEM images seem to display expected features. (Zhai, Su et al. 2017). Our spherical NPs have a sharp contrast with the background, our empty MVs both PMA-CHRF and Mk appear collapsed and shallow, and our wrapped NPs have a white core with a secondary layer surrounding it suggesting wrapping. Although we can visualize wrapping via TEM, it is hard to quantify the number of NPs in a sample and to accurately assess their size as fixation materials can cause the vesicles and NPs to shrink (Dragovic, Gardiner et al. 2011). To further quantify and confirm membrane wrapping, other tools are utilized; notably Nanoparticle Tracking Analysis (NTA) and Flow cytometry.

### **2.3.2 Confirming Wrapping by NTA**

Our TEM images of wrapped NPs show that the membrane layer surrounding the NPs has a thickness of 7 to 10 nm (Figure 5).

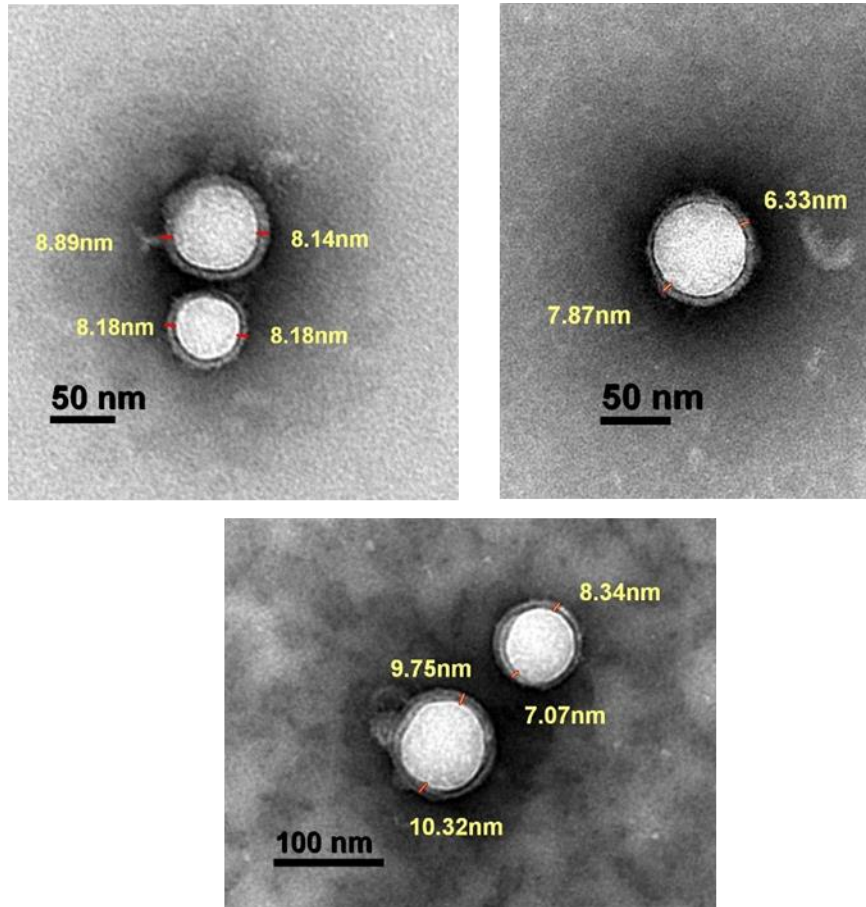


Figure 5. Mk membranes are 7-10nm thick. Mk membranes were extracted and wrapped around NPs. All samples were placed on a 400nm Carbon coated grid and negatively stained with 1% PTA (sodium) (pH 7.2) and visualized with TEM. Membrane thickness was determined by tools used on Libra 120 software.

Therefore, when a Mk membrane wraps around a bare NP, the size of the NP should increase up to 20nm. Figure 6 below and Supplemental Figure B.1 show an example of the NP size increase that we observed. This is consistent with Kang et al, who observed neutrophil membranes, with a thickness of 10nm, wrapped around a NP causing their NPs to increase in size by 20nm (Kang, Zhu et al. 2017).

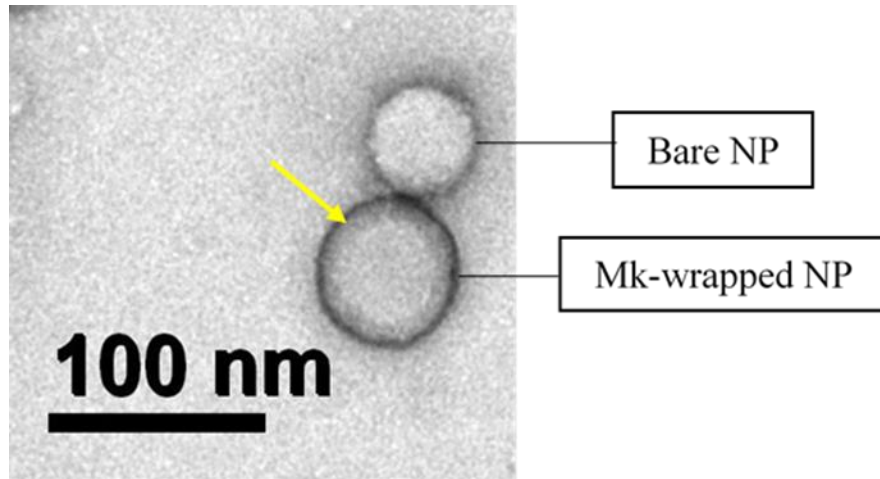


Figure 6. Mk-membrane wrapping increases the size of NPs. Top structure is a bare NP and bottom structure is a Mk-wrapped NP. Vesicles were isolated from  $4.4 \times 10^6$  Day 12 Mk cells and used to wrap NPs ranging in size of 50-75nm on 1/10/2018. Yellow arrow points to the Mk membrane wrapped around the NP.

Previously published papers report that the ideal polymer-to-membrane ratio of 1:1 (1mg of PLGA NPs to 1mg membrane protein) resulted in high wrapping efficiency and long-term stability (Fang, Hu et al. 2014, Kang, Zhu et al. 2017). However, since we are working with a small quantity of membranes, currently, it is not feasible for us to measure membrane protein concentration. Thus, we chose to use NTA to measure small particle size. NTA uses Brownian motion to determine the size and concentration of particles under 1000nm in size and it offers advantages over other methods (Dragovic, Gardiner et al. 2011). It can detect, size and measure the concentration of particles smaller than those possible on flow cytometry, which typically can measure particles down to about 0.03 to 0.05 of a micron (300 to 500 nm). Dynamic Light Scattering is often used to characterize NPs, but with heterogeneous mixtures, DLS cannot distinguish between the different sizes and it

tends to estimate the particle size and distribution based on the larger particles (Dragovic, Gardiner et al. 2011). NTA measures size and scattering intensity on individual particles allowing to determine the particle size in heterogenous mixtures quite accurately (Dragovic, Gardiner et al. 2011). Plots produced by NTA measuring a wrapped sample can be used to distinguished between the number of wrapped and unwrapped NPs or remaining membrane vesicles.

The size and concentration of bare NPs, empty MkmVs, and MknPs were determined using the NS300 instrument (Malvern). Bare NPs and empty MkmVs were analyzed separately to determine their size and concentrations. Mk membranes were extracted and extruded through the 400nm pore membrane filter 11 times to generated MkmVs. NTA determined that the mean diameter of the MkmVs was between 140-160nm post-400nm-extrusion (Figure 7) for each MkmV sample measured.

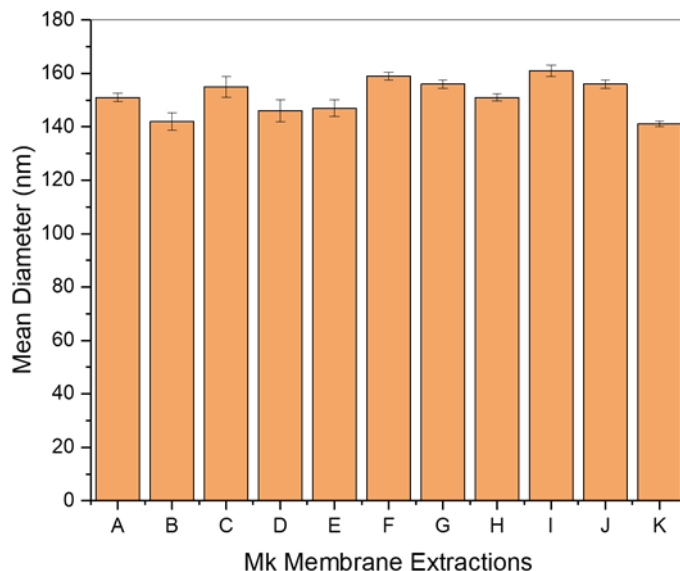


Figure 7. Mean diameter size of MkMVs. Day 12 MkMVs were extruded through 400nm membrane pore filter 11 times. NTA (NS300) was performed on extruded vesicles with three replicates per individual membrane extraction. Error bars represent standard deviation (n=11).

These results were consistent with our TEM images (Figure 3 and Supplemental Fig A2) displaying MkMVs varying in size from 25-400nm. Total concentration of the MkMVs was also determined, with  $10^6/10^7$  whole Mk cells (cells/mL) yielding  $10^8$  particles/ $\mu$ L per extraction and extrusion process.

Once the total concentration of bare and MkMVs samples were determined, we used their concentrations to calculate how many MkMVs to mix with our bare NPs for wrapping. Before wrapping, a ratio of bare NPs to MkMVs was chosen. This ratio is based on the number of NPs to the number of MkMVs added during wrapping. We decided to use one NP for all samples and varied the amount of MVs, with the theory that more MVs will increase the likelihood of wrapping. Using the total concentration

of bare NPs and MkMVs and the volume of each sample, we calculated the number of NPs and MkMVs to mix for wrapping. A sample calculation is shown below in Table 1. This calculation was originally back-calculated once we verified under TEM and co-cultured samples that the NPs were wrapping.

Table 1. Calculating wrapping ratio based on concentration

Bare NPs		MkMVs	
Bare NPs total concentration	$1.32 \times 10^{10}$ NPs/ $\mu$ L	MkMVs total concentration:	$5.39 \times 10^7$ MkMVs/ $\mu$ L
Volume of bare NPs added:	1.0 $\mu$ L	Volume of MkMVs added:	450 $\mu$ L
Number of bare NPs added:	$0.05 \mu\text{l} * 1.32 \times 10^{10} = 1.32 \times 10^{10}$ bare NPs	Number of MkMVs added:	$450 \mu\text{L} * 5.39 \times 10^7 = 2.34 \times 10^{10}$ MkMVs
NPs to Mk membranes:		$2.34 \times 10^{10} / 1.32 \times 10^{10} = 2$	
Ratio of NPs to Mk-membranes:		1:2	
Used 2 Mk mem vesicles to cover 1 NP			

To verify that the membranes are wrapping around the NPs and thus causing the NPs to increase by 20nm, random wrapping ratios were chosen to wrap the NPs, and the wrapped samples were measured using NTA. Based on the concentration of the bare NPs and the empty MkMVs, a ratio of NP to MkMVs was established. Figure 8 below shows that we were able to see if wrapping occurred based on the mean diameter sizes of the wrapped NPs.

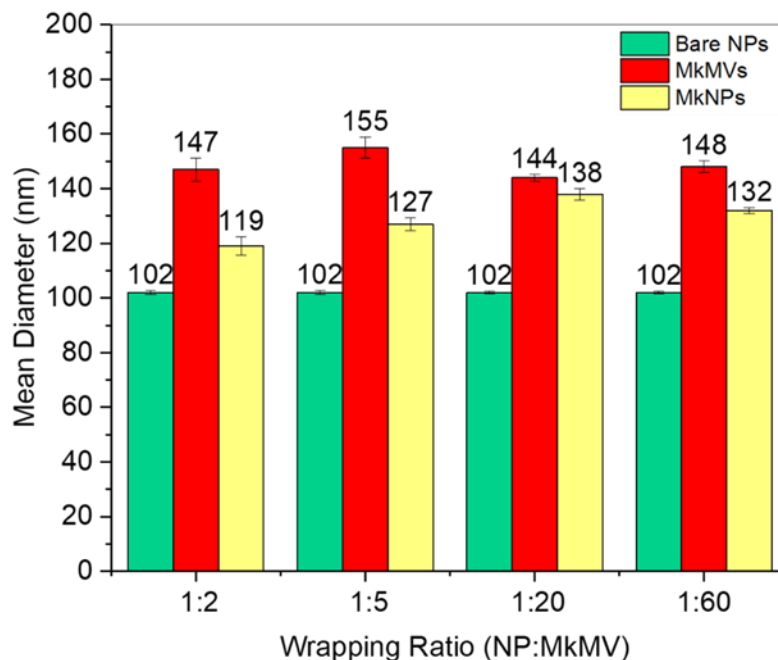


Figure 8. Size distribution of bare NPs, MkMVs, and MkNPs as determined by NTA. Wrapping was performed using the 400nm-pore membrane. The size of bare NPs and extruded MkMVs were determined using NS300 (Malvern). Ratios of NP to MkMVs were calculated (number of NPs: number of MkMVs), wrapped samples were generated and measured for mean size. NTA was performed on each sample with three technical replicates each. Error bars represent standard deviation (n=4).

NPs in Figure 8 were wrapped through extrusion with the 400nm membrane pore. Most of the ratios resulted in the NPs increasing by 20nm in size. Sample 1:2 (1 NP: 2 MkMVs) increased from 102 to 119nm while Sample 1:5 increased from 102 to 128nm. This suggests that the ratios of 1:2, and 1:5 were ideal for wrapping through extrusion using the 400nm membrane pore Samples 1:20 and 1:60 show a mean diameter increase of 36 and 30nm, respectively.

When the 1:60 sample was visualized under TEM excess MkMVs and debris were present, suggesting the mean diameter size of the wrapped NPs may be skewed due the presence of excess MVs (Figure 9). The wide field of view in Figure 9A shows MkMVs strewn throughout the sample post wrapping. Figure 9B shows a close-up of the images in Figure 9A.

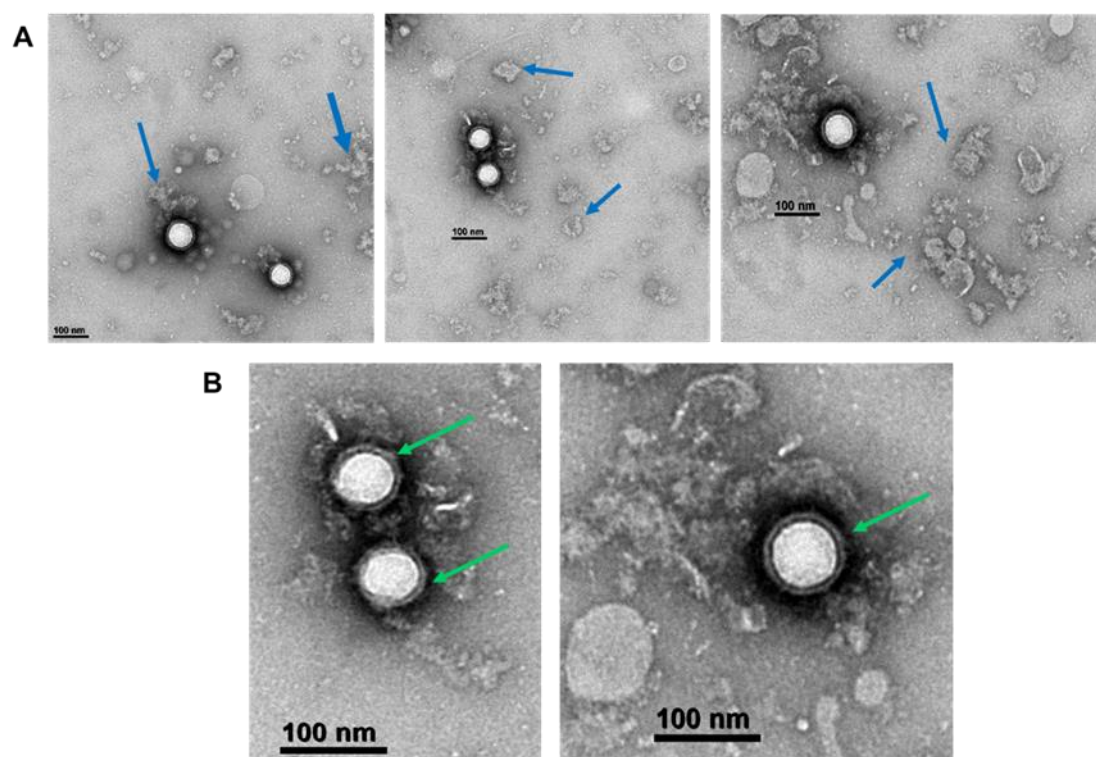


Figure 9. Excess MkMVs and debris are present after wrapping. (A). Bare NPs were wrapped with MkMVs at a 1:60 NP to MkMV ratio (1 NP for 60 MkMVs). Blue arrows point to excess MkMVs or debris. (B). Wrapped NPs in A above were magnified to show wrapping. Green arrows point to wrapped NPs. Samples were placed on 400nm Carbon Cu grids and negatively stained with 2% uranyl acetate and examined under TEM. Scale bars represent 100 $\mu$ m.

To “clean” our wrapped NPs and remove any excess MkMVs, we isolated the wrapped NPs by spinning down our sample at 17,000g for 30mins. At this speed the excess MkMVs “float” in the supernatant while the wrapped NPs pellet down. This allows us to separate any excess MkMVs from MknPs as shown in Figure 10 below.

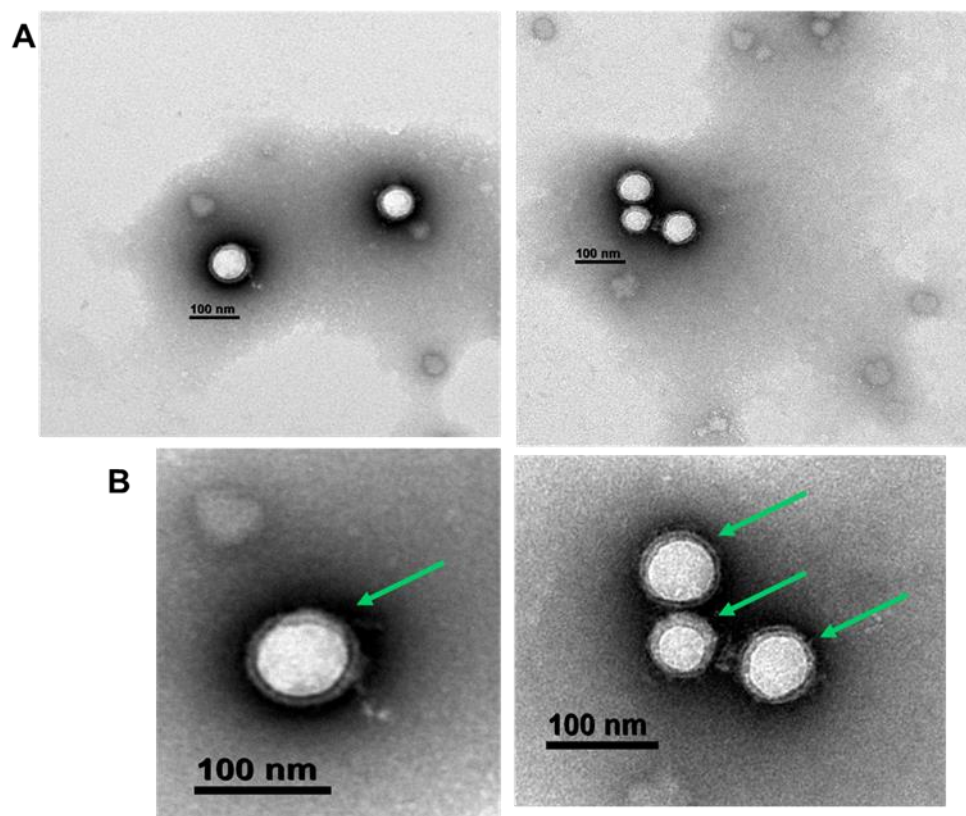


Figure 10. Excess MkMVs are removed after additional ultracentrifugation step. (A) NPs wrapped by MkMVs in a 1:60 NP: MkMV were ultracentrifuged at 17,000rpm for 30mins and then resuspended in water. (B) The samples in A were magnified to show wrapping. Green arrow points to wrapping. Samples were placed on 400nm Carbon Cu grids and negatively stained with 2% uranyl acetate and examined under TEM. Scale bars represent 100 $\mu$ m.

As Sample 1:60 (1 NP per 60 MkMVs) was being “cleaned” we also analyzed the size distribution and concentration of the same sample on NTA during each collection step. The distribution of the particle sizes within the sample are visualized in size distribution curves presented in Figure 11 below. The bare NPs had a sharp distinct peak around 78nm. Once wrapped, the synthesized MkNPs distribution curve displayed two peaks. The first distinct peak was around 92nm; this could represent a mixture of both bare and wrapped NPs, as the wrapping increases size by 20nm, but the bare NPs could also be large. There is a small blip around 110-120nm, suggesting the presence of wrapped NPs, but since this peak is tiny it is hard to say for sure if the peak represents wrapped NPs or a mixture of MkNPs and MkMVs, as indicated by the numerous arrows and question marks. There is a distinct peak at 140nm, however, suggesting presence of excess MkMVs, since MkMVs extruded by the 400nm are 140-160nm in size (see Figure 7). Again, the wrapped NPs could be mixed in with the MkMVs.

Once the synthesized the MkNPs were “cleaned”, or purified, by ultracentrifugation, we see two distinct peaks (Figure 11). The first peak shows bare NPs at 82nm, which was close to the original reading of 78nm, so we can assume that this peak likely represents bare NPs. We also see a separate peak at 123nm; this suggests we have wrapped NPs (which was confirmed visually by TEM. See Figure 10). We no longer see a sharp distinct peak at 140nm suggesting that we were able to remove excess MkMVs (Figure 10).

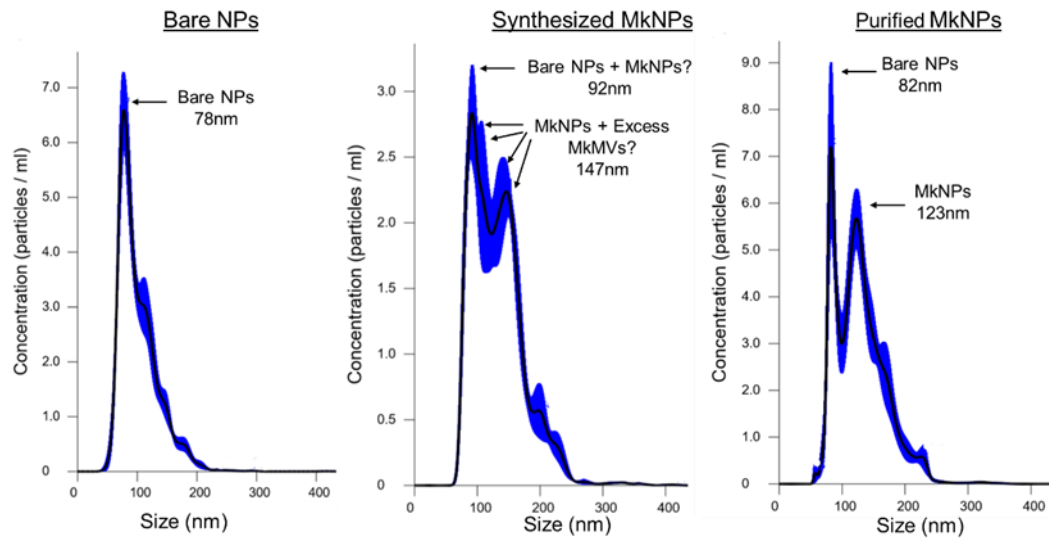


Figure 11. Particle size distribution of bare and wrapped NPs determined by NTA. Bare NPs were wrapped with MkMVs, and synthesized MkNPs were subjected to ultracentrifugation to remove excess MkMVs and generate Purified MkNPs. NTA determined size distribution with three technical replicates.

It should be noted that the peaks in size distribution curves display the mode, or the majority size, of NPs at a specific concentration. For our results, we report the mean size of the particles, but we also include the distribution curves since they demonstrate the heterogeneity of the sample. The mean diameters reported below in Figure 12 correspond to the size distribution curves presented in Figure 11. The synthesized MkNPs were reduced from a mean size of 132nm to 128nm post-cleaning. These purified MkNPs display a 20nm increase in diameter when compared to bare NPs (mean=102nm).

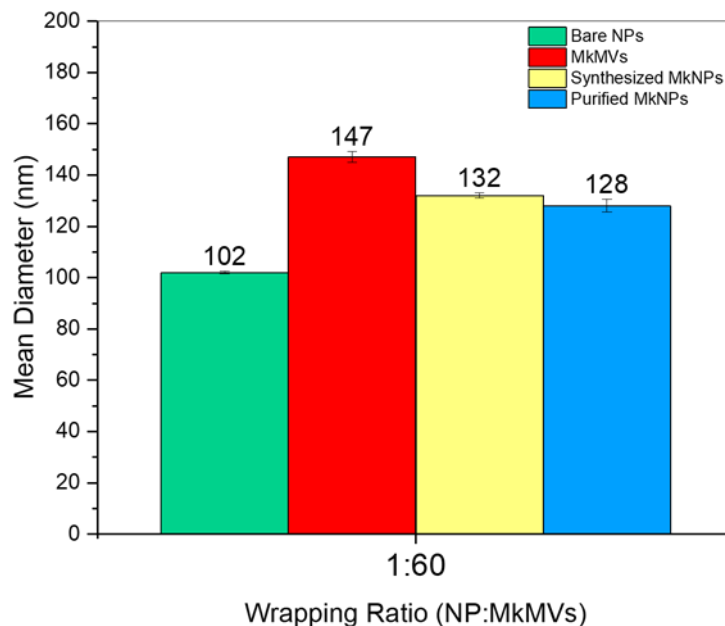


Figure 12. Mean Diameter of Purified MkNPs. Bare DiD-loaded NPs were wrapped with Day 12 MkMVs via extrusion in a 1 to 60 ratio (NP: MkMV) and analyzed on NanoSight300 (Malvern). Synthesized MkMVs were ultracentrifuged to remove excess MkMVs. Once “cleaned” the wrapped NP is referred to as Purified MkNPs. NTA was performed on each sample with three technical replicates each. Error bars represent standard deviation.

The removal of excess MkMVs, or purification, was performed on two additional wrapping ratios. Figure 13 displays how the excess MkMVs can remain in solution post-wrapping, skewing NTA mean readings towards a larger size. The sample with the 1:2 wrapping ratio had synthesized MkNPs with 140nm in size but post-cleaning, the purified MkNPs were now measuring at 119nm. The concentrations of samples between synthesize wrapped NPs and purified wrapped NPs also decreased

(data not shown). Overall, this suggests that excess MkMVs can be removed via ultracentrifugation, allowing for an accurate reading of wrapped NP size.

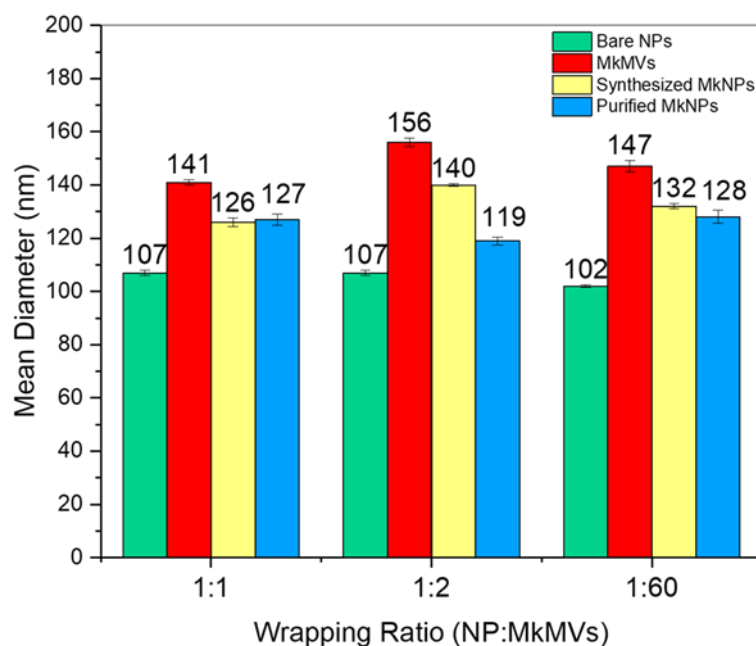


Figure 13. Mean Diameters of Synthesized MkNPs and Purified MkNPs. Bare DiD-loaded NPs were wrapped with Day 12 MkMVs via extrusion and analyzed on NanoSight300 (Malvern). Synthesized MkMVs were ultracentrifuged to remove excess MkMVs. Once “cleaned” wrapped NPs were called Purified MkNPs. NTA was performed on each sample with three technical replicates. Error bars represent standard deviation. (n=3)

However, some NTA distribution curves of purified MkNPs are still suggesting that during the wrapping process some bare NPs may remain unwrapped (see Figure 11 Purified MkNPs). To remove the bare NPs, the synthesized MkNPs

were placed in PBS overnight to swell the bare NPs. PBS induces swelling of bare NPs, so if a mixed population of wrapped and unwrapped NPs are placed in PBS the bare NPs will swell immensely (Fang, Hu et al. 2014). If the membrane is securely wrapped around the NP, it will provide protection against the PBS and prevent swelling. After swelling in PBS overnight, the bare NPs were removed through a 0.22 $\mu$ m filter and the solution was ultracentrifuged at 17,000rpm to remove the excess MkMVs. Figure 14 below displays the size distribution curves of the synthesized MkNPs and the MkNPs after PBS swelling and ultracentrifugation. The purified MkNPs now have a smooth curve with a mode of 105nm  $\pm$  5nm, suggesting we were able to remove bare NPs and excess MkMVs.

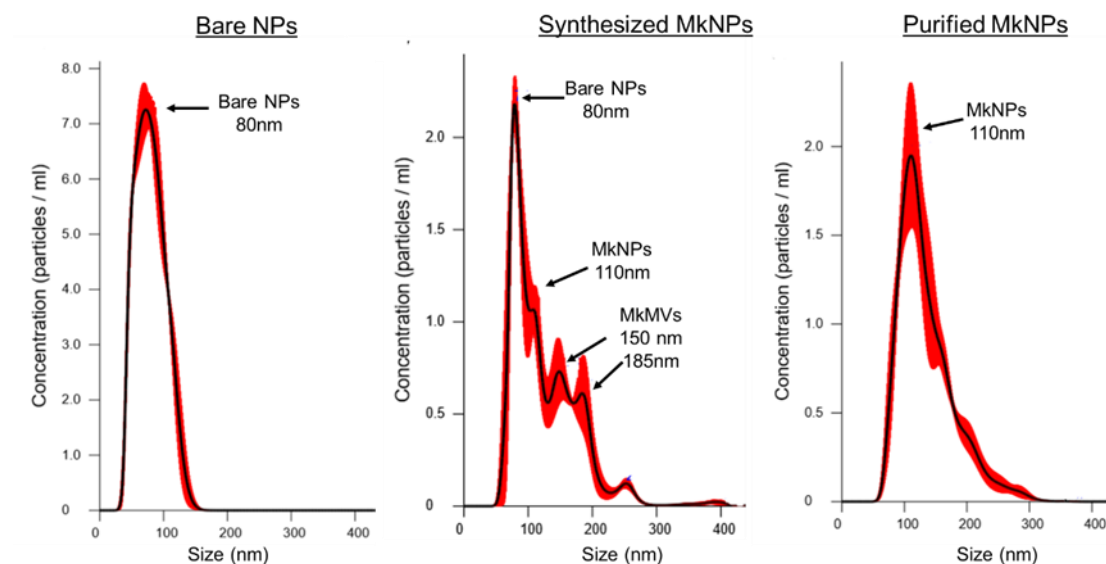


Figure 14. Size distribution curves of Bare NPs, Synthesized MkNPs, and Purified MkNPs. Bare NPs were wrapped with MkMVs via 400nm membrane pore. Synthesized MkNPs were placed in PBS overnight to induce swelling of Bare NPs. The Bare NPs were filtered and excess MkMVs were removed by ultracentrifugation to produce Purified MkNPs. NTA determined size distribution with three technical replicates.

Once the wrapped NPs were purified, the final concentration of MkNPs was determined via NTA. From this concentration (MkMVs/ $\mu\text{L}$ ), we were able to calculate the number of wrapped NPs and bare NPs to add to HSPCs for co-culture studies. The volume ( $\mu\text{L}$ ) of the purified MkNPs was used to determine the number of MkNPs to add to HSPCs. The chosen volume was multiplied by the concentration to determine the number of MkNPs in that volume. Using the calculated number of MkNPs, we then back-calculated to determine volume of bare NPs to add to the HSPCs to ensure that we were adding equal amounts of MkNPs as bare NPs. A sample of this calculation is shown below in Table 2.

Table 2. Sample calculation of wrapped and bare NPs to add to HSPCs

MkNPs		Bare NPs	
Final Concentration	$6.64 \times 10^7$ MkNPs / $\mu\text{L}$	Final Concentration	$2.31 \times 10^{10}$ bare NPs/ $\mu\text{L}$
Volume of MkNPs added per sample	50 $\mu\text{l}$	Number of bare NPs added per cell	$1.33 \times 10^5$ bare NPs/cell
Number of MkNPs per cell	$\frac{(6.64 \times 10^7 \text{ particles}/\mu\text{L})(50 \mu\text{L})}{25,000 \text{ HSPCs}}$  = $1.33 \times 10^5$ MkNPs/cell	Volume of bare NPs to add per sample	$\frac{(1.33 \times 10^5 \text{ NPs}/\text{cell})(25,000 \text{ cell})}{2.31 \times 10^{10} \text{ bare NPs}/\mu\text{L}}$  = 0.14 $\mu\text{L}$ bare NPs

Moving forward, we plan to wrap our NPs based on surface of bare NPs and MkMVs. This will ensure that we are calculating the approximate amount of MkMVs necessary to wrap all NPs in each sample. The calculation will be based on the mean diameter and concentration of the bare NPs, and MkMVs as determined by NTA. Once the diameters are determined we will calculate the surface area of an individual bare NP and total surface area of all NPs in each sample. We will determine the

surface area of extruded MkMVs, assuming they are spheres, and calculate the amount of MkMVs needed to cover all NPs. Based on this value, we will determine the ratio of NPs to MkMVs, or how many NPs will be covered x amount of MkMVs. An example of this calculation is provided below in Table 3.

Table 3. Calculating the wrapping ratio based on Surface Area

Bare NPs		Mk membrane vesicles (MkMVs) (after 400nm extrusion)	
NP mean diameter	102 nm	MkMVs mean diameter	147 nm
NP mean radius	51 nm	MkMVs mean radius	73.5 nm
Surface Area of one NP	32,6888 nm <sup>2</sup>	Surface Area of one MkMV	67,852 nm <sup>2</sup>
# of NPs in sample	1.32x10 <sup>10</sup> NPs		
Total SA of all NPs	4.31x10 <sup>14</sup> nm <sup>2</sup>		
# of MkMVs needed to cover all NPs in sample		6.36x10 <sup>9</sup> MkMVs	
Ratio of NPs to MkMVs		2 (Two NPs will be covered by one MkMV)	
Ratio of MkMVs to NPs		0.48 (Half of an MkMV will cover one NP)	

In the example above, we calculated that we will need 6.36x10<sup>9</sup> MkMVs to cover 1.32x10<sup>10</sup> NPs in each sample based on their surface area. A ratio of 2 tells us that one MkMV will cover two NPs. However, we plan to use this calculation to overdose or add several folds more MkMVs than the bare minimum amount. Adding several folds (5x-10x) of MkMVs will increase the chances of wrapping. It must be taken into consideration that the NTA may be measuring the outer radius of the MV, as opposed to measuring the inner radius of the MV, which is more important for

wrapping. This could lead to overestimating the surface area of the MVs; therefore, adding several folds of MVs will make up for this discrepancy. Then, once wrapping occurs, any excess MVs will be removed with the additional ultracentrifuge step mentioned above.

### **2.3.3 Assessing the Membrane Protein Content of Wrapped NPs Using a Magnetic Bead Assay**

The TEM and NTA based characterizations above can only indicate if the membrane wrapping was successful or not. However, it is more important to assess that membrane integrity, i.e. membrane protein content, is maintained post wrapping. Membranes must wrap around the NP correctly and maintain their integrity so that the wrapped NPs will be able to interact with its environment and perform their desired function (Zhai, Su et al 2017). Analyses of protein content are performed on wrapped NPs to confirm proper functionalization of the NPs with the cell membrane proteins (Fang, Hu et al. 2014). First, sodium dodecyl sulfate polyacrylamide gel electrophoresis (SDS-PAGE) is performed to compare the protein profiles of wrapped NPs to MVs or whole cell lysates (Fang, Hu et al. 2014). This will allow for visualization of all protein levels present in the samples. Second, membrane-specific or intracellular-protein marker levels on wrapped NPs are analyzed using Western Blot and compared to those of native membranes (Zhai, Su et al 2017). Analyzing levels of specific proteins (markers) will confirm if the membrane has maintained its integrity during the wrapping process. However, to perform SDS-PAGE and Western Blots large quantities of membranes and membrane wrapped NPs are required for accurate visualization. Since we are generating small quantities of MkMV from cultured Mk primary cells, we do not have enough membranes for membrane-specific

protein detection with SDS-PAGE or Western Blot. An alternative approach to confirm wrapping and membrane-protein specific detection is to use antibody-decorated magnetic beads and flow cytometry.

As our MkNPs are less than 200nm in size, we had to find an alternative method to detect them on flow cytometry since most flow cytometers cannot detect substances less than 300nm (Dragovic, Gardiner et al. 2011). By using antibody-decorated magnetic beads that are  $\sim 1.0\mu\text{m}$  size we were able to detect our MkMVs and MkNPs on flow cytometry. To collect our MkMVs and MkNPs, we used the selectable membrane marker CD41, which is the characteristic selectable marker of Mks. CD41 is a single-pass transmembrane protein with most of the antigen presented on the extracellular side of the membrane. CD41, also known as Integrin  $\alpha\text{IIb}$ , non-covalently associates with CD61 (Integrin  $\beta 3$ ) to form the Integrin  $\alpha\text{IIb}\beta 3$  complex on Mks and platelets, which plays an important role in thrombus formation (Nishikii, Kurita et al. 2017). Typically, a population of Day 12 whole Mk cells will be  $\sim 90\text{-}95\%$  CD41<sup>+</sup>. Therefore, this selectable marker was chosen since the population of Mk primary cells are largely CD41<sup>+</sup>.

To begin collecting MkMVs and MkNPs, we used magnetic beads that were coated in streptavidin, a bacterial-derived protein that binds to biotin. We used biotin-conjugated anti-CD41 monoclonal antibodies, that when mixed with the magnetic beads, are attracted to the streptavidin coating on the magnetic beads. The magnetic beads were considered “decorated” or primed with anti-CD41 antibodies. We then mixed the magnetic beads with either MkMVs, bare NPs, or MkNPs. The anti-CD41 monoclonal antibody would then attract and bind any CD41<sup>+</sup> materials. As most of the CD41 antigen is located on the extracellular side of the membrane it is believed that

the biotin-anti-CD41 antibodies would recognize and bind to the epitope extracellularly. After mixing, the samples were placed on magnetic stand so that the any CD41<sup>+</sup> materials bound to the magnetic beads will stick to the magnet and any unbound materials will be washed away. Using this assay, we hypothesize that we will be able to isolate MkMVs and MkNPs, as they are CD41<sup>+</sup>, and any bare NPs will wash away, as they are composed of polymers and not CD41<sup>+</sup>. The bare NPs will not be captured by the magnetic beads, as demonstrated below in Figure 15.

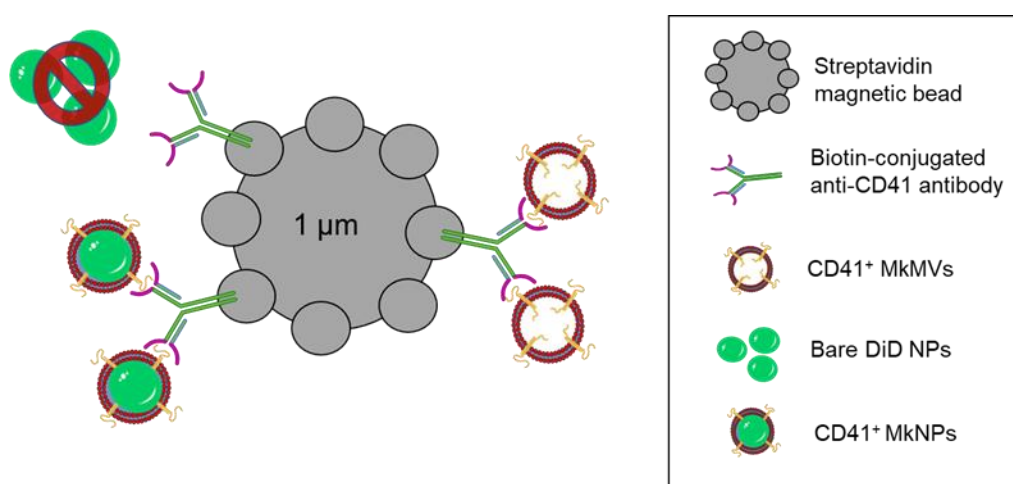


Figure 15. Scheme of Magnetic Bead-antibody assay. The streptavidin-coated magnetic beads will be attracted to biotin-conjugated anti CD41 antibodies. Any material that is CD41<sup>+</sup> (MkMVs and MkNPs) will be attracted to the antibody bound to the magnetic beads. The bare DiD NPs will remain unbound and wash away.

To visualize the particles binding to the beads, we dyed the membranes of whole MK cells with PKH26, a red fluorescent dye, which remains intact during MkMV formation. Our NPs were loaded with DiD, a green, hydrophobic fluorescent dye. By measuring the magnetic beads alone (grey) on flow cytometry, we established

a PKH26 gate using the PE channel to identify PKH26<sup>+</sup> MkmVs and we established a DiD gate using the APC channel to identify DiD<sup>+</sup> NPs. When gating for DiD, we created a PKH26<sup>+</sup>DiD<sup>+</sup> sub-gate within the PKH26 gate to identify any NPs that were also PKH26<sup>+</sup>, suggesting they were wrapped. This sub-gate allowed for us to identify magnetic beads that only captured wrapped NPs, if any residual bare NPs remained in solution they would not appear in our PKH26<sup>+</sup>DiD<sup>+</sup> gate. In Figure 16 below, we see that in our MkmV sample that 30% of magnetic beads sampled were PKH26<sup>+</sup> (red), indicating that our magnetic beads were able to capture CD41<sup>+</sup> MkmVs and that the CD41 marker is oriented properly on the extracellular side of the membrane. With our bare NP sample, 1% of magnetic beads sampled were DiD<sup>+</sup> (green), suggesting most of the NPs had been removed during washing, as expected. The MkmNP sample showed that 21% of magnetic beads sampled were PKH26<sup>+</sup>. Of those 21% PKH26<sup>+</sup> magnetic beads, 81% were DiD<sup>+</sup>, suggesting that these captured particles were wrapped since both signals were detected (yellow). These results suggest that during this particular wrapping process, we were able to wrap most of the bare NPs. It also shows that Mkm marker is properly displayed and oriented on the wrapped NPs in a similar orientation as the MkmVs.

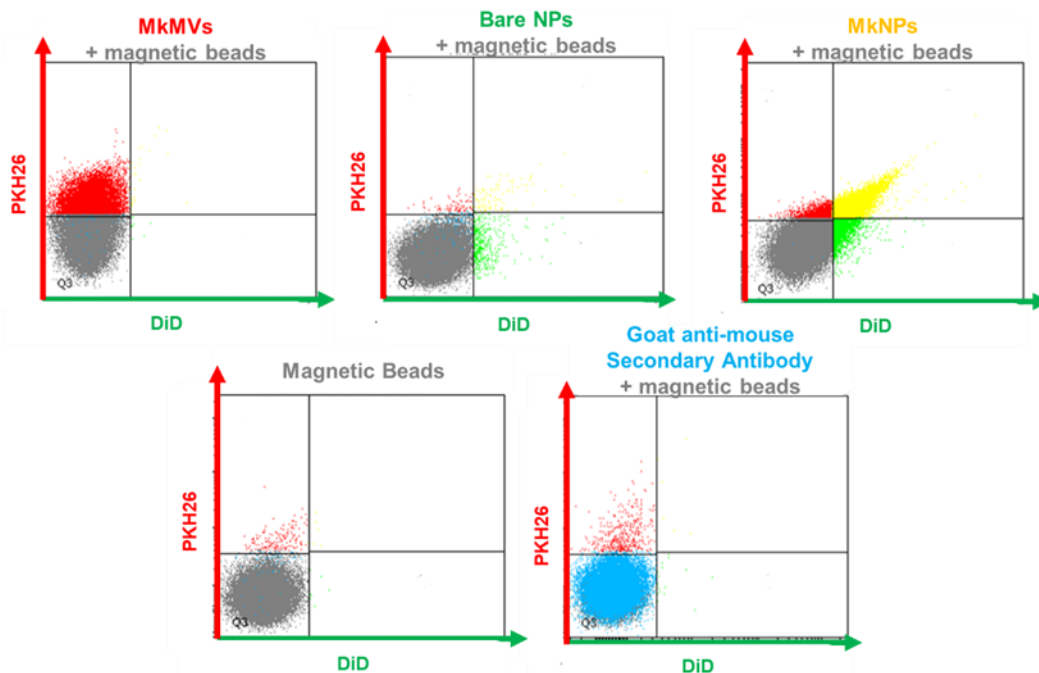


Figure 16. Streptavidin-coated Magnetic beads and biotin-conjugated anti-CD41 antibodies capture MkMVs and MkNPs. Magnetic beads (grey) were mixed with biotin-conjugated anti-CD41 antibodies. MkMVs (red), bare NPs (green), and MkNPs (yellow) were each mixed separately with the magnetic beads and antibodies. Samples were placed on a magnetic stand and washed three times, ensuring only captured material remained. Washed magnetic beads were analyzed via flow cytometry. Goat anti-mouse antibody (blue) was used as a proof-of-principle.

As a proof-of-principle to confirm our assay was working correctly, we used our CD41 antibody-magnetic beads with goat anti-mouse Alexa488-conjugated antibodies. When these secondary antibodies recognize any mouse-antibody, they will bind and produce a fluorescent signal detectable on the FITC channel. The biotin-conjugated CD41 antibodies are mouse anti-human antibodies. Therefore, they will be recognized by goat anti-mouse antibodies. 65% of magnetic beads sampled were Alexa488<sup>+</sup> (blue), suggesting that our assay is working properly, and it can be used to

confirm NP wrapping. This magnetic bead assay to capture wrapped NPs is a novel approach and makes confirming wrapping via flow cytometry easier, as most flow cytometry cannot detect MVs, NPs, or wrapped NPs alone because they are below the size threshold.

Since we verified that our magnetic bead assay can capture MkNPs we next wanted to quantify the amount of MkNPs that were CD41<sup>+</sup>. As mentioned earlier whole Mk cells are ~90-95% CD41<sup>+</sup> and since the Mk membrane should wrap around the NP in such a way that membrane integrity is retained, we hypothesize that the MkMVs and the MkNPs should have similar levels of CD41<sup>+</sup>. We attempted to quantify the amount of MkNPs that were CD41<sup>+</sup> using the magnetic bead assay. MkNPs were captured using the previous system and then any available CD41 present on the wrapped particles were labeled with FITC-conjugated CD41. The data collected from this experiment was inconclusive (not shown). On average 1-4% of magnetic beads sampled were PKH<sup>+</sup>FITC<sup>+</sup>, meaning that those collected membranes had extra CD41 membrane proteins that could be labeled with a FITC antibody. Since the biotin-conjugated anti-CD41 antibody was used to collect the MkMVs and MkNPs initially, it is hard to say if the levels of FITC-CD41 detected are an accurate representation of CD41<sup>+</sup> on MkMVs and MkNPs. This experiment will be redesigned, and further experiments will be discussed in the Discussion Section.

In a separate study performed by Toledano Furman et al., magnetic beads were used to capture membrane vesicles generated from Mesenchymal stem cells (MSCs) and flow cytometry was used to measure the membrane retention for typical MSC markers (Toledano Furman, Lupu-Haber et al. 2013). Initial measurements of surface markers on whole MSC revealed 93% CD90<sup>+</sup>, 79% CD105<sup>+</sup>, 66% CD44<sup>+</sup>, and 66%

CD29<sup>+</sup> (Toledano Furman, Lupu-Haber et al. 2013). After the membranes were extracted and sonicated, MSC membrane vesicles were analyzed for detection of MSC surface markers. It was reported that MSC membrane vesicles conjugated to magnetic beads were 73% CD90<sup>+</sup>, 81% CD105<sup>+</sup>, 72% CD44<sup>+</sup>, and 51% CD29<sup>+</sup> (Toledano Furman, Lupu-Haber et al. 2013). Surface marker detection higher than 50% was considered retained and in correct orientation; therefore, all MSC surface markers were retained on the MSC membrane vesicles (Toledano Furman, Lupu-Haber et al. 2013) despite the decreased levels of some markers.

As a secondary conformational experiment, confocal microscopy was also performed to confirm that the MKNPs are CD41<sup>+</sup>. Briefly, Mk membranes remained unstained while the bare NPs were loaded with DiD dye. FITC-conjugated CD41 monoclonal antibodies were mixed with the MKNPs and viewed under confocal microscopy (Supplemental Figure B2). Colocalization, or overlapping, of the DiD signals with FITC-CD41 signals on the membranes suggested that the MKNPs are CD41<sup>+</sup>, further confirming that the CD41 antigen remains intact during membrane extraction and NP wrapping.

## **2.4 Discussion**

For our MKNPs to be able to target HSPCs and deliver their cargo effectively we must first confirm that the NPs are being wrapped. We hypothesized that the electrostatic repulsion between negatively charge PLGA NPs and Mk membranes will drive the Mk-membrane to wrap around the NP properly, thus allowing the membrane to retain its target recognition function. To test this hypothesis, our wrapping protocol was optimized for membrane collection from CHRf and primary Mk cells. We then characterized the wrapping process using several methods. Through TEM, we were

able to visually confirm that the Mk-membrane was wrapping around the NP with a membrane thickness of 7 to 10nm, increasing the wrapped NP in size by 20nm (Figures 5 and 6). Utilizing NTA, we were able to confirm the size increase and determine the concentration of particles in a sample. The concentrations allowed us to compare different wrapping ratios and analyze the wrapping using extrusion through membranes of 400nm membrane pore sizes. Wrapping through 400nm membrane pore size allows for the best wrapping of NPs ~100nm in size. Determining the concentration of various particles with NTA allowed us to precisely determine the number and concentration of wrapped and unwrapped NPs as would be necessary for the HSPC co-culture studies. Using flow cytometry and magnetic beads, we were able to further visualize wrapping, however, our experiment to determine membrane protein levels must be re-designed.

As we are working with small quantities of membranes and wrapped NPs, alternative methods for characterizing had to be utilized. Characterizing wrapped NPs through NTA and magnetic beads on flow cytometry are two novel approaches that have not yet been published. These two methods allowed us to work with small volumes, determine size/concentration of wrapped NPs, as well as visualize wrapped NPs on flow, which would have otherwise been undetected due to size limitations.

Since we saw smooth distribution curves after filtering out swollen bare NPs and removing excess MkMVs with ultracentrifugation, we will incorporate these steps into our wrapping protocol. In the future, when cargo-loaded wrapped NPs are utilized *in vivo* it will be necessary to remove bare NPs. The excess MkMVs may not be as problematic since they are dead and unloaded. However, since bare NPs are non-specific and may interact with any cell type when delivered *in vivo*, they have the

potential to introduce off-target effects, if taken into the wrong cell. Therefore, removing any NPs that remain unwrapped prior to injection will ensure less of a chance of introducing off-target effects.

To wrap NPs in the future, we would like to utilize the diameter or surface area of the NPs and MkMVs as determined by NTA. Wrapping based on surface area will provide more accuracy in wrapping and allow us to calculate the exact amount of MkMVs needed to cover all NPs in solution. Once the exact amount is determined, we will add excess MkMVs to ensure wrapping is successful and any unwrapped NPs and excess MkMVs will be removed post-wrapping. As cargo loaded NPs are generally larger in size than single emulsion NPs, wrapping by surface area will greatly increase our chances of ensuring all NPs are wrapped.

To detect levels of membrane proteins that accurately represent our wrapped NPs, we must improve the magnetic bead assay. First, all samples must have equal amount of empty membranes as bare NPs and wrapped NPs added to the magnetic bead compound. This will ensure accuracy in percentage when comparing the different samples. Second, since anti-CD41 biotin conjugate antibodies are used to pull out the MkMVs and MkNPs it hard to say if the percentage of magnetic beads with FITC-CD41 was lowered because some CD41 markers are not available, since some are bound to the magnetic, or if it is lowered due to damage during the wrapping process. For better representation of the membrane proteins on the wrapped NPs, there are several improvements that can be made to this study. A suitable control must be used for this study; one could be whole MkMPs that were collected from culture and then captured using the magnetic beads. This will give us a better representation of the level of CD41 on particles captured on the magnetic beads, instead measuring CD41

on whole Mk membranes without capturing on magnetic beads first. Next, as we capture MkMVs and MkNPs and measure PKH<sup>+</sup>CD41<sup>+</sup> magnetic beads, we must also measure the supernatant or materials that were washed off during bead preparation. Prior to initiating the magnetic bead assay, we will determine the concentration of our wrapped sample using NTA and then we will determine the concentration of the supernatant containing the rinsed materials. By comparing these two concentrations we will have a better estimate of the percentage of the sample that is CD41<sup>+</sup>. We can assume that the materials not sticking to the beads were not CD41<sup>+</sup>.

Other selectable markers, such as CD42, CD43, CD61, CD11b, and CD18, should also be detected to further confirm that our MkNPs are maintaining membrane integrity. If enough membrane material and wrapped NPs are generated we can try to use SDS-PAGE to collect a protein profile, and Western Blotting could be performed if we use specific polyclonal antibodies allowing for an increase in protein detection vs monoclonal antibodies which are very specific. Immunogold staining has been utilized in the past to demonstrate that the membrane is wrapping around a NP in a “right-side-out” confirmation by using extracellular and intracellular-domain specific antibodies (Hu, Zhang et al. 2011). However, this method is faulty and based on personal interpretation. Perhaps a better method would be to use the extracellular and intracellular domain antibodies and analyze on flow cytometry. This would allow you to determine the percentage of extracellular vs intracellular antigens, and when compared back to whole cells, you would be able to conclude if the membranes are wrapping in a “right-side-out” confirmation.

## Chapter 3

### **MK-WRAPPED NANOPARTICLES INTERACT WITH HEMATOPOIETIC STEM CELLS**

#### **3.1 Background**

MkMPs target and bind to HSPCs (Jiang 2017). Specifically, they target the uropod region of the HSPC (Jiang 2017). MkMPs bind through a receptor-mediated response utilizing CD54, CD11b, CD18, and CD43 that are highly expressed in the HSPC uropod region (Jiang 2017). Uptake of MkMPs occurred 5 hours after the co-culture of HSPCs with MkMPs was initiated. HSPCs either contained MkMPs or the CFDA-SE dye contained inside the MkMPs was transferred to the HSPCs, indicating that the MkMPs delivered cargo to the HSPCs (Jiang 2017). MkMPs are taken into the HSPCs by either membrane fusion, and/or processes engaging lipid rafts, clathrin-mediated endocytosis, and/or macropinocytosis (Jiang 2017).

Since MkMPs possess the same physical properties as their parent cells, we expect Mks, or at least their membranes, to target and interact with HSPCs. We hypothesize that Mk membrane-wrapped NPs will enhance targeting of HSPCs due to the ability of the MkMPs' natural ability to target HSPCs. To test this hypothesis, we exposed our MkNPs to HSPCs, explored the time needed for uptake, and explored the mechanism of how MkNPs are entering HSPCs.

## **3.2 Materials and Methods**

### **3.2.1 Co-Culture with HSPCs and Mk-wrapped NPs**

Frozen CD34<sup>+</sup> HSPCs were cultured as previously described. At Day 3, HSPCs were isolated from culture by centrifuging at 300xg for 8mins. Pellet was washed with 500 $\mu$ L of IMDM and centrifuged at 500xg for 4mins. Co-cultures were created taking approximately 25,000 HSPCs per sample by placing the cells on a 0.4 $\mu$ m pore size tissue culture treated polyester transwell membrane (Costar 3470) inserted inside of a 24 well tissue culture plate (Falcon 353047, Corning) for 30mins. Co-culture media was composed of IMDM + 20% BIT + 1% Anti-Anti, 100ng/mL rhTPO and rhSCF. The co-culture media was placed on the outside of the transwell membrane. After adjusting to the transwell membrane for 30mins, MkMVs, bare NPs, or MkNPs were added directly to the transwell membrane and mixed with the HSPCs. The plate was incubated at 5% CO<sub>2</sub>, 20% O<sub>2</sub>, 95% relative humidity, and 37°C. To maximize the interaction between the particles and HSPCs, the 24-well tissue culture plate was spun at 600xg for 30mins, then placed in the incubator for 24hrs.

### **3.2.2 Confocal and Super Resolution Microscopy**

After 24hrs in the co-culture system, live cells were collected, placed on an  $\mu$ -slide 8 chamber poly-L-lysine (Ibidi 80826) plate and visualized using confocal microscopy under 40x oil Confocal (Zeiss LMS880 multiphoton confocal microscope).

To perform Super Resolution (SuperRes) microscopy, cells were washed and mounted on slides with paraformaldehyde and visualized using 63x oil SuperRes (Zeiss Elyra PS1).

### **3.2.3 Endocytosis of Bare PLGA NPs and Mk-wrapped NPs**

Day 3 HSPCs were pre-treated with 10 $\mu$ M dimethylamiloride (DMA, Sigma), 80 $\mu$ M Dynasore (Sigma), 5mM Methyl- $\beta$ -Cyclodextrin (M $\beta$ CD, Sigma) or 50 $\mu$ M LY29400 (Sigma Aldrich) for 45 mins at 37°C, which were used to inhibit macropinocytosis, dynamin-dependent (clathrin-dependent) endocytosis, lipid raft-mediated endocytosis, and macropinocytosis, specifically blocking PI3K, respectively. Cells and inhibitors were vortexed for 30secs and incubated at 37°C for 45min with the tubes open. After 45mins, around 50,000 HSPCs were exposed to either bare NPs or wrapped NPs. Samples were vortexed in the tubes for 30secs and then transferred to 12-well plate. The 12-well plated was incubated at 37°C for 30mins. After incubation, 1mL PBS was added to the wells to remove and wash the cells. Cells were centrifuged at 500xg for 5mins to collect washed cells. Supernatant was removed, and cells were re-suspended in 300 $\mu$ L of PBS and analyzed using flow cytometry. Mean Fluorescent Intensity was used to determine the intensity of the DiD dye within the NPs and detected using the APC channel. Each sample was measured in triplicate. Paired student t-test on all data was performed using Excel.

## **3.3 Results**

### **3.3.1 Mk-wrapped NPs Interact with HSPCs after 24hrs**

Once we were able to confirm that our membranes were wrapping around the NPs, we next wanted to look at the interaction between the MkNPs and the HSPCs. As previously reported by Jiang et al, when the MkMPs were cultured with Day 3 HSPCs at 5 hours there were fluorescent MkMPs inside of the HSPCs as well as on their surface (Jiang 2017). Since our Mks possess similar membrane properties as MkMPs,

we hypothesized that our MkNPs would interact with Day 3 HSPCs and be taken in by the cells.

Our Mk membranes were dyed with membrane dye, PKH26, and our NPs were loaded with fluorescent dye DiD to enable visualization. Our MkNPs were co-cultured with Day 3 HSPCs for 12-24 hours and then examined under the confocal microscope. Examination at 5 hours showed no interaction of any sample (MkMVs, bare NPs, MkNPs) with the HSPCs (data not shown). At 12 hours, Supplementary Figure C1 shows that we saw MkNPs interacting with the HSPCs along the HSPCs' membrane. At 40x magnification it is hard to tell if the MkNPs are on the extracellular side of the HSPCs or if they are beginning to enter the cells. However, we can assume the NPs are wrapped based on the colocalization of the two signals, as demonstrated in Figure 17 below. When the red PKH26 signal for MkMVs overlaps with the green signal for DiD-loaded NPs a yellow signal is produced, suggesting wrapping; both signals are present.

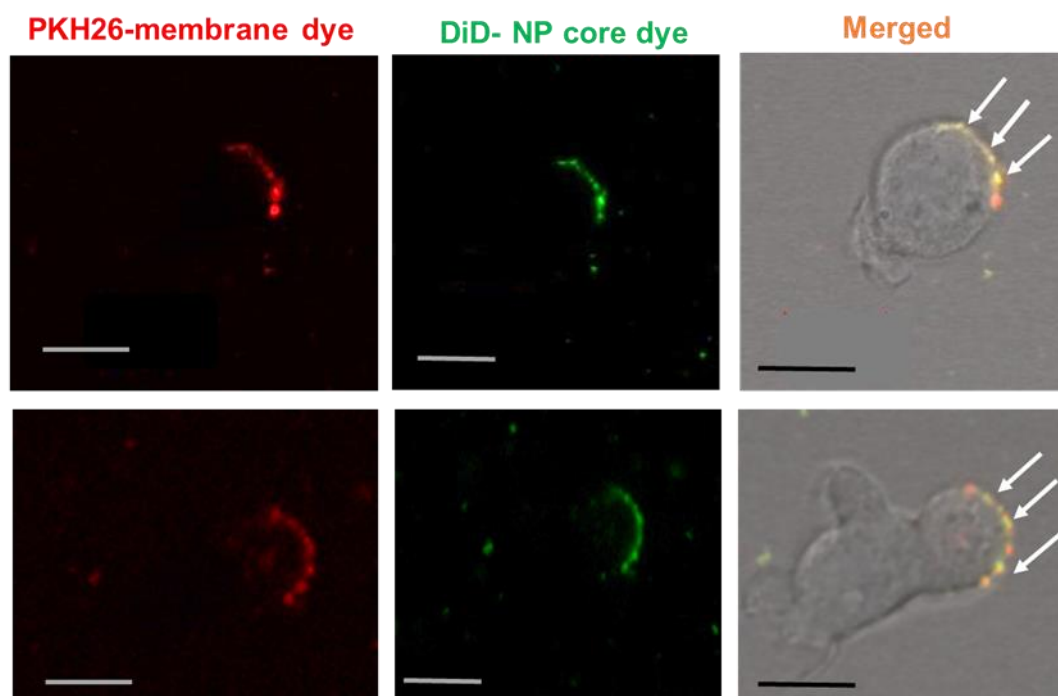


Figure 17. Colocalization of signals suggests NPs are wrapped and targeting HSPCs. NPs (green) were wrapped with PKH-26 dyed Mk membranes (red) and exposed to Day 3 HSPCs in a co-culture system. Yellow signal suggests colocalization. Live cells were washed with PBS and visualized under Confocal (LMS880) under 40x oil. Arrows point to examples of MkNPs. Scale bar represents 10 $\mu$ m.

Although the wrapped particles were interacting with the HSPCs, as predicted, we did not see any internalization of MkNPs in the cytoplasm, despite seeing internalization of MkMVs and bare NPs (Supplementary Figures C2). We decided to wait an additional 12 hours to see if the MkNPs would enter the cytoplasm of the HPSCs. Twenty-four hours after initializing co-culture, we saw uptake of MkNPs (Figure 18a). Figure 18b below, displays static images taken from a Z-stack video of an HSPC that has internalized a few MkNPs, as indicated by the yellow signal. When

the nucleus, stained with DAPI, comes into focus we see that the MkNPs are also in focus, indicating that they are inside the cell.

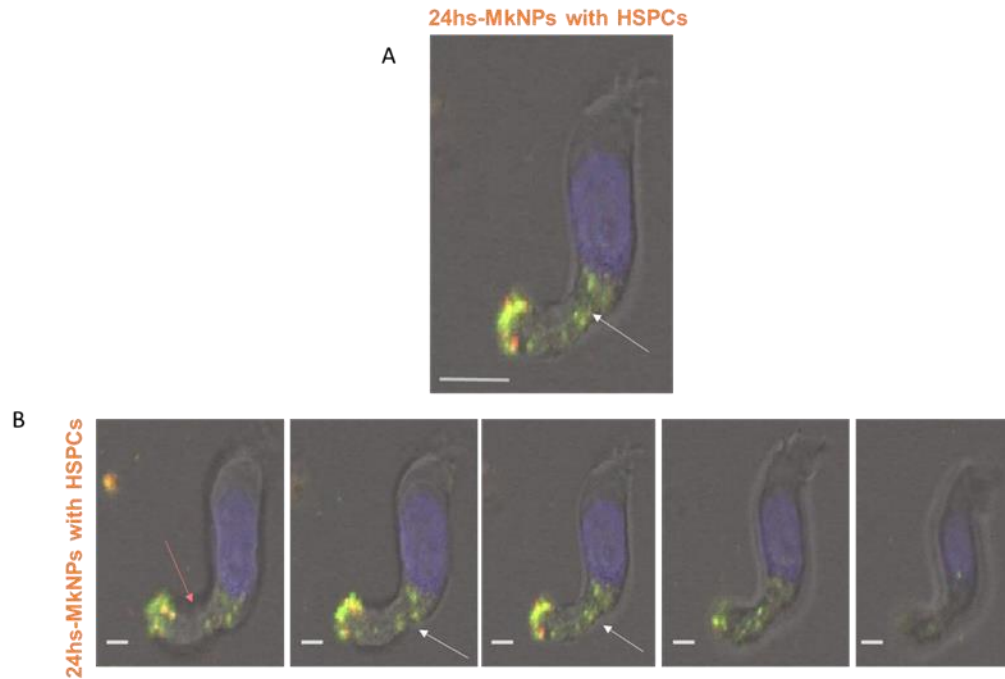


Figure 18. HSPCs uptake Mk-wrapped NPs after 24hrs. (A) Static image of HSPC with taken in MkNPs indicated by the yellow colocalization of signals. (B) Static images taken from Z-stacks in sequence. Z-stacks and image taken on Confocal LMS880. Red arrow points to uropod region of HSPC. White arrow points to the MkNPs in cytoplasm. Nuclei stained with DAPI. Scale bar represents 10 $\mu$ m.

Interestingly, we also observed both bare and wrapped NPs interacting with the uropod region of the stem cell, indicated by the red arrow in Figure 18b. This finding was similar to Jiang et al's observations when he exposed MkMPs to HSPCs (Jiang 2017). The uropod region is the polarized rear edge of the stem cell containing markers CD54 and CD43, and is the preferred binding site of MkMPs (Jiang 2017).

To further confirm that the MkNPs are internalized by HSPCs, we fixed our live samples to slides for observation under Super Resolution (SuperRes) Microscopy. SuperRes further confirmed uptake of MkNPs after 24hrs (Figure 19). We also stained our HSPCs' membranes using phalloidin, which stains actin within cell membranes. This created an outline along the membrane of the HSPC so that we could easily visualize if the MkNPs were internalized in the cell cytoplasm or trapped in the cell membrane. Although there is a low amount of uptake shown in Figure 19 below, we can further confirm that there is wrapping by the colocalization of signals and that the MkNPs are in the cytoplasm. The low amount of uptake could be due to a low quantity of successfully wrapped NPs introduced to the cells, or perhaps the cells that appeared to have internalized large quantities of MkNPs under Confocal were washed away during the fixation step.

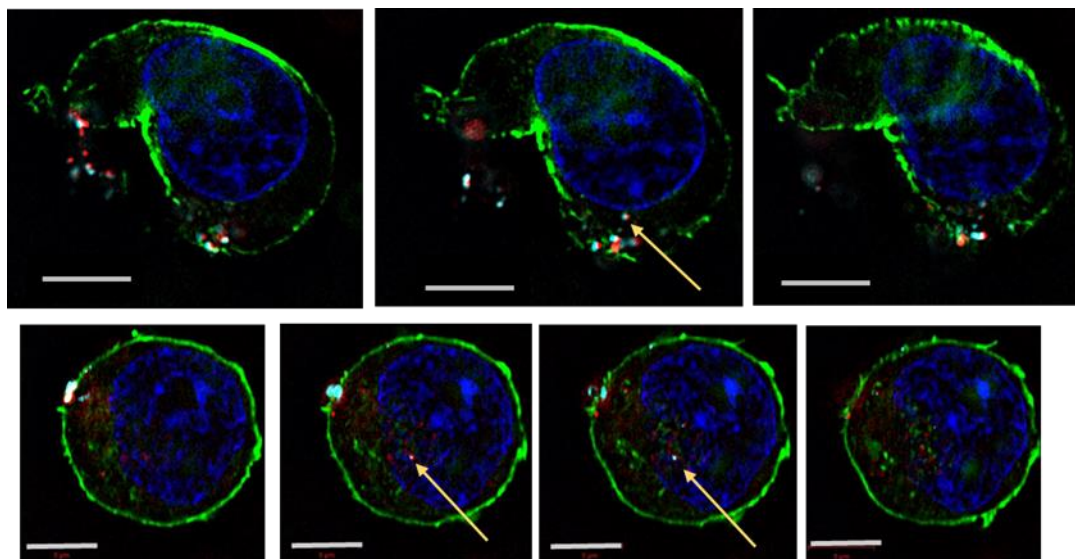


Figure 19. Super Resolution Microscopy further confirms MkNPs are inside HSPCs. Mk membranes were stained with PKH26 (red). NPs were loaded with DiD (light blue). HSPCs' membranes were stained with phalloidin (green) and nuclei were stained with DAPI. Z-stack recorded on SuperRes Zeiss Elyra PS 1 under 63x oil and static images taken from Z-stack video in sequence are presented. Yellow arrows point to colocalization in static images.

While visualizing uptake using microscopy, we also utilized flow cytometry to confirm the wrapped NPs are interacting with the HSPCs. Our co-cultured cells (~25,000 cells for each sample) were washed with PBS and ran through flow cytometry for detection. We first established a threshold to capture live cells without any particles, acting as the control (blue). We then gated for PKH26 signals and DiD signals to assess the percentage of live cells that indicated there was interaction. Based on our bare NP sample in Figure 20, we created a gate to show NPs that were both PKH26<sup>+</sup> (red membrane dye) and DiD<sup>+</sup> (green NP dye), suggesting wrapping (yellow). As expected, at both 12 and 24hrs (Supplementary Figure C4) 0% of live HSPCs were PKH26<sup>+</sup>DiD<sup>+</sup> when exposed to bare NPs. However, 84% and 91% of live

cells sampled, were DiD<sup>+</sup>, suggesting that a large portion of the live cells were interacting with the bare NPs.

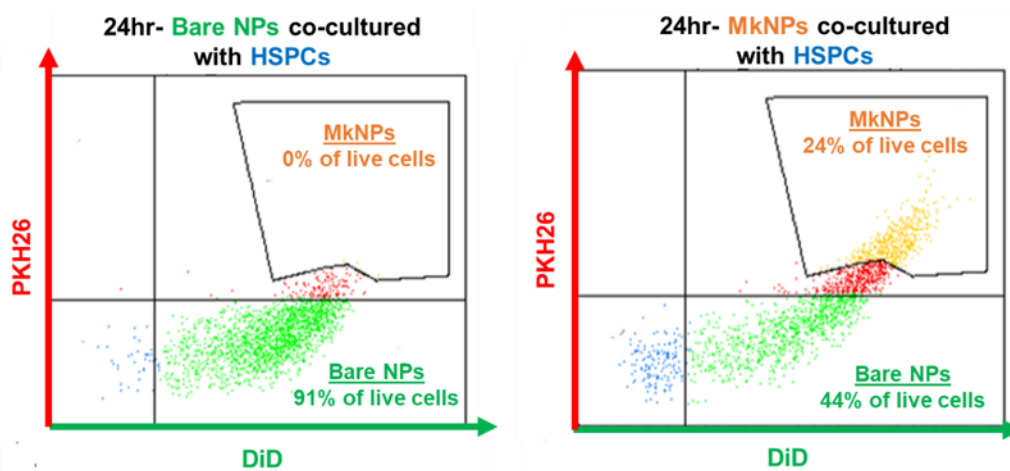


Figure 20. MkNPs interact with HSPCs at 24hrs, as detected by flow cytometry. Mk membranes stained with PKH26 (red) and NPs loaded with DiD (green) were extruded to form MkNPs (yellow). Particles were co-cultured with Day 3 HSPCs for 24 hours and then measured using flow cytometry (FACS Aria). Gate in upper right corner represents wrapped NPs. Blue color shows live cells positive for interaction.

At 24hrs, 24% of live cells were PKH26<sup>+</sup>DiD<sup>+</sup>, suggesting that 24% of HSPCs were interacting with the MkNPs, as indicated by the yellow color gated in the upper right corner of Figure 20. However, 44% of live cells were DiD<sup>+</sup> (green color). This suggests that some of our MkNPs, in this sample, remained unwrapped; perhaps the bare NP concentration was too high and not enough excess MkMVs were added to provide enough wrapping. At 12hrs (Supplementary Figure C4), we also saw similar detection levels; 27% of live cells were PKH26<sup>+</sup>DiD<sup>+</sup>, suggesting interaction with MkNPs, and 39% of live cells were DiD<sup>+</sup>. When we compare these findings to the

confocal images where we saw little to no uptake at 12hrs (Supplementary Figure C1), we can assume that most of these detected interactions are from the particles (wrapped or bare) aggregating along the outer surface of the HSPCs. It is hard to say if they are just aggregating on the outer surface or if the particles are about to be taken into the cell. Currently, we do not have a reliable method for flow cytometry to differentiate between on the surface or inside of the cell.

It should be noted that the data presented in Figures 17-20 were not acquired from using the NTA concentration calculations presented in Chapter 1 Table 2. At the time these studies were performed, the concentration of MkNPs vs bare NPs was not known. There was no way to count how many MkNPs or bare NPs we were introducing to the HSPCs. Therefore, some co-culture samples may have had a higher concentration of bare NPs introduced to the HSPCs, skewing some results. However, utilizing the NTA we can confirm wrapping and calculate the concentrations of wrapped NPs and bare NPs to ensure equal numbers of each type of particle are added.

Once we confirmed wrapping via NTA, we next determined a method to increase the interaction between MkNPs with HSPCs in co-culture. We added 100,000 HSPCs to a 0.4 $\mu$ m pore size tissue culture treated polyester transwell membrane (Costar 3470) which was inserted inside of a 24 well tissue culture plate. Once the HSPCs adjusted to the well, we added our MkNPs, bare NPs, or MkMVs. To maximize the interaction between the particles and the HSPCs, we centrifuged the tissue culture plate for 30mins. The centrifugal force increased the rate of interaction by physically forcing the particles to interact with HSPCs. With the transwell membrane and the additional centrifugation step we saw uptake of MkNPs after 24hrs (Figure 21 and Figure 22) (Supplemental Figures C5-C7).

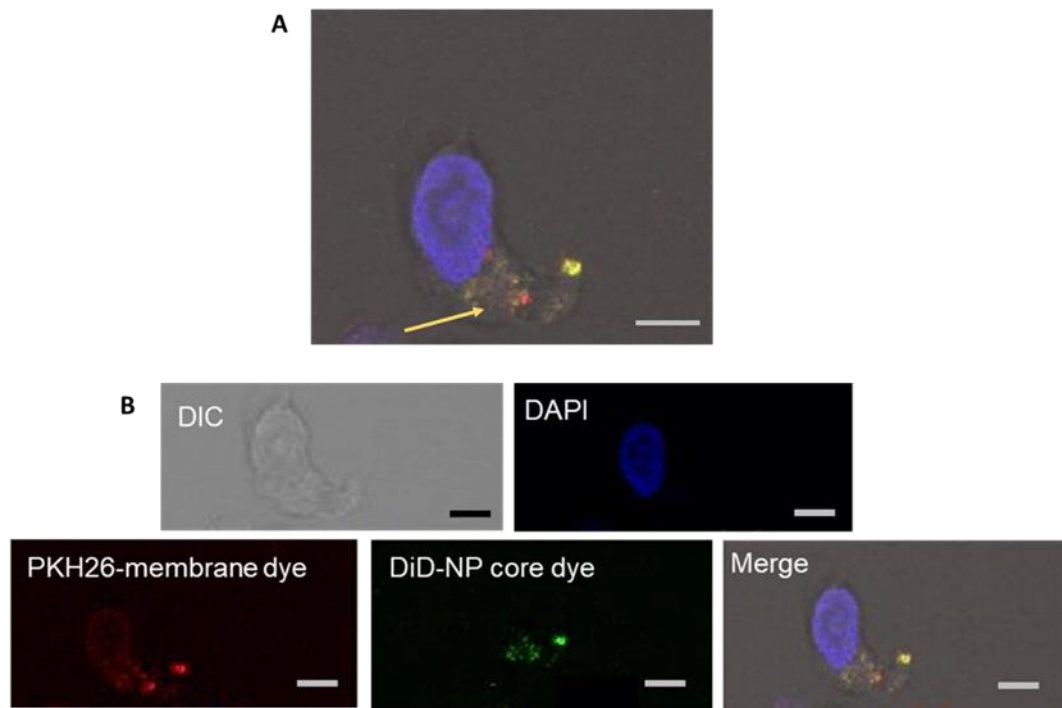


Figure 21. Transwell membrane and additional centrifugation step allow for increase uptake of MKNPs by HSPCs. HSPCs were co-cultured with 44,000 MKNPs/cell for 24hrs. (A) Static image of HSPC with MKNPs taken in (B) Split screen of static image displaying different channels. Mk membranes stained with PKH26 membrane dye (red), NPs loaded with DiD dye (green), nuclei stained with DAPI (blue). Arrows point to uptake when nuclei are in focus. Yellow signals suggest colocalization. Visualized with Confocal LMS880 under 40x oil. Scale bar is 5µm.

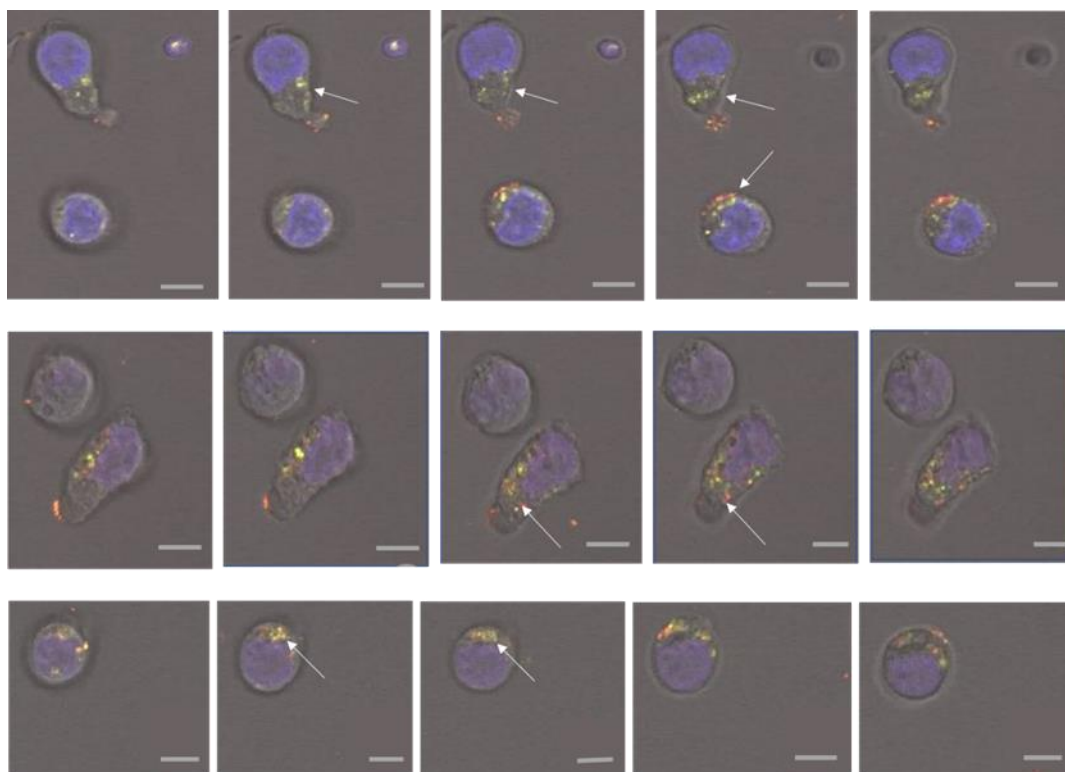


Figure 22. HSPCs take up MKNPs after 24 hrs. Day 3 HPSCs were seeded with 10,000 MKNPs/cell. Mk membranes stained with PKH26 membrane dye (red), NPs loaded with DiD dye (green), nuclei stained with DAPI (blue). Arrows point to uptake when nuclei are in focus. Yellow signals suggest colocalization. Visualized with Confocal LMS880 under 40x oil. Images are static images taken from Z-stacks in sequence Scale bar is 5 $\mu$ m.

To further confirm that the wrapped NPs are internalized and delivered to the cytoplasm, we again used actin-staining to visualize the HSPCs' membrane and higher magnification.

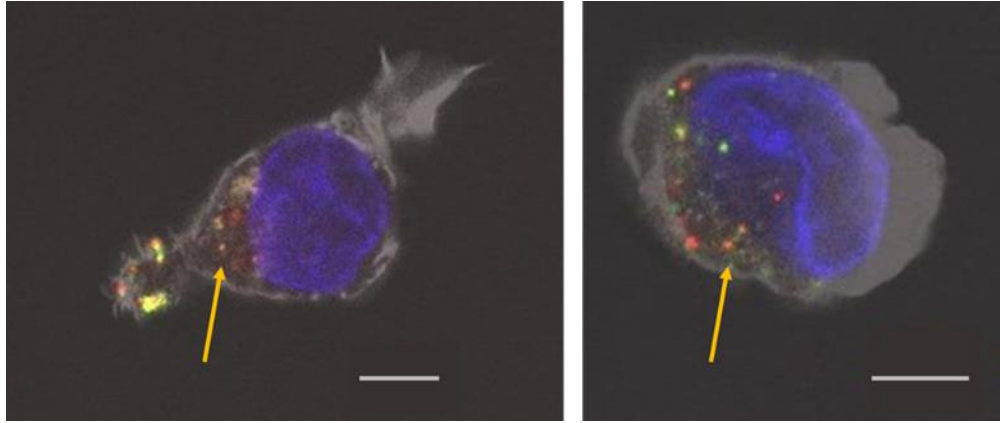


Figure 23. MKNPs are in cell cytoplasm of HSPCs. Day 3 HSPCs were co-cultured with 77,000 MKNPs for 24hrs. Mk membranes were dyed with PKH26 (red), NPs were loaded with DiD (green), nuclei were stained with DAPI (blue), and HSPCs' membranes stained with phalloidin (white). Samples were fixed to slides and visualized on Confocal LMS880 under 63x oil. Scale bars are 5 $\mu$ m. Arrows point to uptake of wrapped NPs.

With actin staining and higher magnification, the static (Figure 23) and the static images taken from the Z-stacks (Figure 24) displayed a high amount of successfully wrapped NPs internalized by the HSPCs, as suggested by the yellow colocalization signal.

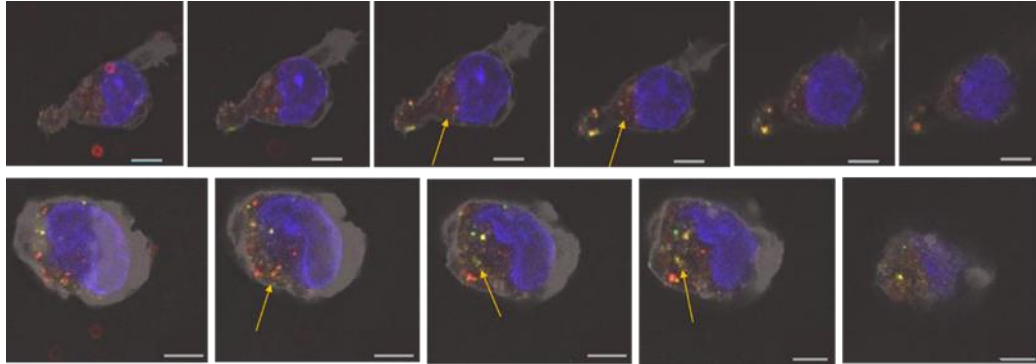


Figure 24. Static images taken from Z-stack in sequence display internalization of MkNPs in cell cytoplasm. Day 3 HSPCs were co-cultured with 77,000 MkNPs for 24hrs. Mk membranes were dyed with PKH26 (red), NPs were loaded with DiD (green), nuclei were stained with DAPI (blue), and HSPCs' membranes stained with phalloidin (white). Samples were fixed to slides and visualized on Confocal LMS880 under 63x oil. Scale bars are 5 $\mu$ m. Arrows point to uptake of wrapped NPs.

To ensure that we were adding the same number of MkNPs as bare NPs to the HSPCs, we used the sample concentration determined by NTA to calculate the total number of wrapped NPs and bare NPs to add to each cell (Chapter 1 Table 2). Using the calculation generated in Chapter 1 Table 2 10,000 MkNPs per cell were added to Day 3 HSPCs. After 24hrs HSPCs were viewed under Confocal (Figure 25). The MkNPs displayed in Figure 25 below were wrapped using a 1:4 wrapping ratio of 1 NP to 4 MkMVs. This ratio was determined by the NTA concentration of bare NPs and MkMVs prior to wrapping (demonstrated in Chapter 1 Table 1). A similar comparison was made for MkNPs wrapped using a 1:2 wrapping ratio, 1 NP to 2 MkMVs (Supplemental Figure C8).

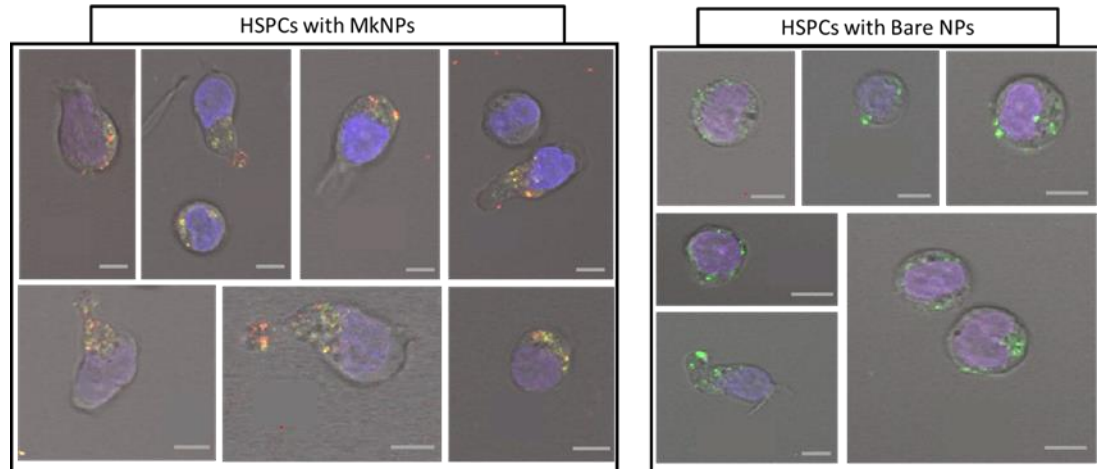


Figure 25. Comparison of HSPCs exposed to 10,000 particles/cell for 24hrs. Day 3 HSPCs were co-cultured with either 10,000 MkNPs (left panels) or 10,000 bare NPs (right panels) for 24hrs, as determined NTA. Mk membranes are dyed with PKH26(red), NPs are dyed with DiD (green), nuclei are stained with DAPI (blue). The yellow signals suggest colocalization. Visualized using Confocal LMS880. Scale bars are 5 $\mu$ m.

HSPCs also displayed uptake after 24hrs of MkNPs wrapped in 1:1 wrapping ratio (1 NP to 1 MkMV), 1:2 wrapping ratio (1 NP to 2 MkMVs) and a 1:4 wrapping ratio (1 NP to 4 MkMVs), further confirming that our MkNPs are entering HSPCs' cytoplasm.

In a different experiment, McNeer et al loaded PLGA NPs with coumarin 6 (C6), a hydrophobic dye, and introduced the NPs to Day 3 CD34<sup>+</sup> HSPCs to track cellular uptake (McNeer, Chin et al. 2011). Cells were co-cultured for 24hrs and then viewed under Confocal for uptake. McNeer noted that the low cytoplasm to nucleus ratio of CD34<sup>+</sup> cells made internalization difficult to see but Confocal confirmed the C6-NPs were internalized in the cytoplasmic space of the CD34<sup>+</sup> cells (McNeer, Chin et al. 2011). C6-NPs were not detected in the nucleus (McNeer, Chin et al. 2011). These results are consistent with what we are seeing with our wrapped DiD-loaded

PLGA NPs targeting CD34<sup>+</sup> HSPCs. It is difficult at times to visualize a signal internally, but we have visually documented that several HSPCs have internalized our MKNPs after 24hrs.

### 3.3.2 Uptake of Mk-wrapped NPs is Dynamin-Dependent

Since we obtained visual confirmation that the MKNPs are interacting and entering HSPCs, we wanted to examine potential mechanism by which the MKNPs and bare NPs are taken up by HSPCs.

When NPs reach the exterior membrane of a target cell, they can interact with components of the plasma membrane or extracellular matrix and enter the cell through endocytosis (Behzadi 2017). Endocytosis leads to the uptake of particles, less than 500nm in diameter, through the target cell membrane invaginating and collecting the particles, budding, and finally pinching off to form endocytic vesicles that are transported to specialized intracellular sorting compartments (Paulo, Pires das Neves et al. 2011, Behzadi 2017). The different mechanisms of endocytosis are summarized below in Table 4.

Table 4. Brief description of major endocytic pathways (Verma and Stellacci 2010, Mulcahy 2014).

Type of endocytosis	Brief description	Size of vesicle formed
Phagocytosis	Internalization of large solid particles such as bacteria and yeast by specialized cells.	Depends on the particles being engulfed
Pinocytosis	Fluid phase uptake of particles. Many pathways discussed below	See below

Table 4 continued

Macropinocytosis	Extracellular fluid internalized by membrane protrusions or ruffling	<1 $\mu\text{m}$
Clathrin-mediated endocytosis	Transmembrane receptors and ligands on membrane invaginated and form clathrin-coated pits	~120nm
Caveolae-mediated endocytosis	Flask-shaped invaginations that involve the use of caveolin-1	~50-60nm
Clathrin- and caveolae-independent endocytosis	Internalization of particles void of clathrin and caveolin-1; lipid rafts.	~200nm

Previously, Jiang et al found that MkMPs co-cultured with HSPCs, are taken up by HSPCs through macropinocytosis, lipid rafts, and dynamin-dependent (clathrin-dependent) endocytosis (Jiang 2017). Since the NPs are wrapped with membranes from Mks, it is expected that a MkNP will be taken up by the HSPCs in a similar manner. Therefore, the endocytic pathways chosen to be studied in this project were macropinocytosis, dynamin-dependent endocytosis, and lipid rafts, and accordingly specific or specialized inhibitors were chosen to block the corresponding endocytic pathways

Dimethylamiloride (DMA) was chosen to block macropinocytosis. The membrane ruffling mechanism in macropinocytosis is rich in rac1-, actin-, and cholesterol-dependent and requires  $\text{Na}^+/\text{H}^+$  exchange activity (Mulcahy 2014). DMA inhibits macropinocytosis by blocking the  $\text{Na}^+/\text{H}^+$  exchange at the cell surface and may affect actin (Dutta 2012). Macropinocytosis may also be stimulated by Phosphatidylinositol-3-kinase (PI3K) (Mulcahy 2014) and therefore the inhibitor LY29400 was chosen to block PI3K activity.

To block clathrin-dependent endocytosis, the inhibitor Dynasore was chosen. During the formation of the clathrin-coated pits the protein dynamin-2 is recruited to the site of the pit where it forms a collar-like structure at the neck of the coated pit (Mulcahy 2014). Once the pit is formed Dynamin-2 undergoes GTPase hydrolysis and the pit pinches off from the membrane (Mulcahy 2014). Dynamin-2 also helps with membrane binding and curvature during clathrin-dependent endocytosis (Mulcahy 2014). Therefore, Dynasore blocks the GTPase activity of Dynamin-2 thus inhibiting clathrin-mediated endocytosis (Dutta 2012). However, it should be noted that Dynamin-2 is also involved in caveolae-dependent endocytosis as it performs a similar function in pinching off caveolin-1 coated vesicles (Dutta 2012, Mulcahy 2014, Behzadi 2017).

Caveolae that participate in caveolae-dependent endocytosis are subdomains of glycolipid rafts and are rich in cholesterol, sphingolipids, and caveolins (Mulcahy 2014). Methyl- $\beta$ -cyclodextrin (M $\beta$ CD) was chosen to block caveolae-dependent endocytosis since it depletes cholesterol, thus preventing caveolin-coated pits forming at high cholesterol sites. Similarly, M $\beta$ CD may affect entry through lipid rafts, which are areas of the plasma membrane that have high levels of cholesterol and can mediate endocytosis independent of clathrin and caveolin-independent endocytosis (Dutta 2012, Mulcahy 2014). So M $\beta$ CD acts as an inhibitor of both lipid rafts and caveolin-dependent endocytosis.

To examine which endocytic pathways were involved in bare and MknPs uptake, Day 3 HSPCs were pre-incubated with DMA, M $\beta$ CD, Dynasore, or LY29400, which target macropinocytosis, lipid rafts, dynamin-dependent endocytosis, and macropinocytosis through PI3K, respectively. HSPCs were exposed to the inhibitors

for 45mins at 37°C, then co-cultured with bare NPs or MKNPs for 30mins at 37°C. Mean Fluorescence Intensity (MFI) of DiD was measured under flow cytometry for both bare NPs and MKNPs.

For bare NPs (Figure 26), we found that M $\beta$ CD treatment significantly decreased bare NP uptake by 22% and Dynasore treatment significantly decreased bare NP uptake by 50%, compared to the bare NP control. These data suggest that lipid rafts and dynamin-dependent endocytosis play a role in bare NP uptake by HSPCs. As bare NPs absorb serum proteins when incubated in cell culture media allowing them to be taken in through receptor-mediated endocytosis (Verma and Stellacci 2010), these results are fairly consistent with published literature to the effect that PLGA NPs are internalized through clathrin-based endocytosis (Danhier, Ansorena et al. 2012, Dizaj, Jafari et al. 2014). DMA treatment and LY29400 treatment were not significant, rendering these treatments ineffective for blocking endocytosis of bare NPs. Based on these results we can assume that macropinocytosis does not play a role in uptake of our bare NPs. In a similar experiment, uptake of bare PLGA NPs decreased when 4T1 breast cancer cells were blocked with chlorpromazine, BFA, NaN<sub>3</sub> with deoxglucose, cyto-D, and nocodazole, suggesting that PLGA NPs enter 4T1 breast cancer cells through clathrin-dependent endocytosis (Kang, Zhu et al. 2017).

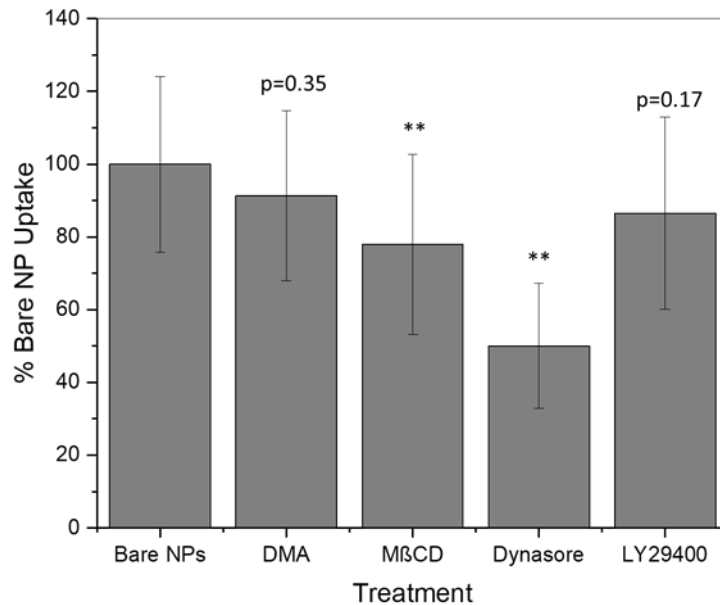


Figure 26. Lipid rafts and Dynamin are involved in the uptake bare PLGA NPs by HSPCs. Day 3 HSPCs were pre-incubated with specific inhibitors of endocytic pathways. Inhibitors used were Dimethylamiloride (DMA), Methyl- $\beta$ -cyclodextrin (M $\beta$ CD), Dynasore, and LY29400, which target macropinocytosis, lipid raft, dynamin-dependent endocytosis, and macropinocytosis through PI3K, respectively. 5mM M $\beta$ CD, 10 $\mu$ M DMA, 80 $\mu$ M Dynasore, and 50 $\mu$ M LY29400 for 45mins at 37°C, before co-culture with bare NPs for 30mins. Uptake of Bare NPs were analyzed by flow cytometry. Data represent the average of 6 biological replicates  $\pm$  standard error of the mean. \*, p<0.05; \*\*, p<0.01

When we examined the MFI for the MkNPs, we found that the Dynasore treatment significantly decreased MkNP uptake by 39% (Figure 27) when compared to the MkNP control. This datum suggests that uptake of MkNPs involves dynamin-dependent endocytosis. The M $\beta$ CD treatment decreased MkNP uptake by 21%; however, this was not statistically significant, suggesting that lipid rafts do not play as large as a role in MkNP uptake by HSPCs. Like the bare NPs, DMA and LY29400

treatments showed no statistically significant effect on uptake of MkNPs suggesting that macropinocytosis is not involved.

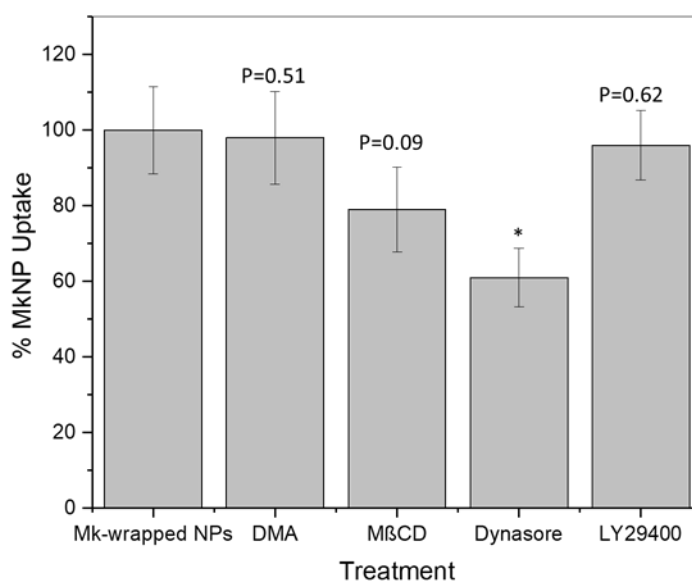


Figure 27. Dynamin-dependent endocytosis is involved in uptake of MkNPs by HSPCs. Day 3 HSPCs were pre-incubated with specific inhibitors against endocytic pathways. Inhibitors used were Dimethylamiloride (DMA), Methyl- $\beta$ -cyclodextrin (M $\beta$ CD), Dynasore, and LY29400, which target macropinocytosis, lipid raft, dynamin-dependent endocytosis, and macropinocytosis through PI3K, respectively. 10 $\mu$ M DMA, 5mM M $\beta$ CD, 80 $\mu$ M Dynasore, and 50 $\mu$ M LY29400 for 45mins at 37°C, before co-culture with Mk-wrapped NPs for 30mins. Uptake of MkNPs were analyzed by flow cytometry. Data represent the average of 6 biological replicates  $\pm$  standard error of the mean. \*,  $p < 0.05$ ; \*\*,  $p < 0.01$

In the 4T1 breast cancer cell experiment mentioned above, uptake of neutrophil membrane wrapped PLGA NPs decreased when 4T1 breast cancer cells

were blocked with  $\text{NaN}_3$ , Cyto-D, filipin, genistein, and monensin suggesting neutrophil-wrapped NPs enter 4T1 breast cancer cells through caveolae-dependent endocytosis. It is believed that membrane attachment on the NP induced a different endocytic pathway (Kang, Zhu et al. 2017). This is suggestive of our wrapped NPs; however, this data cannot be conclusive. As mentioned above, this study set was performed without knowing the concentrations of the bare NPs or the MkNPs. Therefore, the data are presented as two separate studies and cannot be compared to each other.

### **3.4 Discussion**

Jiang et al previously shown that MkMPs target and are taken in by HSPCs through membrane fusion and endocytosis (Jiang 2017). Therefore, we hypothesized that the Mk-membrane would target the wrapped NPs towards the HSPCs and that the HSPCs would uptake the wrapped NPs. We see that the Mk membranes are wrapping around the NPs based on the colocalization of the signals (Figure 17) and that the wrapped NPs are interacting with the HSPCs. We have visualized internalized MkNPs at 24hrs through Confocal and Super Resolution microscopy (Figure 18 and 19) and confirmed with flow cytometry (Figure 20). To improve our flow cytometry analysis, it may be possible to use Trypan blue, or some other reagent that does not interfere with our fluorophores, to quench external signals on our HSPCs after co-culture. Trypan blue was used to quench signals from externally attached C6 loaded PLGA NPs to differentiate between cell-associated (external) and internal signals when the C6-NPs were co-cultured with HSPCs (McNeer, Chin et al. 2011). This may be a useful tool for our flow cytometry analysis and worth further investigating.

The endocytic mechanism in which the bare and wrapped NPs were entering the HSPCs was also of interest to us. We observed that bare PLGA NPs were taken in through lipid rafts and dynamin-dependent endocytosis (Figure 26) while MkNPs are taken into HSPCs through dynamin-dependent endocytosis (Figure 27). To further determine how the MkNPs are getting into the HSPCs, we can perform an antibody-blocking assay that will block specific surface molecules on the MkNPs and HSPCs to see if MkNPs are still internalized. Previously, when CD54 on HSPCs, and CD11b and CD18 on MkMPs were blocked, uptake of MkMPs was reduced (Jiang 2017). When CD43 on HSPCs was blocked, however, MkMP uptake increased (Jiang 2017). Utilizing the same assay, we plan to block CD11b and CD18 on the MkNPs and CD43 and CD54 on the HSPCs to see if uptake of MkNPs still occurs.

To further assess the target specificity of MkNPs, we plan to expose MkNPs to different cell types such as granulocytes, MSCs, HUVECs. We hypothesize that as Mks naturally target HSPCs, membranes derived from Mks will wrap NPs correctly, preserving its natural targeting abilities, producing MkNPs that will only target HSPCs. We should not see any uptake of MkNPs with the different cell types mentioned above.

## Chapter 4

### FUTURE DIRECTIONS

Understanding the route of NP uptake is important for mediating their intracellular fate and biological response (Chou 2011). As we would like to load the NPs with genetic cargo in future, it is necessary to ensure they are being delivered to the cytoplasm or nucleus to initiate a genotypic response in HSPCs. Once substances are internalized through endocytosis into endosomal vesicles they are often end up in degradative lysosomes (Behzadi 2017). For genetic cargo to be delivered to the cytoplasm and nucleus it must escape out of the endosome and avoid lysosomal degradation. PLGA NPs possess the ability to escape endosomal degradation by selectively reversing the surface charge of PLGA (from anionic to cationic) under acidic conditions (Paulo, Pires das Neves et al. 2011) making them ideal candidates for delivery of genetic cargo. However, it also been shown that after internalization, PLGA NPs enter early endosomes, Golgi apparatus, and endoplasmic reticulum (Paulo, Pires das Neves et al. 2011). The final location of the NP depended on the size, surface coverage, and charge of the NPs (Paulo, Pires das Neves et al. 2011). Therefore, the membrane wrapped around of NP may influence whether the cargo is delivered to the cytoplasm or nucleus.

Currently, the MKNPs are entering through dynamin-dependent endocytosis. This means the wrapped NPs are recognizing receptors on the HSPCs, causing the clathrin-coated pits to invaginate and dynamin causing the vesicles to pinch off. At this point we cannot tell if the bare or wrapped NPs are degrading and releasing their

cargo once internalized by the cell. This step is crucial for delivery of genetic cargo. To ensure that our MkNPs can deliver cargo to HSPCs to induce a genotypic/phenotypic response we must load our NPs with genetic cargo.

A type of genetic cargo considered for delivery are small RNA molecules (19-40 nucleotides) that induce gene silencing at a post-transcriptional level (Paulo, Pires das Neves et al. 2011), known as small interfering RNAs (siRNAs). siRNAs bind to Argonaut proteins (AGO) to form RNA-induced silencing complexes (RISCs), which recognize target RNAs and induce repression of gene expression (Paulo, Pires das Neves et al. 2011). These siRNAs can be useful to knockdown specific targets in various diseases or for genetic enhancement. Unfortunately, naked siRNA is quickly degraded by endogenous enzymes and is unable to cross cellular membranes due to its large size (~13kDa) and high negative charge (Paulo, Pires das Neves et al. 2011). Therefore, loading siRNA into NPs will provide protection against endogenous enzymes and will allow the siRNA to be released into the cytoplasm and knock down the target (Paulo, Pires das Neves et al. 2011).

As proof-of-principle, some siRNA targets we are interested in studying would be to use an siRNA against GFP or CD34. For GFP expression, we would first have to transfect the HSPCs with a GFP-plasmid either through nucleofection or electroporation. GFP expression would be easily confirmed by flow cytometry or Confocal. Then, we would load MkNPs loaded with siRNA-GFP and use Confocal or flow cytometry to see if GFP expression decreases. A decreased GFP expression suggests that siGFP was delivered to the cytoplasm and bound to AGO to form RISC. The complex would then recognize GFP RNAs and knock them down, decreasing

GFP expression. Negative control in this study would be NPs loaded with scrambled siRNA and positive control would be naked siRNA.

Another siRNA of interest is siRNA-CD34. Young HSPCs highly express the selectable marker CD34 before they differentiate into other blood lineage cell types. If we deliver NPs loaded with siCD34 to HSPCs we would expect to see a decrease in CD34 expression. To test this hypothesis, we would deliver siCD34 NPs to HSPCs and monitor their CD34 expression levels over the course of a couple of days. We would compare a normal culture (control), to bare siCD34 NPs, to Mk-wrapped siCD34 NPs. As the Mk membrane enhances interaction and uptake with the HSPCs we expect to see a larger decrease of CD34 expression in HSPCs co-cultured with MkNPs. The decrease in CD34 expression may cause the HPSCs to differentiate into other blood lineage cell types faster, thus allowing for faster turnover for Mks, MkMPs, or platelets.

Since our cargo-loaded NPs could be utilized in genetic therapies, we are interested in seeing where the NPs travel *in vivo*. Using a mouse model, we plan on injecting MkNPs loaded with DiD intravenously to study their biodistribution. It was previously found that intravenously injected fluorescently labeled RBC-membrane wrapped PLGA NPs were mostly distributed mainly in the blood and liver (Hu, Zhang et al. 2011). The large quantity of NPs found in the blood was attributed to the RBC membrane covering the NP and allowing for longer circulation time (Hu, Zhang et al. 2011). In a different study, it was found that cancer cell membrane wrapped indocyanine green-loaded lipid polymer NPs with PLGA cores were able to evade liver and kidney and target tumors more effectively than unwrapped NPs (Chen 2016). It was also found, in a separate small pilot study, that when mice were intravenously

or intraperitoneally injected with bare C6-loaded PLGA NPs small percentages of the NPs localized to bone marrow after 6 hours with clearance by 24hrs (McNeer, Schleifman et al. 2011). Intravenous injections led to higher percentage of NPs in the bone marrow compared to intraperitoneal injections possibly due to widespread distribution and less NPs being cleared by the liver, as seen with intraperitoneal injections (McNeer, Schleifman et al. 2011).

Based on these results and knowing that MkMPs target and interact with HSPCs, we hypothesize that, once intravenously injected, we will see a higher distribution of MkNPs in the mice bone marrow compared to bare NPs. This will confirm that our Mk membrane is allowing for targeted specificity and that our wrapped NPs can reach the bone marrow once intravenously injected. We could also inject our cargo-loaded NPs to see if any phenotypic response is produced in our mice.

## REFERENCES

- Behzadi, S., Serpooshan, V., Tao, W., Hamaly, M.A., et al. (2017). "Cellular uptake of nanoparticles: journey inside of the cell " Chem Soc Rev.
- Cabrita, G. J., B. S. Ferreira, C. L. da Silva, R. Goncalves, G. Almeida-Porada and J. M. Cabral (2003). "Hematopoietic stem cells: from the bone to the bioreactor." Trends Biotechnol **21**(5): 233-240.
- Chen, J., Z. Guo, H. Tian and X. Chen (2016). "Production and clinical development of nanoparticles for gene delivery." Mol Ther Methods Clin Dev **3**: 16023.
- Chen, Z. (2016). "Cancer cell membrane-biomimetic nanoparticles for homologous-targeting dual-modal imaging and photothermal therapy." ACS Nano **10**: 10049-10057.
- Chou, L. Y. T., Ming, K., Chan, W.C.W. (2011). "Strategies for the intracellular delivery of nanoparticles." Chem Soc Rev **40**: 233-245.
- Danhier, F., E. Ansorena, J. M. Silva, R. Coco, A. Le Breton and V. Preat (2012). "PLGA-based nanoparticles: an overview of biomedical applications." J Control Release **161**(2): 505-522.
- Diener, Y., A. Bosio and U. Bissels (2016). "Delivery of RNA-based molecules to human hematopoietic stem and progenitor cells for modulation of gene expression." Exp Hematol **44**(11): 991-1001.
- Diener, Y., Jurk, M., Kandil, B., Choi, YH., Wild, S., Bissels, U., Bosio, A. (2015). "RNA-based, transient modulation of gene expression in human haematopoietic stem and progenitor cells." Scientific Reports **5**(1-10).
- Dizaj, S. M., S. Jafari and A. Y. Khosroushahi (2014). "A sight on the current nanoparticle-based gene delivery vectors." Nanoscale Res Lett **9**(1): 252.
- Domen, J., Wagers, A., Weissman, I.L. (2006). Bone marrow (Hematopoietic) stem cells. Regenerative Medicine: 13-34.
- Dragovic, R. A., C. Gardiner, A. S. Brooks, D. S. Tannetta, D. J. Ferguson, P. Hole, B. Carr, C. W. Redman, A. L. Harris, P. J. Dobson, P. Harrison and I. L. Sargent (2011).

"Sizing and phenotyping of cellular vesicles using Nanoparticle Tracking Analysis." Nanomedicine **7**(6): 780-788.

Dutta, D. a. D., J.G. (2012). "Search for inhibitors of endocytosis." Cellular Logistics **2**(4): 203-208.

Escobar, C. (2017). Human megakaryocytic microparticles target murine hematopoietic stem cells to stimulate in vivo platelet biogenesis. MS in Biological Sciences, University of Delaware.

Fang, R. H., C. M. Hu, B. T. Luk, W. Gao, J. A. Copp, Y. Tai, D. E. O'Connor and L. Zhang (2014). "Cancer cell membrane-coated nanoparticles for anticancer vaccination and drug delivery." Nano Lett **14**(4): 2181-2188.

Flaumenhaft, R., J. R. Dilks, J. Richardson, E. Alden, S. R. Patel-Hett, E. Battinelli, G. L. Klement, M. Sola-Visner and J. E. Italiano, Jr. (2009). "Megakaryocyte-derived microparticles: direct visualization and distinction from platelet-derived microparticles." Blood **113**(5): 1112-1121.

Fuhrken, P. G., C. Chen, W. M. Miller and E. T. Papoutsakis (2007). "Comparative, genome-scale transcriptional analysis of CHR-288-11 and primary human megakaryocytic cell cultures provides novel insights into lineage-specific differentiation." Exp Hematol **35**(3): 476-489.

Goodman, M. A. and P. Malik (2016). "The potential of gene therapy approaches for the treatment of hemoglobinopathies: achievements and challenges." Ther Adv Hematol **7**(5): 302-315.

Hu, C. M. J., L. Zhang, S. Aryal, C. Cheung, R. H. Fang and L. F. Zhang (2011). "Erythrocyte membrane-camouflaged polymeric nanoparticles as a biomimetic delivery platform." Proceedings of the National Academy of Sciences of the United States of America **108**(27): 10980-10985.

Jiang, J., Kao, CY., Papoutsakis, E.T. (2017). "How do megakaryocytic microparticles target and deliver cargo to alter the fate of hematopoietic stem cells?" Journal of Controlled Release **247**: 1-18.

Jiang, J., D. S. Woulfe and E. T. Papoutsakis (2014). "Shear enhances thrombopoiesis and formation of microparticles that induce megakaryocytic differentiation of stem cells." Blood **124**(13): 2094-2103.

- Kang, T., Q. Zhu, D. Wei, J. Feng, J. Yao, T. Jiang, Q. Song, X. Wei, H. Chen, X. Gao and J. Chen (2017). "Nanoparticles Coated with Neutrophil Membranes Can Effectively Treat Cancer Metastasis." ACS Nano **11**(2): 1397-1411.
- Kroll, A. V., R. H. Fang and L. Zhang (2017). "Biointerfacing and Applications of Cell Membrane-Coated Nanoparticles." Bioconjug Chem **28**(1): 23-32.
- Kuhn, D. A., D. Vanhecke, B. Michen, F. Blank, P. Gehr, A. Petri-Fink and B. Rothen-Rutishauser (2014). "Different endocytotic uptake mechanisms for nanoparticles in epithelial cells and macrophages." Beilstein J Nanotechnol **5**: 1625-1636.
- Luk, B. T., C. M. Hu, R. H. Fang, D. Dehaini, C. Carpenter, W. Gao and L. Zhang (2014). "Interfacial interactions between natural RBC membranes and synthetic polymeric nanoparticles." Nanoscale **6**(5): 2730-2737.
- Luk, B. T. and L. Zhang (2015). "Cell membrane-camouflaged nanoparticles for drug delivery." J Control Release **220**(Pt B): 600-607.
- Machlus, K. R. and J. E. Italiano, Jr. (2013). "The incredible journey: From megakaryocyte development to platelet formation." J Cell Biol **201**(6): 785-796.
- McNeer, N. A., J. Y. Chin, E. B. Schleifman, R. J. Fields, P. M. Glazer and W. M. Saltzman (2011). "Nanoparticles deliver triplex-forming PNAs for site-specific genomic recombination in CD34+ human hematopoietic progenitors." Mol Ther **19**(1): 172-180.
- McNeer, N. A., E. B. Schleifman, P. M. Glazer and W. M. Saltzman (2011). "Polymer delivery systems for site-specific genome editing." J Control Release **155**(2): 312-316.
- Mulcahy, L. A., Pink, R.C., Carter, D.R.F. (2014). "Routes and mechanisms of extracellular vesicle uptake." Journal of Extracellular Vesicles **3**(1).
- Nishikii, H., N. Kurita and S. Chiba (2017). "The Road Map for Megakaryopoietic Lineage from Hematopoietic Stem/Progenitor Cells." Stem Cells Transl Med **6**(8): 1661-1665.
- Ogawa, M. (1993). "Differentiation and Proliferation of Hematopoietic Stem Cells." Blood **81**(11): 2844-2853.
- Panuganti, S., A. C. Schlinker, P. F. Lindholm, E. T. Papoutsakis and W. M. Miller (2013). "Three-stage ex vivo expansion of high-ploidy megakaryocytic cells: toward large-scale platelet production." Tissue Eng Part A **19**(7-8): 998-1014.

Patel, S. R., Hartwig, J.H., Italiano, J.E. (2005). "The biogenesis of platelets from megakaryocyte proplatelets." Journal of Clinical Investigation **115**(12): 3348-3354.

Paulo, C. S., R. Pires das Neves and L. S. Ferreira (2011). "Nanoparticles for intracellular-targeted drug delivery." Nanotechnology **22**(49): 494002.

Toledano Furman, N. E., Y. Lupu-Haber, T. Bronshtein, L. Kaneti, N. Letko, E. Weinstein, L. Baruch and M. Machluf (2013). "Reconstructed stem cell nanoghosts: a natural tumor targeting platform." Nano Lett **13**(7): 3248-3255.

Verma, A. and F. Stellacci (2010). "Effect of surface properties on nanoparticle-cell interactions." Small **6**(1): 12-21.

Yin, H. e. a. (2014). "Non-viral vectors for gene-based therapy." Nature Reviews: Genetics **15**: 541-555.

Yu, K. R., H. Natanson and C. E. Dunbar (2016). "Gene Editing of Human Hematopoietic Stem and Progenitor Cells: Promise and Potential Hurdles." Hum Gene Ther **27**(10): 729-740.

Zhai, Y., J. Su, W. Ran, P. Zhang, Q. Yin, Z. Zhang, H. Yu and Y. Li (2017). "Preparation and Application of Cell Membrane-Camouflaged Nanoparticles for Cancer Therapy." Theranostics **7**(10): 2575-2592.

## Appendix A

### MEMBRANE-COLLECTION AND NP WRAPPING

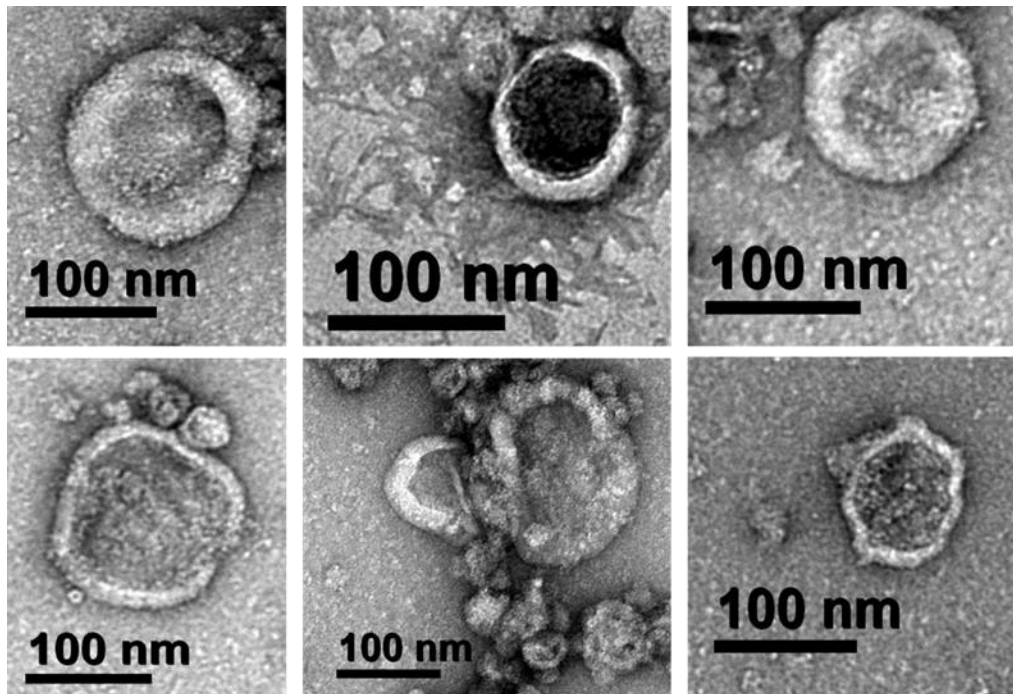


Figure A1. PMA-CHRF membrane vesicles visualized on TEM. PMA-CHRF vesicles were generated by membrane extraction process and extruded through 400nm membrane pore. All samples were placed on a 400nm Carbon coated grid and negatively stained with 1% PTA (sodium) (pH 7.2) and visualized with TEM.

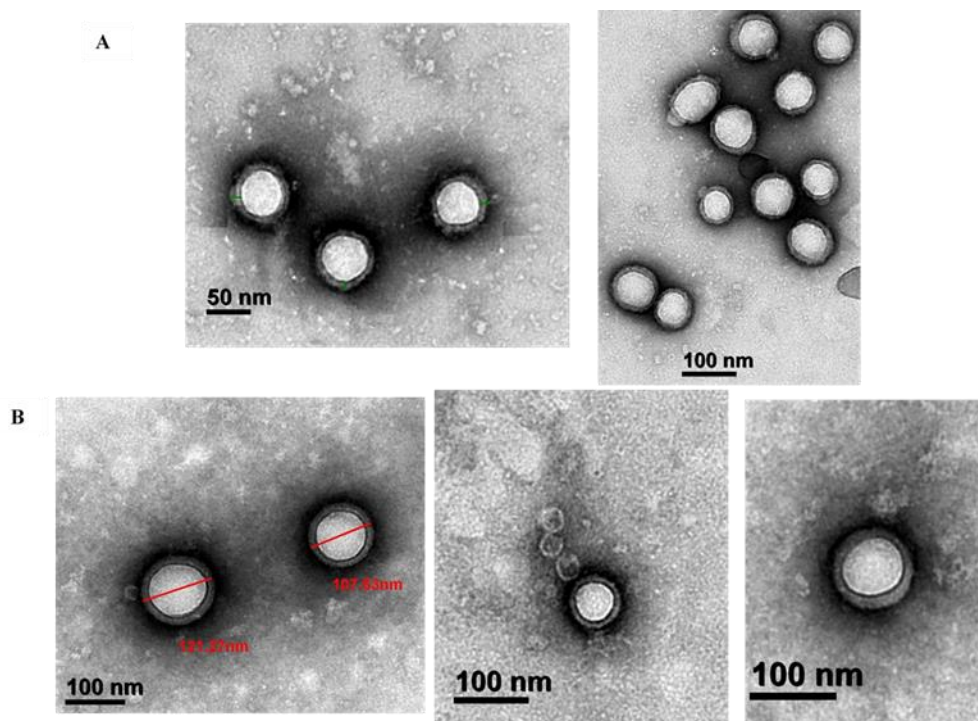


Figure A2. PMA-CHRF wrapped NPs visualized on TEM. (A) PMA-CHRF wrapped 5.2mg/mL NPs generated on 9/26/17 (B) PMA-CHRF wrapped 4.83 mg/mL NPs generated on 10/03/17. All samples were placed on a 400nm Carbon coated grid and negatively stained with 1% PTA (sodium) (pH 7.2) and visualized with TEM.

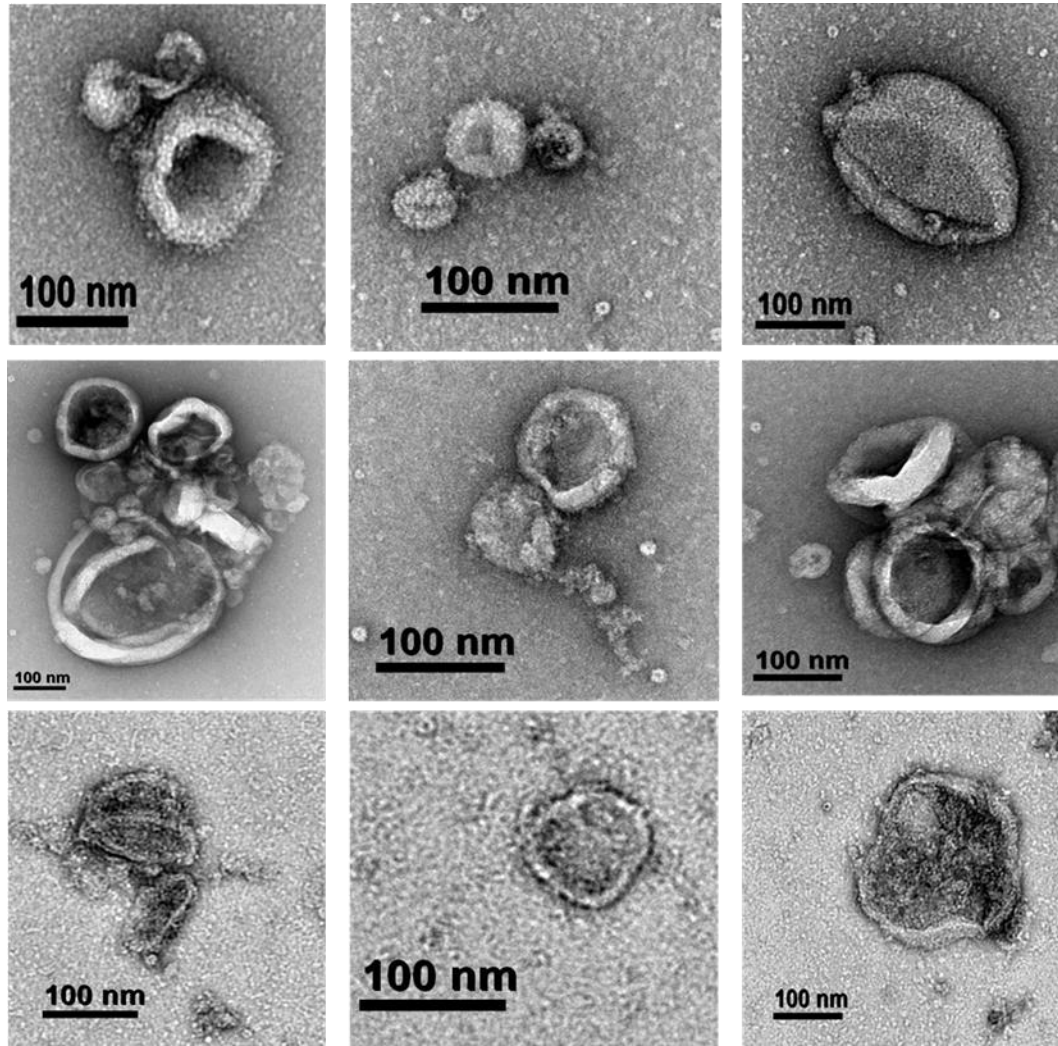


Figure A3. MkMVs. Top row: MkMVs isolated from  $2.0 \times 10^7$  Day 12 Mk cells on 5/28/2018. Middle row: Mk membrane vesicles isolated from  $1.1 \times 10^7$  Day 12 Mk cells on 6/19/2018. Bottom row: Mk membrane vesicles isolated from  $6.0 \times 10^6$  D12 Mk cells on 7/10/2018. All membrane vesicles were extruded through 400nm membrane pore 11 times. All samples were placed on a 400nm Carbon coated grid and negatively stained with 2% uranyl acetate and visualized with TEM.

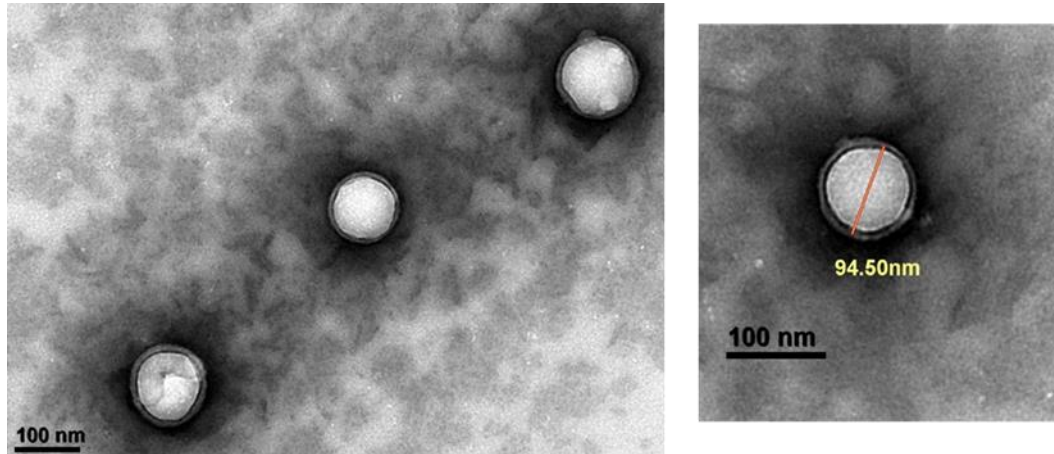


Figure A4. MnPs visualized on TEM. Day 12 Mk membranes wrapped 0.25 mg/mL NPs through extrusion of 400nm pore on 2/02/2018. All samples were placed on a 400nm Carbon coated grid and negatively stained with 1% PTA (sodium) (pH 7.2) and visualized with TEM.

## Appendix B

### FURTHER CHARACTERIZATION OF MK-WRAPPED NPs

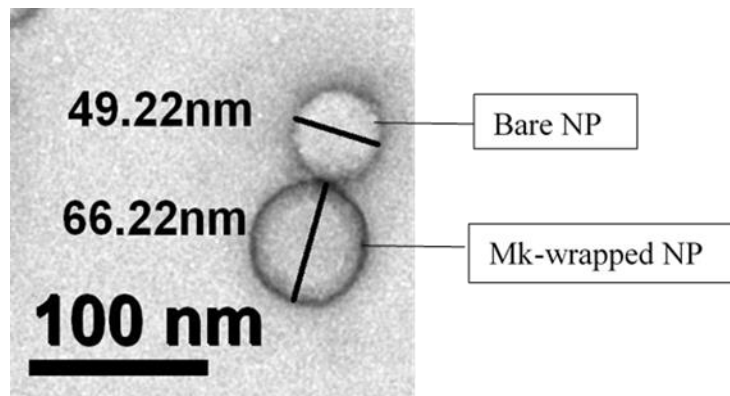


Figure B1. Secondary layer surrounding the NP indicates wrapping and increases size of NPs. Top structure is a bare NP and bottom structure is a Mk-wrapped NP. Vesicles were isolated from  $4.4 \times 10^6$  Day 12 Mk cells and use to wrap NPs ranging in size of 50-75nm on 1/10/2018. Particles labeled using a tool on Libra 120 Software to show size increase.

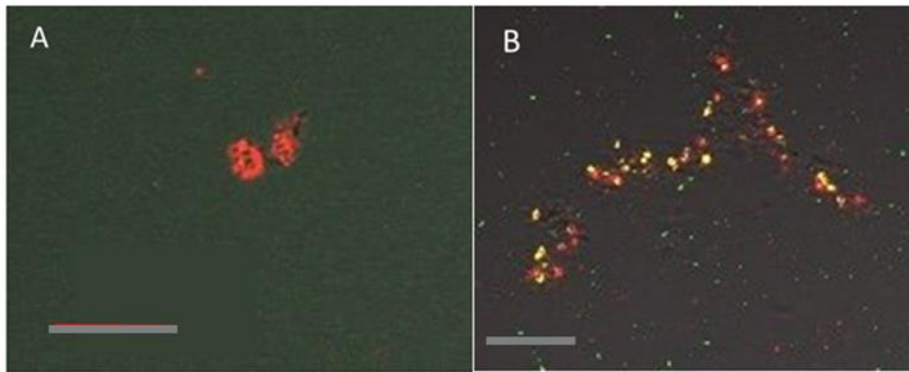


Figure B2. MkNPs are FITC-CD41<sup>+</sup>. Bare NPs (A) loaded with DiD (red) were wrapped with un-dyed Mk membranes. Wrapped NPs (B) were exposed to FITC-CD41 (green) and visualized under 40X oil on Confocal 880. The scale bare is 20 $\mu$ m. Any yellow suggests colocalization of both signals.

## Appendix C

### MK-WRAPPED NPS INTERACTING WITH HSPCs

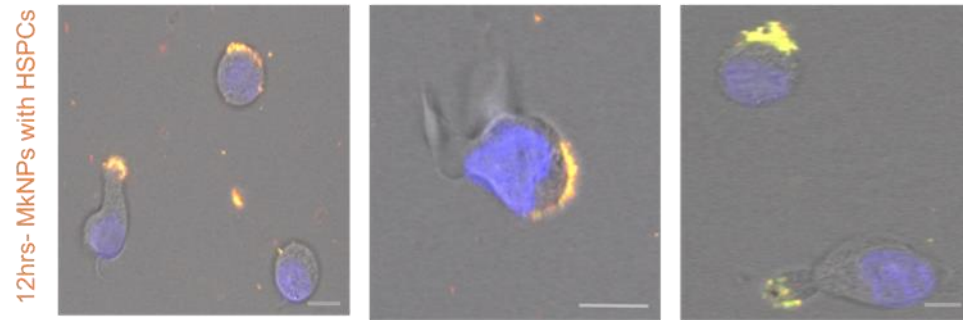


Figure C1. MkNPs appear to aggregate at HSPCs' membrane surface at 12hrs. MkNPs show colocalization of signals but no uptake when exposed to Day 3 HSPCs for 12hrs. Images taken on Confocal LMS880. Nuclei stained with DAPI. Scale bar represents 10 $\mu$ m.

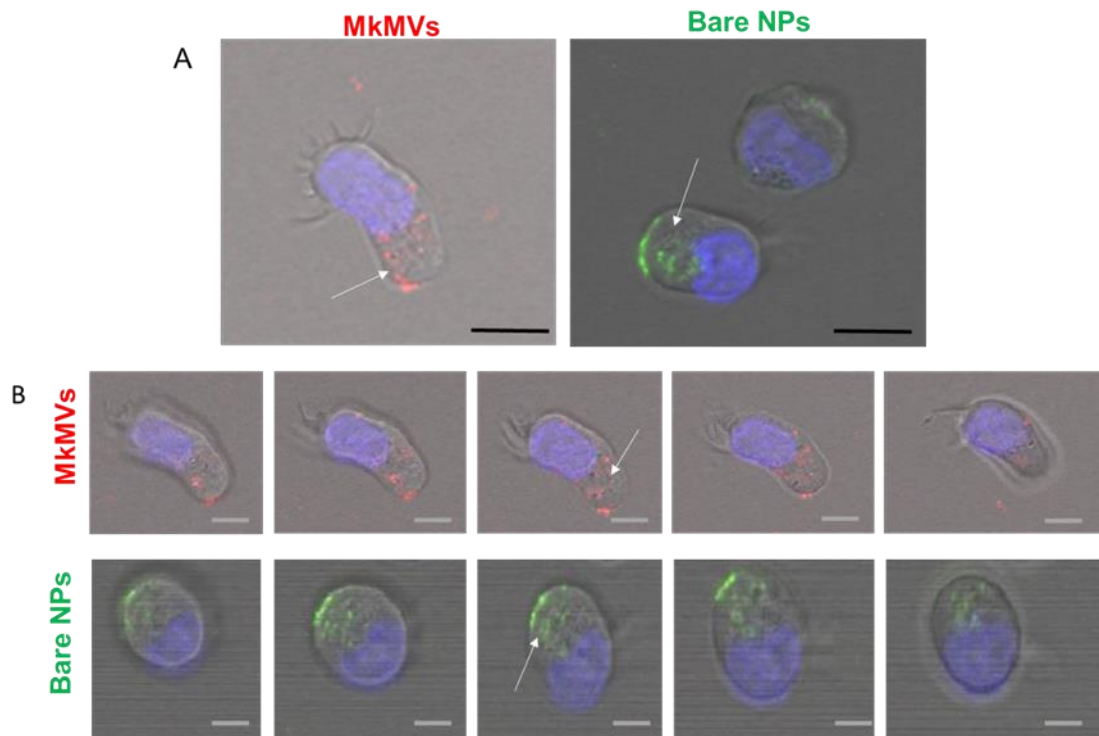


Figure C2. HSPCs take in MkmVVs and Bare NPs at 12hrs. (A) Static images of HSPCs with MkmVVs stained with PKH26 (red) and Bare NPs (green) (B) Static images taken from Z-stacks in sequence. Z-stacks and images taken on Confocal LMS880. Arrows point to uptake of either MkmVVs or Bare NPs. Nuclei stained with DAPI. Scale bar represents 10µm.

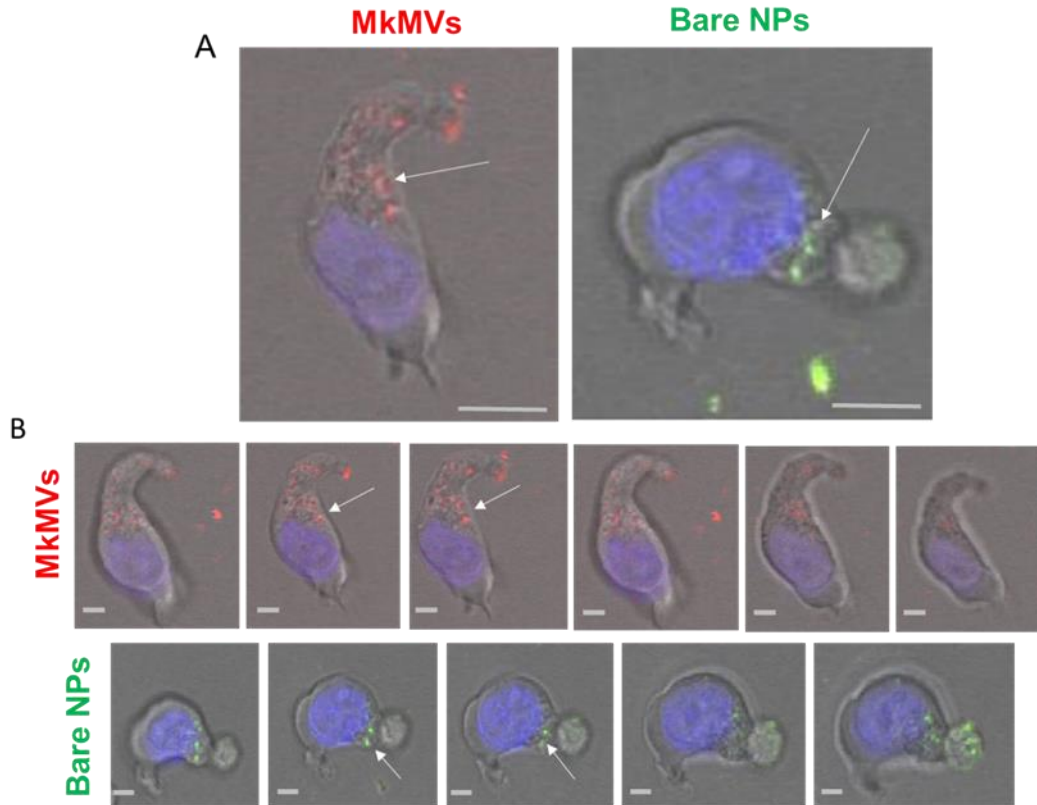


Figure C3. HSPCs take in MkmVVs and Bare NPs at 24hrs. (A) Static images of HSPCs with MkmVVs stained with PKH26 (red) and Bare NPs (green). (B) Static images taken from Z-stacks in sequence. Z-stacks and images taken on Confocal LMS880. Arrows point to uptake of either MkmVVs or Bare NPs. Nuclei stained with DAPI. Scale bar represents 10 $\mu$ m.

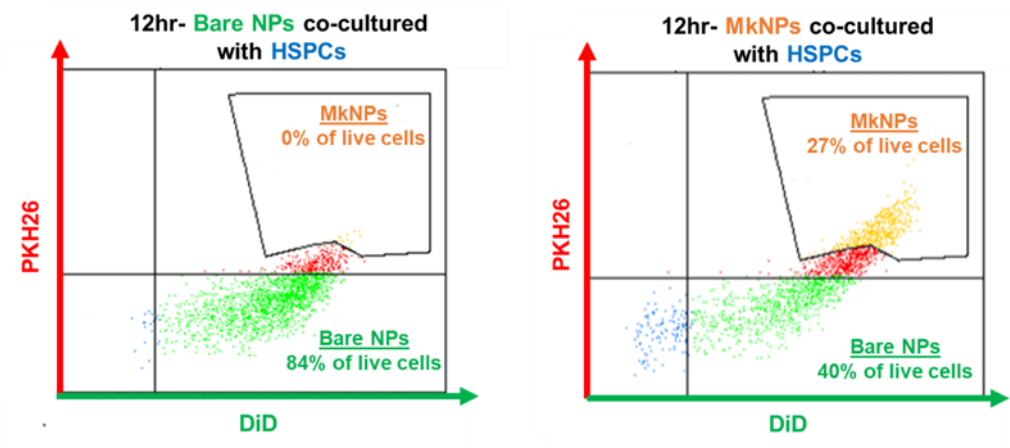


Figure C4. MkNPs detected on flow cytometry interacting with HSPCs at 12hrs. Mk membranes stained with PKH26 (red) and NPs loaded with DiD (green) were extruded to form MkNPs (yellow). Particles were co-cultured with Day 3 HSPCs for 12 hours and then measured using flow cytometry (FACS Aria). Gate represents wrapped NPs. Blue color shows live cells positive for interaction.

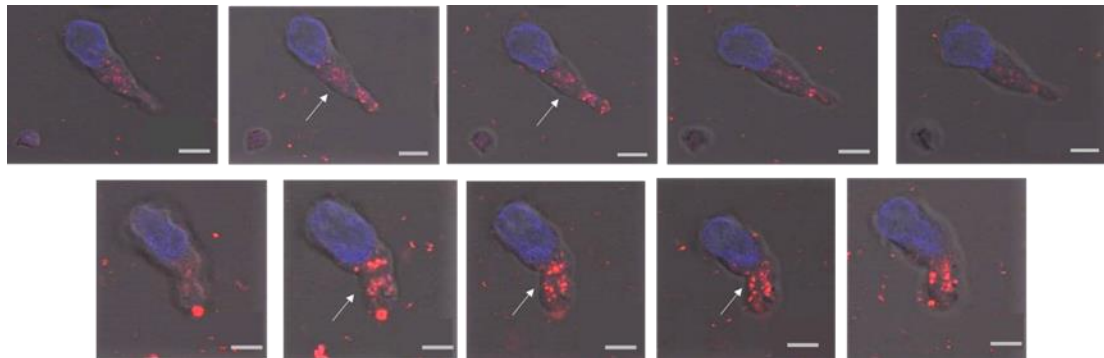


Figure C5. Uptake of MkMVs by HSPCs after 24hrs. Day 3 HSPCs were co-cultured with 175,000 MkMVs per cell for 24hrs. Mk membranes were dyed with PKH26 (red). Nuclei stained with DAPI (blue). Arrow points to uptake as nucleus comes into focus. Static images taken from Z-stack in sequence. Visualized on Confocal LMS880 under 40x oil. Scale bar is 5 $\mu$ m.

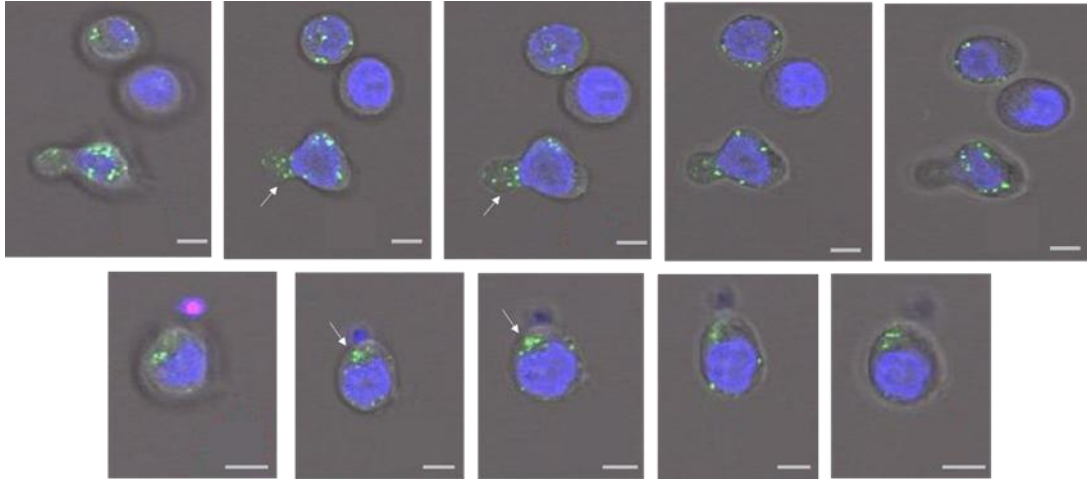


Figure C6. Uptake of bare NPs by HSPCs after 24hrs. Day 3 HSPCs were co-cultured with 43,900 bare NPs per cell for 24hrs. Bare NPs were dyed with DiD. Nuclei stained with DAPI. Arrow points to uptake as nucleus comes into focus. Static images taken from Z-stack in sequence. Visualized on Confocal LMS880 under 40x oil. Scale bar is 5 $\mu$ m.

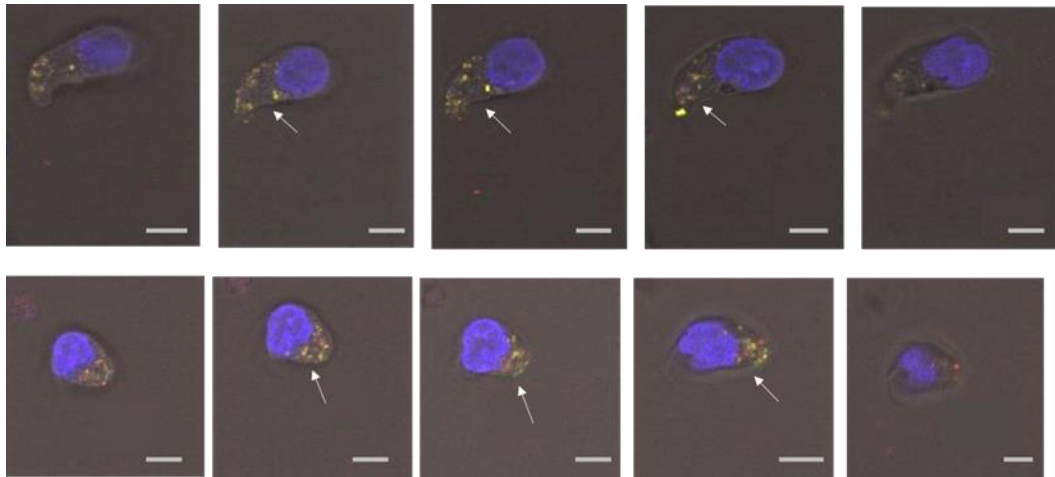


Figure C7. HSPCs uptake Mk-wrapped NPs after 24 hrs. Day 3 HPSCs were seeded with 77,000 MkNPs/cell. Mk membranes stained with PKH26 membrane dye (red), NPs loaded with DiD dye (green), Nuclei stained with DAPI (blue). Arrows point to uptake when nuclei are in focus. Yellow signals suggest colocalization. Visualized on Confocal LMS880 under 40x oil. Static images are taken from Z-stacks in sequence. Scale bar is 5 $\mu$ m.

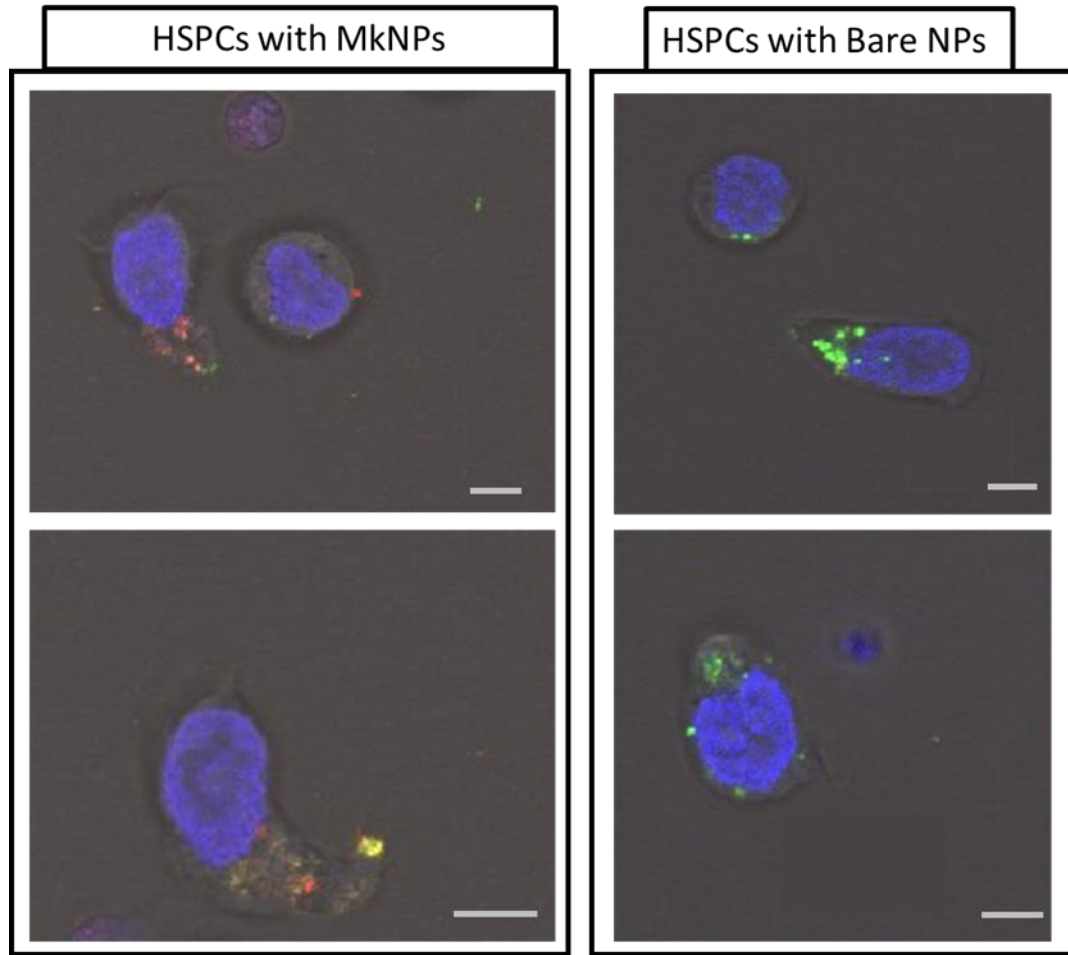


Figure C8. Comparison of HSPCs exposed to 43,000 particles/cell for 24hrs. Day 3 HSPCs were co-cultured with 43,000 MkNPs (left panels) or bare NPs (right panels) for 24hrs. Mk membranes are dyed with PKH26(red), NPs are dyed with DiD (green), Nuclei are stained with DAPI (blue). The yellow signals indicate colocalization. Visualized under Confocal LMS880. Scale bars are 5µm.

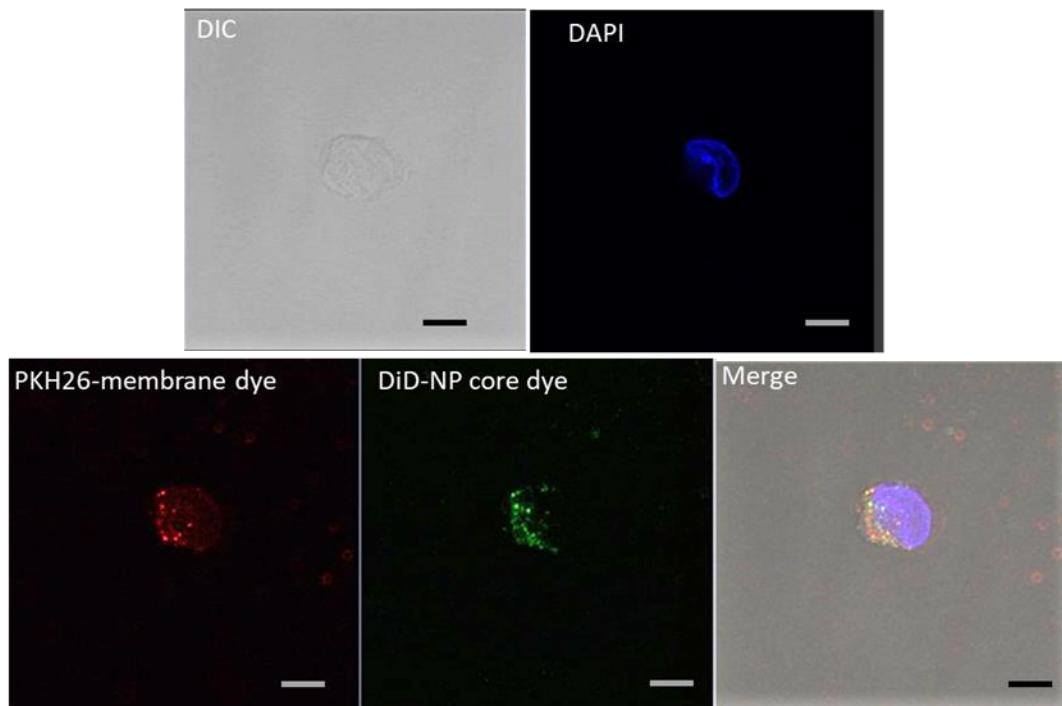
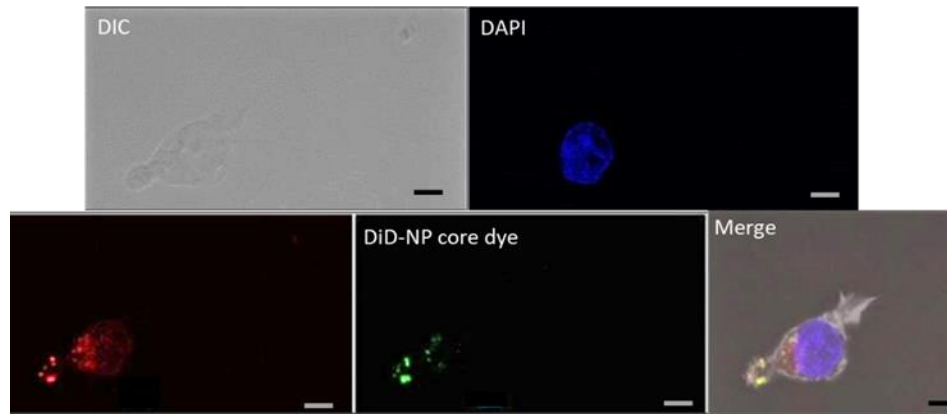


Figure C9. Split screens showing different channels. HSPCs were co-cultured with 77,000 MkNPs per cell for 24hrs. Mk-membranes were dyed with PKH26 (red), NPs were loaded with DiD dye (green), and nuclei were stained (blue), HSPCs were stained with phalloidin (white). Slides were fixed in 4% formaldehyde and visualized using Confocal LMS880 under 63X oil. Scale bar is 5 $\mu$ m.

**Appendix D**  
**HUMAN CONSENT FORM**

HUMAN SUBJECTS PROTOCOL  
University of Delaware

Protocol Title: Utilizing Primary Human Cells in the Papoutsakis Lab

Principal Investigator

Name: Eleftherios T. Papoutsakis  
Department/Center: Chemical and Biomolecular Engineering  
Contact Phone Number: 302-831-8376  
Email Address: epaps@udel.edu

Advisor (if student PI): N/A

Name:  
Contact Phone Number:  
Email Address:

Other Investigators: N/A

Investigator Assurance:

By submitting this protocol, I acknowledge that this project will be conducted in strict accordance with the procedures described. I will not make any modifications to this protocol without prior approval by the IRB. Should any unanticipated problems involving risk to subjects occur during this project, including breaches of guaranteed confidentiality or departures from any procedures specified in approved study documents, I will report such events to the Chair, Institutional Review Board immediately.

Rev. 05/2017

HUMAN SUBJECTS PROTOCOL  
University of Delaware

Protocol Title: Generation of Platelet-derived Microparticles

Principal Investigator

Name: Eleftherios T. Papoutsakis  
Department/Center: Chemical and Biomolecular Engineering  
Contact Phone Number: 302-831-8376  
Email Address: epaps@udel.edu

Advisor (if student PI): N/A

Name:  
Contact Phone Number:  
Email Address:

Other Investigators: N/A

Investigator Assurance:

By submitting this protocol, I acknowledge that this project will be conducted in strict accordance with the procedures described. I will not make any modifications to this protocol without prior approval by the IRB. Should any unanticipated problems involving risk to subjects occur during this project, including breaches of guaranteed confidentiality or departures from any procedures specified in approved study documents, I will report such events to the Chair, Institutional Review Board immediately.

## Appendix E

### INSTITUTIONAL ANIMAL CARE AND USE COMMITTEE FORM AUP# 1326-2017-0

University of Delaware  
Institutional Animal Care and Use Committee  
Application to Use Animals in Research  
(New and 3-Yr submission)

RECEIVED  
JUL 24 2017  
IACUC

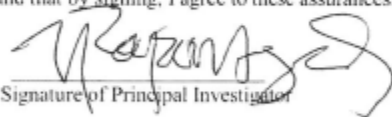
Title of Protocol: Utilization of Hybrid Nanoparticles for Targeted Cargo Delivery to Stem Cells	
AUP Number: 1326-2017-0	← (4 digits only — if new, leave blank)
Principal Investigators: Emily Day and E. Terry Papoutsakis	
Common Name (Strain/Breed if Appropriate): Mouse	
Genus Species: <i>Mus Musculus</i>	
Date of Submission:	

<b>Official Use Only</b>
IACUC Approval Signature: <u>Ann T. Talkington</u>
Date of Approval: <u>8/29/2017</u>

**Primary Principal Investigator Assurance**

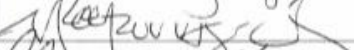
1. I agree to abide by all applicable federal, state, and local laws and regulations, and UD policies and procedures.	
2. I understand that deviations from an approved protocol or violations of applicable policies, guidelines, or laws could result in immediate suspension of the protocol and may be reportable to the Office of Laboratory Animal Welfare (OLAW).	
3. I understand that the Attending Veterinarian or his/her designee must be consulted in the planning of any research or procedural changes that may cause more than momentary or slight pain or distress to the animals.	
4. I declare that all experiments involving live animals will be performed under my supervision or that of another qualified scientist. All listed personnel will be trained and certified in the proper humane methods of animal care and use prior to conducting experimentation.	
5. I understand that emergency veterinary care will be administered to animals showing evidence of discomfort, ailment, or illness.	
6. I declare that the information provided in this application is accurate to the best of my knowledge. If this project is funded by an extramural source, I certify that this application accurately reflects all currently planned procedures involving animals described in the proposal to the funding agency.	
7. I assure that any modifications to the protocol will be submitted to by the UD-IACUC and I understand that they must be approved by the IACUC prior to initiation of such changes.	
8. I understand that the approval of this project is for a maximum of one year from the date of UD-IACUC approval and that I must re-apply to continue the project beyond that period.	
9. I understand that any unanticipated adverse events, morbidity, or mortality must be reported to the UD-IACUC immediately.	
10. I assure that the experimental design has been developed with <b>consideration of the three Rs: reduction, refinement, and replacement, to reduce animal pain and/or distress and the number of animals used in the laboratory.</b>	
11. I assure that the proposed research does not unnecessarily duplicate previous experiments. <i>(Teaching Protocols, including cooperative extension demonstrations, Exempt)</i>	
12. I understand that by signing, I agree to these assurances.	
 Signature of Principal Investigator	7-19-2017 Date

**Secondary Principal Investigator Assurance**

13. I agree to abide by all applicable federal, state, and local laws and regulations, and UD policies and procedures.	
14. I understand that deviations from an approved protocol or violations of applicable policies, guidelines, or laws could result in immediate suspension of the protocol and may be reportable to the Office of Laboratory Animal Welfare (OLAW).	
15. I understand that the Attending Veterinarian or his/her designee must be consulted in the planning of any research or procedural changes that may cause more than momentary or slight pain or distress to the animals.	
16. I declare that all experiments involving live animals will be performed under my supervision or that of another qualified scientist. All listed personnel will be trained and certified in the proper humane methods of animal care and use prior to conducting experimentation.	
17. I understand that emergency veterinary care will be administered to animals showing evidence of discomfort, ailment, or illness.	
18. I declare that the information provided in this application is accurate to the best of my knowledge. If this project is funded by an extramural source, I certify that this application accurately reflects all currently planned procedures involving animals described in the proposal to the funding agency.	
19. I assure that any modifications to the protocol will be submitted to by the UD-IACUC and I understand that they must be approved by the IACUC prior to initiation of such changes.	
20. I understand that the approval of this project is for a maximum of one year from the date of UD-IACUC approval and that I must re-apply to continue the project beyond that period.	
21. I understand that any unanticipated adverse events, morbidity, or mortality must be reported to the UD-IACUC immediately.	
22. I assure that the experimental design has been developed with <b>consideration of the three Rs: reduction, refinement, and replacement, to reduce animal pain and/or distress and the number of animals used in the laboratory.</b>	
23. I assure that the proposed research does not unnecessarily duplicate previous experiments. <i>(Teaching Protocols, including cooperative extension demonstrations, Exempt)</i>	
24. I understand that by signing, I agree to these assurances.	
 Signature of Principal Investigator	 Date

**NAMES OF ALL PERSONS WORKING ON THIS PROTOCOL.**

I certify that I have read this protocol, accept my responsibility and will perform only those procedures that have been approved by the IACUC.

Name	Signature
1. Erica Winter	
2. Jenna Harris	
3. Christian Escobar	
4. Chen-Yuan Kao	
5. Emily Day	
6. Terry Papoutsakis	
7. Gwen Talham	
8. Click here to enter text.	
9. Click here to enter text.	
10. Click here to enter text.	

If after hours participation is required by students on project involving **agricultural animals**, please describe how this is handled and the times and days that students may be on site.

Click here to enter text.

## Appendix F

### INSTITUTIONAL ANIMAL CARE AND USE COMMITTEE FORM AUP# 1290-2016-0

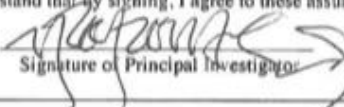
University of Delaware  
Institutional Animal Care and Use Committee  
Application to Use Animals in Research and Teaching

**RECEIVED**  
FEB 24 2017  
IACUC

Title of Protocol: Observation of Microparticle Injection and the Correlation between Induced Thrombocytopenia	
AUP Number: 1290-2016-0	← (4 digits only — if new, leave blank)
Principal Investigator: E. Terry Papoutsakis	
Common Name: Mouse	
Genus Species: Mus Muculus	
Pain Category: <i>(please mark one)</i>	
<b>USDA PAIN CATEGORY: (Note change of categories from previous form)</b>	
<input type="checkbox"/> B	Breeding or holding where NO research is conducted
<input checked="" type="checkbox"/> C	Procedure involving momentary or no pain or distress
<input checked="" type="checkbox"/> D	Procedure where pain or distress is alleviated by appropriate means (analgesics tranquilizers, euthanasia etc.)
<input type="checkbox"/> E	Procedure where pain or distress cannot be alleviated, as this would adversely affect the procedures, results or interpretation

<b>Official Use Only</b>	
IACUC Approval Signature:	<u><i>E. Terry Papoutsakis, DVM</i></u>
Date of Approval:	<u>3/27/17</u>

**Principal Investigator Assurance**

1. I agree to abide by all applicable federal, state, and local laws and regulations, and UD policies and procedures.	
2. I understand that deviations from an approved protocol or violations of applicable policies, guidelines, or laws could result in immediate suspension of the protocol and may be reportable to the Office of Laboratory Animal Welfare (OLAW).	
3. I understand that the Attending Veterinarian or his/her designee must be consulted in the planning of any research or procedural changes that may cause more than momentary or slight pain or distress to the animals.	
4. I declare that all experiments involving live animals will be performed under my supervision or that of another qualified scientist. All listed personnel will be trained and certified in the proper humane methods of animal care and use prior to conducting experimentation.	
5. I understand that emergency veterinary care will be administered to animals showing evidence of discomfort, ailment, or illness.	
6. I declare that the information provided in this application is accurate to the best of my knowledge. If this project is funded by an extramural source, I certify that this application accurately reflects all currently planned procedures involving animals described in the proposal to the funding agency.	
7. I assure that any modifications to the protocol will be submitted to by the UD-IACUC and I understand that they must be approved by the IACUC prior to initiation of such changes.	
8. I understand that the approval of this project is for a maximum of one year from the date of UD-IACUC approval and that I must re-apply to continue the project beyond that period.	
9. I understand that any unanticipated adverse events, morbidity, or mortality must be reported to the UD-IACUC immediately.	
10. I assure that the experimental design has been developed with consideration of the three Rs: reduction, refinement, and replacement, to reduce animal pain and/or distress and the number of animals used in the laboratory.	
11. I assure that the proposed research does not unnecessarily duplicate previous experiments. ( <i>Teaching Protocols Exempt</i> )	
12. I understand that by signing, I agree to these assurances.	
 Signature of Principal Investigator	 Date

**SIGNATURE(S) OF ALL PERSONS LISTED ON THIS PROTOCOL**

I certify that I have read this protocol, accept my responsibility and will perform only the procedures that have been approved by the IACUC.

Name	Signature
1. Christian Escobar	
2. Chen-Yuan Kao	
3. Erica Winter	
4. Click here to enter text.	
5. Click here to enter text.	
6. Click here to enter text.	
7. Click here to enter text.	
8. Click here to enter text.	
9. Click here to enter text.	
10. Click here to enter text.	
11. Click here to enter text.	
12. Click here to enter text.	
13. Click here to enter text.	
14. Click here to enter text.	
15. Click here to enter text.	

Proposed Changes to an Existing Protocol